

University  
of Dundee

Testing the Reliability of the Schmidt Hammer to measure glacial  
recession at the Schlatenkees in the Austrian Alps

Michael Neuwirth



Dissertation submitted as part of the final examination for the  
degree of:

MA with Honours in Geography

University of Dundee, 2025

Word count: 9929

## Acknowledgements

Firstly, I would like to express my gratitude to my supervisor, Dr Simon Cook whose expertise and advice was greatly appreciated throughout this project. Secondly, I would like to thank my Mum and Dad who made this whole project possible and provided me with support through my degree. Finally, I want to thank Florian from the Hohe Tauren National Park who granted access for parking and data collection at the site.

## Table of Contents

Acknowledgements .....	ii
List of Tables .....	v
List of Figures .....	vi
Abstract .....	xiii
<b>Chapter 1. Introduction</b> .....	1
1.1 – Background .....	1
1.2 – Aims and Objectives .....	4
1.3 – Study Area .....	5
1.4 – Dissertation Overview .....	7
<b>Chapter 2. Literature Review</b> .....	8
2.1 - Glacial recession .....	8
2.2 – The Schmidt hammer .....	14
<b>Chapter 3. Methodology</b> .....	20
3.1 - Geomorphological Map .....	20
3.2- Schmidt Hammer .....	24
3.3- Data Analysis – Schmidt hammer .....	31
<b>Chapter 4. Results</b> .....	33
4.1 - Geomorphological Map .....	35
4.1.1 - Geomorphological Features – Scoured Bedrock.....	36
4.1.2 - Geomorphological Features – Moraines .....	38
4.1.3 - Geomorphological Features – Gullies.....	42
4.1.4 - Hydrological Features .....	42
4.1.5 - Glaciological Features .....	44
4.1.6 – Vegetation .....	45
4.2 – Schmidt Hammer .....	47
4.2.1 – Transects.....	49
4.2.2 - Individual Transects Compared .....	55
4.2.3 - Additional sites .....	56
4.2.4 – Transect Average Vs. Elevation .....	58
4.2.5 – Exposure Dates of the Sites.....	58
<b>Chapter 5. Discussion</b> .....	60

5.1 - <i>Geomorphological Map</i> .....	60
5.1.1 – Scoured Bedrock .....	61
5.1.2 – Moraines .....	61
5.1.2.1 – <i>Lateral Moraines</i> .....	62
5.1.2.2 – <i>Recessional Moraines</i> .....	65
5.1.3 – Hydrological Features.....	68
5.2 - <i>Schmidt Hammer</i> .....	71
5.2.1 – R-values across the Schlatenkees Foreland .....	71
5.2.2 – Retreat Pattern of Schlatenkees Affecting R-Values .....	72
5.2.3 – Assessing the Outlier of Site 2 on Transect 4.....	73
5.2.4 – Limitations of the Schmidt Hammer .....	76
<b>Chapter 6. Conclusion</b> .....	78
6.1 – <i>Addressing the Objectives</i> .....	79
<b>7 – Reference List</b> .....	80
<b>8 – Appendices</b> .....	92
Appendix A – ‘RockSchmidt’ programme .....	92
Appendix B – Excel spreadsheet with outliers removed .....	93
Appendix C – R-studio code .....	94

## List of Tables

Table 2. 1: Table showing the Austrian GI's, their reference year and their authors. <sup>1</sup>For shapefile download see Fischer et al. 2015b, all other GI's can be downloaded from author listed. .... 12

*Table 2. 2: Previous annual losses during the Alpenverein's annual measurements for the Schlatenkees. Source: Alpenverein (2016; 2018; 2020; 2021; 2022; 2023b; 2024; 2025)..... 14*

Table 3. 1: Table showing the features mapped within the foreland of the Schlatenkees along with its feature type classification and the geometry typed used to map the feature. .... 23

Table 4. 1: Table showing the total area (or highest length of a linear feature) of the mapped features across the Schlatenkees foreland. The feature type on the map and the occurrence of each feature is also acknowledged. Table based off (Kjær et al., 2008). <sup>1</sup>Gullies drawn only signify that gullies are present on that section of hillside. Does not signify quantity of gullies .. 35

Table 4. 2: Table showing the data for the additional sites sampled at the Schlatenkees. .... 57

Table 4. 3: Table showing the exposure date of the sites along the transects and for the additional sites. .... 59

## List of Figures

Figure 1. 1: <i>LIA maximum of the glaciers within the Venediger group.</i> .....	2
Figure 1. 2: <i>The reduction in size of the Schlatenkees from the LIA to 2015 based of the glacial inventories.</i> .....	3
Figure 1. 3: <i>Overview of the Schlatenkees and the study area.</i> .....	6
Figure 1. 4: <i>Historical watercolour painting of the Schlatenkees from Innergschlöss in 1840 showing the glacier reaching the valley floor. Painting from Gletscher: Klimazeugen von der Eiszeit bis zur Gegenwart (Patzelt, 2019).</i> .....	7
Figure 2. 1: <i>Predicted regional mass balance change and sea level contribution for each of the worlds glaciated regions from 2015-2100. The discs show the projections of glacier mass for each region and globally in 2100 relative to 2015. Source Rounce et al. (2023)</i> .....	9
Figure 2. 2: <i>Graphs showing the period of advance in the 1970s/early 80s of Austrian glaciers, followed by a strong downward trend in length. Graph A shows the mean change in length of all glaciers, and graph B shows the status of the measured glaciers. The period of advance is highlighted in green. Source: Alpenverein (2023a)</i> .....	11
Figure 2. 3: <i>Shows the data type used for compiling GI3 ('L' for lidar DEMs and 'O' for orthophoto) and the individual mountain ranges with the year they were measured. Source: Fischer at al. (2015a)</i> .....	13
Figure 2. 4: <i>Graph from Shakesby et al. (2006) showing the decrease in r-value from the LIA surfaces to the Younger Dryas surfaces.</i> .....	18

*Figure 3. 1: Field sketch taken while walking a moraine in the site. Features such as where the path was and where a smaller group of moraines were noted down as well. Source: Author. .... 22*

*Figure 3. 2: Image showing the digital N-type Schmidt hammer used in this study, specifically, the ‘Rockschmidt’ manufactured by Proceq in Switzerland. Source: Author. .... 24*

*Figure 3. 3: Image showing the author applying the Schmidt hammer to a section of bedrock at a perpendicular angle. Source: Author. .... 26*

*Figure 3. 4: Example of notes taken for site 3 on transect 3. Source: Author ..... 27*

*Figure 3. 5: Image showing the average r-value calculated in the field after data collection at the site was complete. Average r-value is displayed in the top left of the screen of the Schmidt hammer. Source: Author. .... 28*

*Figure 3. 6: Aerial image showing an overview of the sample sites on transects and the additional sites in the Schlattenkees foreland. .... 30*

*Figure 4. 1: Geomorphological map of the Schlattenkees foreland. .... 34*

*Figure 4. 2a: Photo of striations in the bedrock at additional site 3; Figure 4. 2b: Channel incised into the bedrock below site 4 on transect 3; Figure 4. 2c: Streamlined features at additional site three. The feature under the furthest right red arrow is a small roche moutonnée. Red arrows indicate streamline features, green arrows show ice flow direction. Source: All photos – Author. .... 37*

*Figure 4. 3: Image showing large sections of exposed bedrock either side of the narrow tongue of the Schlatenkees. Purple hatchings highlight bedrock either side of the tongue. Source: Author*  
..... 38

*Figure 4. 4: Map showing the LIA, 1969 and 1998 glacier margins for the Schlatenkees in comparison to the moraines. The LIA margin follows the lateral moraines whilst the 1969 and 1998 margins follow the moraine cutting across the site from north-west to south-east. ....* 39

*Figure 4. 5a: Image showing the southern moraine which sits above the foreland of the Schlatenkees. Red lines highlight the ridges of the moraines; Figure 4. 5b: Image showing the moraines on the northern slope above the foreland of the Schlatenkees. Highlighted with red arrows. Source: Author. ....* 40

*Figure 4. 6 a: 3 Image looking downhill as the moraine cuts across the landscape; 4. 6b: Image showing the moraine where it was deposited on a section of bedrock at site 3, transect; 4. 6c: Side view of a section of the moraine further down from figures 4. 6a and 4. 6b. The red line shows the ridge of the moraines. Source: Author. ....* 41

*Figure 4. 7: Photo showing gullying on the large moraine on the south side of the site. Source: Author. ....* 42

*Figure 4. 8: Image showing the meltwater stream which drains the proglacial lake at the Schlatenkees. Source: Author. ....* 43

*Figure 4. 9: Image showing the proglacial lake where the Schlatenkees terminates as seen from site 1 on transect 4. Various icebergs which have calved from the snout can be seen floating in the lake. Source: Author. ....* 44

*Figure 4. 10 a: The Schlatenkees as seen from the proglacial lake where it terminates; Figure 4. 10b: The terminus of the debris covered section of the Schlatenkees. Source: Both photos - Author ..... 45*

*Figure 4. 11: Photo from valley bottom showing trees and shrubs on the lower part of the Schlatenkees foreland which drops down into the valley floor. Source: Author. .... 46*

*Figure 4. 12: Overview showing all sites with their r-values and the glacial margins from the glacial inventories. .... 48*

*Figure 4. 13: A very smooth area of bedrock at site 2 on transect 1. Source: Author ..... 49*

*Figure 4. 14: Graph showing the average site r-value against the distance from the glacier for transect 1. With the standard deviations shown in the error bars. Source: Author. .... 50*

*Figure 4. 15: Boxplot showing the differences between the sites on transect 1. Blue square represents the mean and red crosses represent outliers. Source: Author. .... 50*

*Figure 4. 16: Graph showing the average site r-value against the distance from the glacier for transect 2. With the standard deviations shown in the error bars. Source: Author. .... 51*

*Figure 4. 17: Boxplot showing the differences between the sites on transect 2. Blue square represents the mean and red crosses represent outliers. Source: Author. .... 51*

*Figure 4. 18: Graph showing the average site r-value against the distance from the glacier for transect 3. With the standard deviations shown in the error bars. Source: Author. .... 52*

*Figure 4. 19: Boxplot showing the differences between the sites on transect 3. Blue square represents the mean and red crosses represent outliers. Source: Author. .... 53*

*Figure 4. 20: Graph showing the average site r-value against the distance from the glacier for transect 4. With the standard deviations shown in the error bars. Source: Author. .... 54*

*Figure 4. 21: Boxplot showing the differences between the sites on transect 4. Blue square represents the mean and red crosses represent outliers. Source: Author. .... 54*

*Figure 4. 22: An area of bedrock sampled at site 2 on transect four. Vegetation and a rougher rock surface can be observed. Source: Author. .... 55*

*Figure 4. 23: Graph showing a comparison between all 4 transects plotted against the distance from the glacier. Source: Author. .... 56*

*Figure 4. 24: Overview of the eight additional sites sampled at the Schlatenkees. See Table 4.2 for the distance from the ice and SD. .... 57*

*Figure 4. 25: Graph showing the average r-value of each transect plotted against the average elevation of each transect. Source: Author. .... 58*

*Figure 5. 1 a: Photograph showing a section of the moraine on the northern side of the site comprised of larger clasts surrounded by vegetation; Figure 5. 1b: Photograph looking down the southern moraine above the debris covered tributary of the Schlatenkees which shows some clasts mixed in with finer sediments. Both photos sourced from Author. .... 63*

*Figure 5. 2: Annotated photo showing the possible sources for the abundance of debris covering the debris covered tributary of the Schlatenkees which had formed the southern lateral moraine. The area shaded in red is a scree slope, the north face of the Kristallwand is shaded in a yellow hatching and the glacier is outlined in green. Source: Author. .... 64*

*Figure 5. 3: Annotated photo of the Schlatenkees from between 1920-1940, showing the difference between the clean surface of the Schlatenkees on the right compared to the*

*debris covered tributary on the left. The southern moraine is highlighted in red. Source: Austrian National Library – Photo L 51918-B POR*

*MAG ([https://data.onb.ac.at/rep/BAG\\_18956337](https://data.onb.ac.at/rep/BAG_18956337)). ..... 65*

*Figure 5. 4: Satellite imagery from 1997 showing the actual distance the glacier had receded from the recessional moraine. Red arrows show sections of the moraine and white arrows show the rough distance between the moraine and terminus. Source: See bottom left of figure. .... 66*

*Figure 5. 5: Annotated historical Image between the 1920s-1930s showing the glacial margin at points where recessional moraines were identified on the geomorphological map. Source: Austrian National Library – Photo L 51918-B POR MAG ([https://data.onb.ac.at/rep/BAG\\_18956337](https://data.onb.ac.at/rep/BAG_18956337)) ..... 67*

*Figure 5. 6: Aerial imagery showing the location of the recessional moraines which were left behind by the glacier as it retreated from the location seen in Figure 5.5. .... 68*

*Figure 5. 7: Map of glacial lakes in Austria, showing the Venediger group (labelled as group ‘3’) with the 3<sup>rd</sup> highest lake density in the Austrian Alps. Source: Buckel et al. (2018). ..... 69*

*Figure 5. 8 a: Satellite imagery of the Schlatenkees in 2015 showing little indication of proglacial lake development; Figure 5.8b; Satellite imagery of the Schlatenkees from 2019 showing circular crevasses and disintegration of the snout with the proglacial lake in development; Figure 5.8c: Satellite imagery of the Schlatenkees from 2022 showing the proglacial lake which has become a prominent feature in the landscape. .... 70*

*Figure 5. 9a: Smooth bedrock surface at site 1 on transect 3. Figure 5.9b: Rougher and lichen covered section of bedrock at site 4, transect 3 with moss, lichen and oxidisation, highlighting the difference between two sites on the same surface. Source: Both photos – Author. .... 74*

*Figure 5. 10a: Bedrock sampled from site 1 on transect 4 (r-value 66.5), showing a smooth profile with no lichen present. Figure 5. 10b: Bedrock sampled at site 2 on transect 4 (r-value 49) showing the presence of lichen and a rougher profile. Source: Both photos – Author. .... 75*

## Abstract

This study aims to test the reliability of the Schmidt hammer for measuring glacial recession at the Schlatenkees in the Austrian Alps. Most Schmidt hammer studies use relative dating on landforms, however in this study, sites can be absolutely dated through historical and aerial imagery. As there is little literature on the application of the Schmidt hammer on recently deglaciated gneissic terrain, this study helps to fill in this literature gap by testing the Schmidt hammer's reliability on twenty-six sites across the Schlatenkees foreland.

Geomorphological mapping was undertaken and identified several features that related to glacial retreat in the Schlatenkees foreland. The results from the Schmidt hammer were variable, none of the four transects showed a statistically significant relationship between r-value and distance from the ice. Although, the r-value closest to the ice was higher than the site furthest away on all transects. This highlighted that there was some general reliability in the Schmidt hammer, despite the variation along the transects. A statistically significant relationship was observed between the transect r-value and elevation which showed its reliability as aerial imagery documented its retreat from higher to lower elevation. The Schmidt hammer did prove unreliable in some cases however, one site highlighted the effect of lithology on the Schmidt hammer and suggested that lichen may also have an influence on the r-value. Highlighting that gneiss may not be suitable for Schmidt hammer application and the affect lichen cover has on rock surfaces requires further work.

# **Chapter 1.**

## **Introduction**

This chapter introduces this study by setting some context behind the rationale and equipment used. It also sets out the aim and objectives and introduces the study site.

The final section details the structure of the rest of the study.

### **1.1 – Background**

Glaciers have seen significant melting since the turn of the century, with many predictions stating that if greenhouse gas emissions are not drastically reduced, many regions will suffer unprecedented mass loss by the year 2100 (Zekollarim et al., 2019; Han et al., 2023). It has been predicted that mass loss for glaciers in Alaska (Wahr et al., 2016) and Svalbard (Geyman et al., 2022) alone will double by 2100, contributing to sea level rise (Zemp et al., 2019), affecting low lying regions globally and leading to doubts over water security (Han et al., 2023). This highlights the critical role glaciers play in numerous regions across the globe and why understanding their retreat is important for modelling climate change accurately to inform regions that are the most vulnerable.

One specific region that has been affected by glacier retreat is the Austrian Alps and this has been quantified in numerous studies through the four Austrian Glacial Inventories (GI's). These are crucial in quantifying mass loss (Fischer et al., 2015a) for separate regions such as the Glockner group or the Venediger group (Figure 1.1) and individual glaciers. The GI's have been used on the Schlatenkees in the Venediger group to show retreat from the LIA to 2015 (Figure 1.2), however, the Schlatenkees retreat is also well

documented through historical imagery from the 1920s-30s and aerial imagery from 1953-2022. This means that the Schlatenkees lends itself to be a suitable location to test other methods of measuring glacial recession.

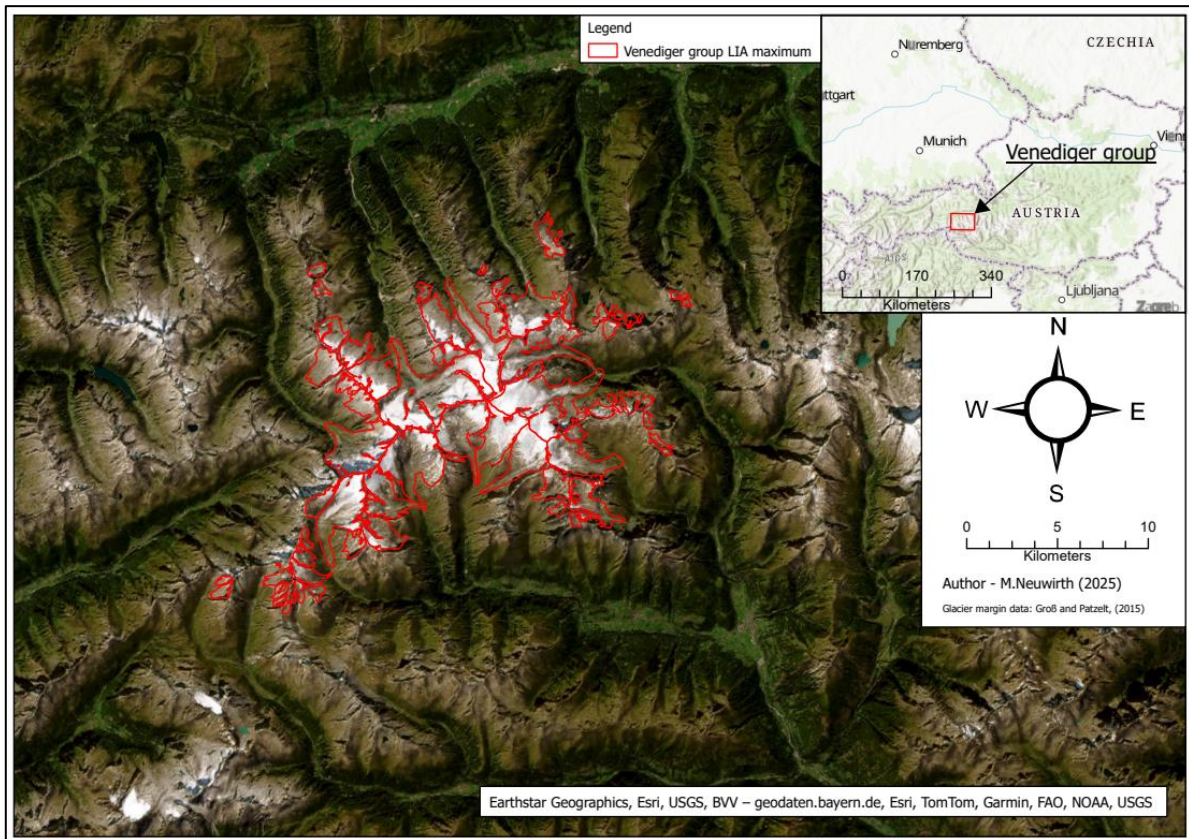


Figure 1. 1: LIA maximum of the glaciers within the Venediger group.

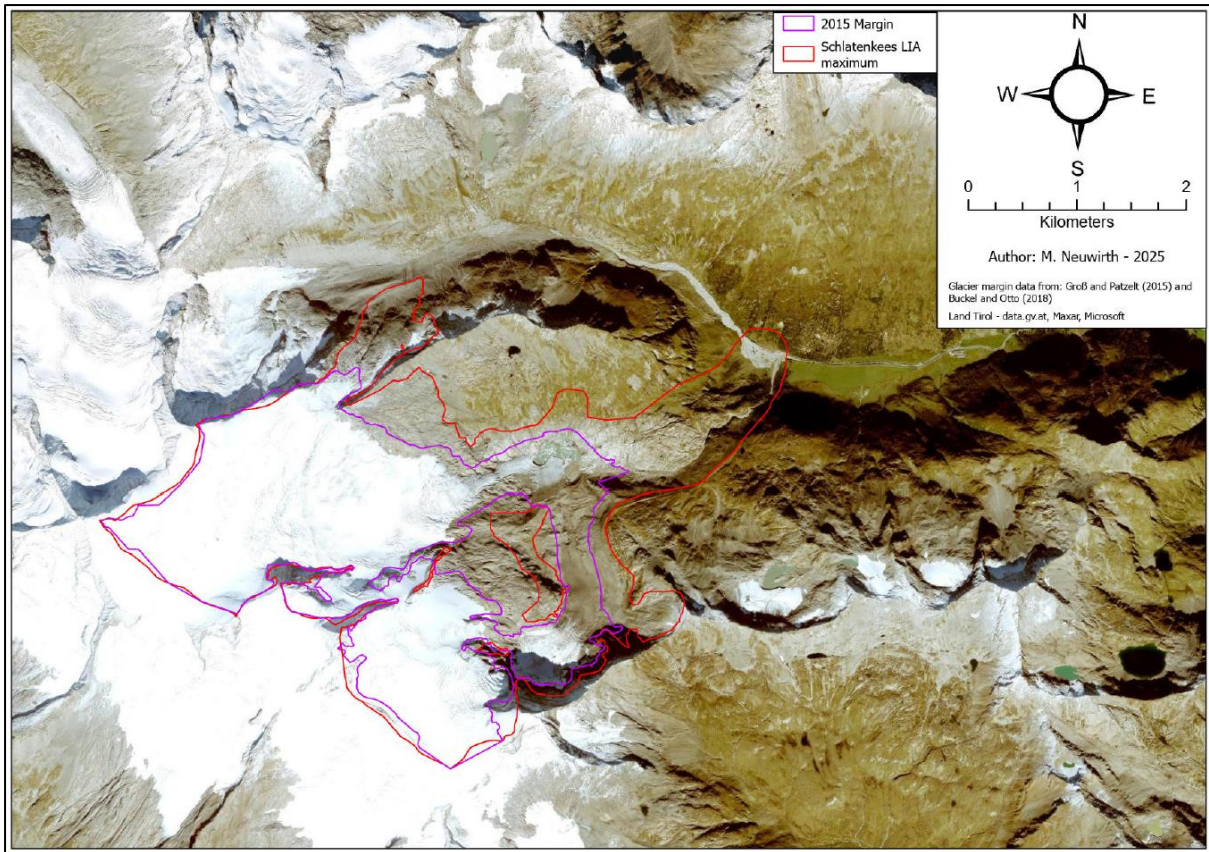


Figure 1. 2: *The reduction in size of the Schlatenkees from the LIA to 2015 based of the glacial inventories.*

The Schmidt hammer is a lightweight piece of equipment that was first used in geomorphology by Matthews and Shakesby (1984) and is a cheaper alternative to absolute dating. The basic principle of the Schmidt hammer is that lower r-values indicate older rock surfaces (Tomkins et al., 2016) which can be used to distinguish surfaces that have been deglaciated from different time periods. This principle has been successfully observed in differentiating LIA surfaces from Holocene surfaces by Shakesby et al. (2006), however, one clear limitation is that sampling different lithologies will cause inaccuracies within the dataset (Matthews et al., 2024). Some other rock characteristics to be avoided are rough surfaces and lichen/moss cover (Winkler, 2005; Shakesby et al., 2006; Rode and Kellerer-Pirklbauer, 2011). This study aims to test the Schmidt hammer in an area where the chronology of glacier retreat is well documented,

providing the opportunity to test its reliability and efficiency in measuring glacial recession.

### 1.2 – Aims and Objectives

The aim of this study is to test the reliability of the Schmidt hammer to measure glacial recession at the Schlatenkees in the Austrian Alps. This will be supported by three research objectives that are to help achieve the aim and they are as follows:

1. Create a geomorphological map to locate features related to previous glacier terminus positions and features relating to glacier retreat.
2. To collect Schmidt hammer rebound values across the Schlatenkees foreland to be used in identifying old glacier positions.
3. To identify a relationship between the rebound values collected and the distance from the glacier.

### 1.3 – Study Area

The study focuses on the foreland of the Schlatenkees which is in the Venediger group (Figure 1.3), in the Osttirol province of Austria and is situated the Hohe Tauern National Park. This valley glacier descends from the peak of the Großvenediger, Austria's fourth highest peak at 3666m, and currently terminates in a proglacial at ~2300m. There is also a debris covered section which sits below the north-east face of the Kristallwand (Figure 1.3). The foreland of the Schlatenkees consists of a large area of exposed bedrock that slopes downwards from north to south with the lowest point situated where the meltwater stream is located. During the LIA, the Schlatenkees reached the bottom of the valley at 1700m (Figure 1.4). The lithology of the site predominately gneiss, a metamorphic rock, and more specifically migmatitic gneiss and paragneiss (Geological Survey of Austria, 1987).

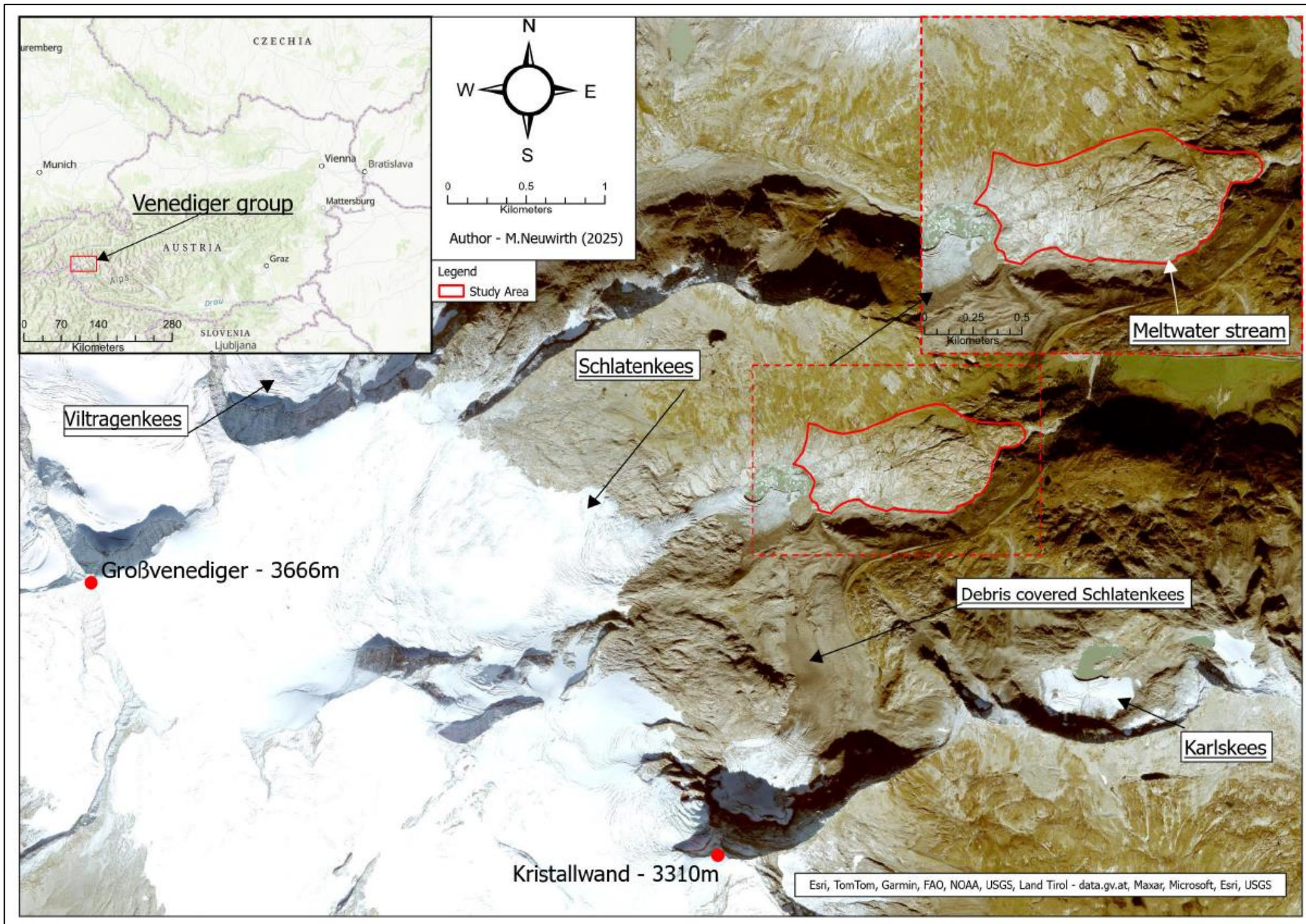


Figure 1. 3: Overview of the Schlattenkees and the study area.



Figure 1. 4: *Historical watercolour painting of the Schlatenkees from Innerschlöss in 1840 showing the glacier reaching the valley floor. Painting from Gletscher: Klimazeugen von der Eiszeit bis zur Gegenwart (Patzelt, 2019).*

#### 1.4 – Dissertation Overview

This study is divided up into six chapters, with chapter one being the introduction. The second chapter consists of a literature review of glacial recession, and Schmidt hammer application in similar landscapes. In chapter 3 the methodology is detailed, for both the geomorphological mapping and the Schmidt hammer data collection and analysis. In the fourth chapter the results are presented for the geomorphological map and the Schmidt hammer, followed by the discussion (chapter five) where features from the geomorphological map are discussed and the Schmidt hammer data is interpreted, and its reliability is discussed. The sixth and final chapter is the conclusion where the aims and objectives are addressed.

## **Chapter 2.**

### **Literature Review**

In this this chapter the key literature is discussed regarding glacial recession from the global context down to the study area in the Austrian Alps, and how past glacial recession in Austria has been measured. The second section covers the Schmidt hammer and how past studies have applied it and discusses a gap in the literature.

#### **2.1 - Glacial recession**

Since the turn of the century there has been unprecedented glacial retreat in all the worlds glaciated regions (Zemp et al, 2015). With large scale regional mass balance change predicted to occur, even if temperatures were to stay below +2<sup>0</sup>C relative to preindustrial levels by 2100 (Rounce et al., 2023) (Figure 2.1), the retreat of ice sheets and glaciers will have an adverse effect on local and global eco systems and human populations globally. For example, the Antarctic ice sheet is crucial for the planet's albedo and ocean circulation (Fricker et al., 2025), and Himalayan Mountain glaciers are a crucial freshwater supply for drinking water but also agriculture (Kehrwald et al., 2008). This could potentially lead to glacially fed rivers becoming the centre of political disputes as in the future there are significant doubts over water security (Haines, 2017).

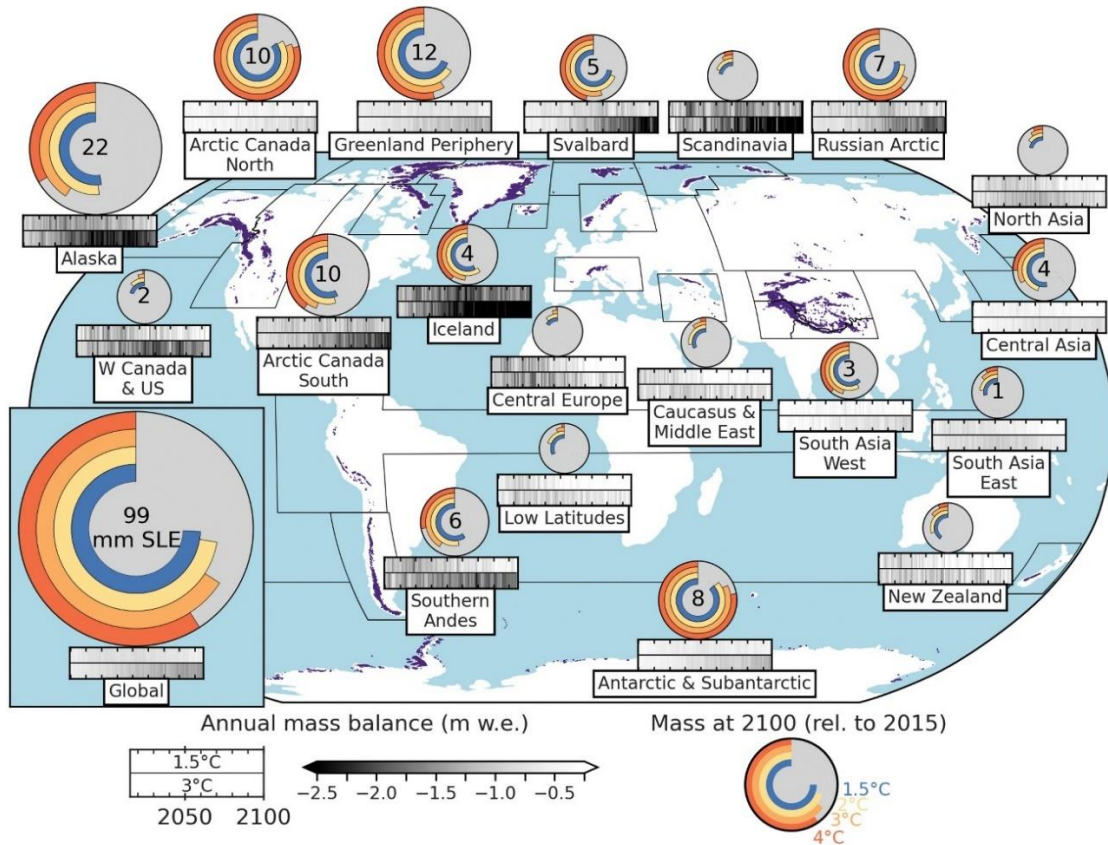


Figure 2. 1: Predicted regional mass balance change and sea level contribution for each of the worlds glaciated regions from 2015-2100. The discs show the projections of glacier mass for each region and globally in 2100 relative to 2015. Source Rounce et al. (2023)

Both ice sheets and glaciers account for sea level rise (Zemp et al., 2025), and it is thought that if temperature thresholds are broken, Antarctica may cause sea levels to rise 28cm by 2100 (Fricker et al., 2025). Recent studies have observed the effect of glaciers (excluding icesheets) on sea level rise, Zemp et al. (2025) found that global sea levels rose  $18 \pm 1$  mm from 2000-2023 or  $0.74 \pm 0.04$  mm annually. Hugonnet et al. (2021) and Rounce et al. (2023) found similar results at  $0.74 \pm 0.04$  mm annually between 2000-2019. With future predictions showing high mass losses to continue under various emissions scenarios (Rounce et al., 2023) (Figure 2.1) gaining a better understanding of

glacier recession is vital for the creation of accurate climate change models (Wytiahlowsky et al., 2024) (e.g. sea level rise prediction).

The European alps are sensitive to climate change (Koboltschnig and Schöner, 2011) and have retreated significantly since the LIA (Zemp 2006; Reinthaler and Paul, 2024; Palacios et al., 2024). Glaciers in the alps lost an overall 35% in area between 1850 and the 1970s, which increased to a reduction of 50% by 2000 (Zemp, 2006; Zemp et al., 2008). A study by Sommer et al. (2020) found that all regions in the alps have lost mass and area in the 21<sup>st</sup> century, highlighting that ranges at lower altitudes within the alps could be ice free by the end of the century. Palacios et al., (2024) state that the rising average temperatures have been the primary catalyst for their retreat, especially in the 21<sup>st</sup> century with average summer air temperatures having increased 1.3°C from 1986-2015 (Luterbacher et al., 2016; Wytiahlowsky et al., 2024). Rounce et al. (2023) and Zekollari et al. (2019) further support this and state that if temperatures keep rising, under a high emissions scenario of +3°C or higher, more than 80% of the glaciers in the alps will be gone by 2100 (Figure 2.1). This intense retreat and mass loss observed in the European alps highlights the need for strict global temperature thresholds to protect the freshwater supply these glaciers bring to Alpine communities (Lambrecht and Kuhn, 2007).

Austria has seen dramatic glacier loss since the turn of the century along with the other countries in the Alps. The alps in Austria are lower when compared to Switzerland or France, with no peaks reaching above 4000m in altitude which leaves the glaciers in Austria, especially valley glaciers (Stocker-Waldhuber et al., 2017), at greater risk to the rising summer temperatures (Luterbacher et al., 2016). The glaciers in Austria are small

to medium sized and in the 1970s it had an estimated 925 glaciers with none being larger than 20km<sup>2</sup> (Zemp et al., 2008). The most recent recorded advance of Austrias glaciers was in the 1970s/early 80s (Figure 2.2) (Lambrecht and Kuhn, 2007; Fischer et al., 2015a), due to a period of positive mass balance, however, since 1982 the trend reversed more towards negative mass balance (Schöner et al., 2000). Work by Fischer et al., (2015a) used the various Austrian GI's to calculate overall area loss since the LIA and found that from the LIA to 2006 (GI3) there was a 44% reduction in glacier area.

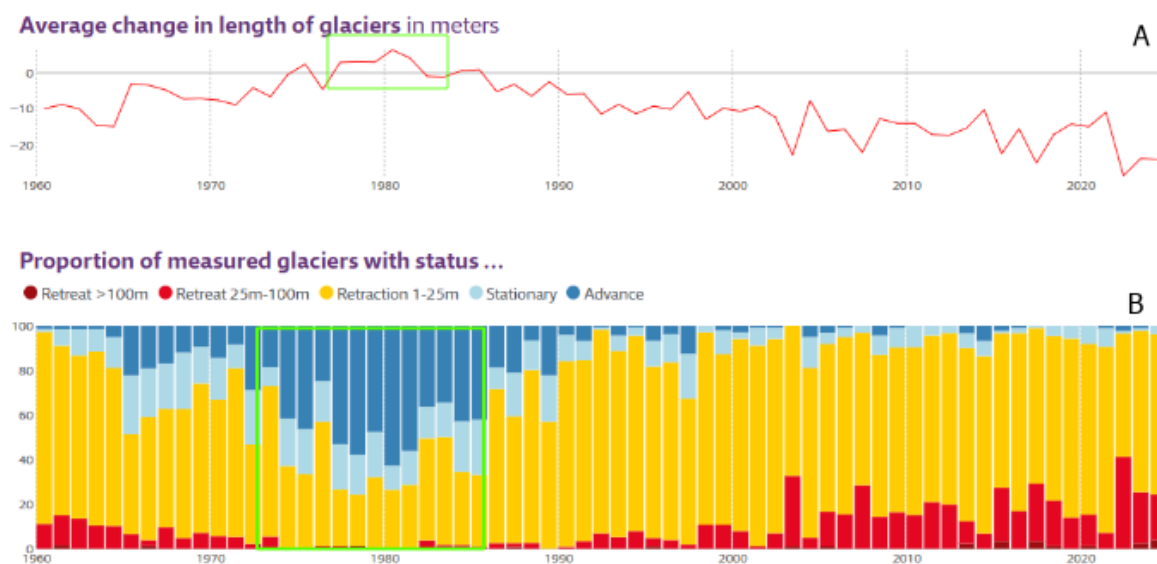


*Figure 2. 2: Graphs showing the period of advance in the 1970s/early 80s of Austrian glaciers, followed by a strong downward trend in length. Graph A shows the mean change in length of all glaciers, and graph B shows the status of the measured glaciers. The period of advance is highlighted in green. Source: Alpenverein (2023a)*

Austria has four GI's (Table 2.1), and they play a key role in quantifying overall mass loss, retreat over time and modelling future extent (Alps et al., 2009). The first one (GI1) was originally an analogue data set (Patzelt, 1980; Groß, 1987) and was later digitised by Lambrecht and Kuhn (2007). For GI3 (Fischer et al., 2015b), Fischer et al. (2015a) used orthophotos and lidar digital elevation models (DEMs) from 2004-2012 (Figure 2.3) to update the inventory and the latest GI was undertaken in 2015 (GI4), for Buckel et al. 2018

using Google Earth. These glacial inventories have been used in studies to track area loss (Fischer et al., 2015a), total ice volume (Lambrecht and Kuhn, 2007) and increases in proglacial lake formation from the LIA-2015 (Buckel et al., 2018).

*Table 2. 1: Table showing the Austrian GI's, their reference year and their authors. <sup>1</sup>For shapefile download see Fischer et al. 2015b, all other GI's can be downloaded from author listed.*

<b>Name</b>	<b>Reference Year</b>	<b>Author</b>
<i>GI1</i> <sup>1</sup>	1969	Patzelt, 1980
<i>GI2</i> <sup>1</sup>	1998	Lambrecht and Kuhn, 2007
<i>GI3</i>	2006	Fischer et al. 2015b
<i>GI4</i>	2015	Buckel and Otto, 2018
<i>GI LIA</i>	~1850	Groß and Patzelt 2015

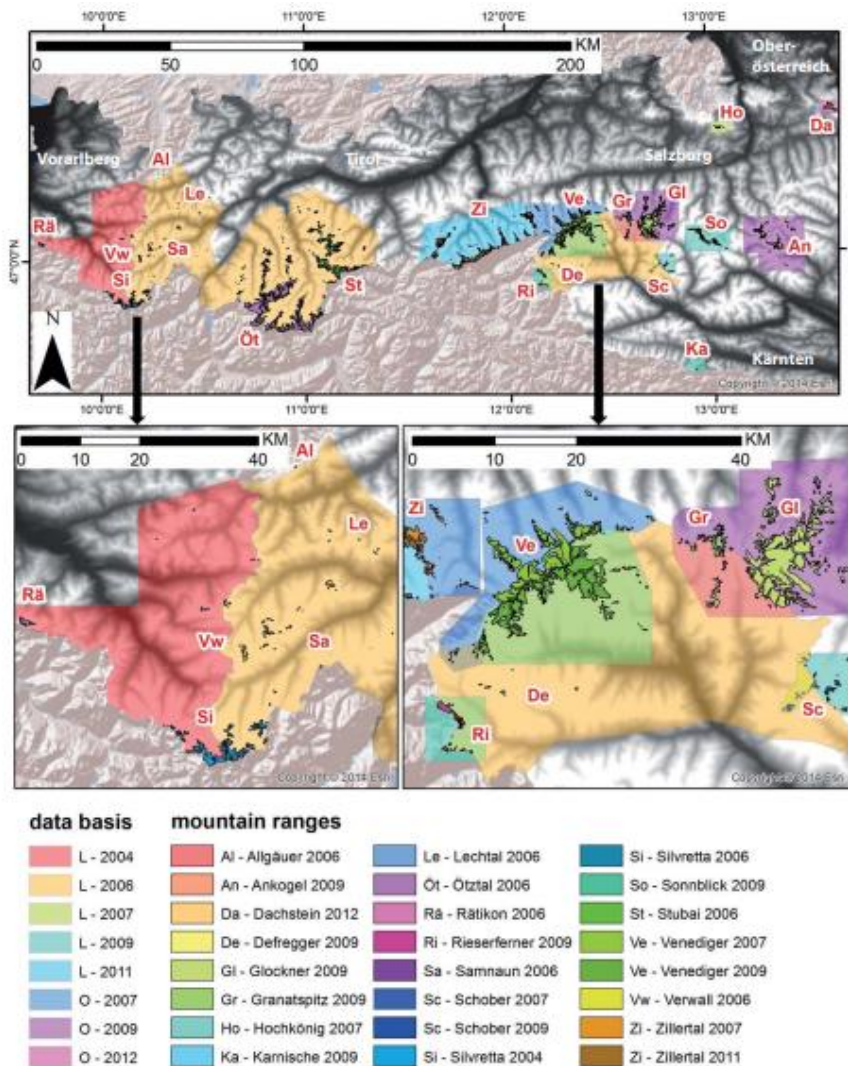


Figure 2. 3: Shows the data type used for compiling GI3 ('L' for lidar DEMs and 'O' for orthophoto) and the individual mountain ranges with the year they were measured. Source: Fischer et al. (2015a)

For the last 134 years the Alpineverein have observed ~90 glaciers each year. Their latest report from the year 2023/24 showed an average loss of 24.1m in length (Alpenverein, 2025) which was the 3<sup>rd</sup> highest observed in the 134 years of this annual measurement (Alpen Verein, 2025). This was also the second consecutive year where a glacier has lost over 200m and reported that the 2023/2024 year was 1.9°C too warm and very dry. The Schlatenkees recorded the highest loss in length for two consecutive years from 2020/2021 to 2021/2022 with a 54.5m loss and an 89.5m loss (Table 2.2). Glacier retreat

at the Schlatenkees has little literature surrounding it, although it was measured to be 9.321km<sup>2</sup> using GI2 (Fischer and Kuhn, 2013). However, retreat for the Venediger group (where the Schlatenkees is located) has been quantified through to the Austrian glacial inventories with Fischer et al. (2015a) observing a 20.9% decrease in area between GI2 and GI3 and Buckel et al. (2018) reporting a high density of proglacial lakes formed from the LIA to 2015. Developing a better understanding of glacial retreat at the Schlatenkees is needed to understand future landscape changes and changes to the water supply for downstream communities.

*Table 2. 2: Previous annual losses during the Alpenverein's annual measurements for the Schlatenkees. Source: Alpenverein (2016; 2018; 2020; 2021; 2022; 2023b; 2024; 2025)*

<b>Glacier Budget Year</b>	<b>Loss (m)</b>
2023/2024	Not measured
2022/2023	-92m
2021/2022	-89.5
2020/2021	-54.5m
2019/2020	-50m
2018/2019	-23m
2016/2017	-70m
2014/2015	-60.3m

## 2.2 – The Schmidt hammer

The Schmidt hammer is a piece of equipment that was originally designed to conduct *in situ* concrete hardness tests (Goudie, 2006). It was pioneered in geomorphology by Matthews and Shakesby (1984) and is used in the relative dating of landforms and calculating rock weathering rates (Goudie, 2006; Matthews and Winkler, 2022). It is a cheap, lightweight piece of equipment that can give *in situ* readings of rock hardness in the field with digital ones having the ability to calculate the mean r-value and standard

deviation instantly. The most common type of Schmidt hammer used by geomorphologists is the 'N' type Schmidt Hammer (Goudie, 2006), and it has been successfully applied to various landforms in glacial environments, such as rock glaciers (Rode and Kellerer-Pirklbauer, 2011), moraines (Rune Aa and Sjøstad, 2000; Winkler, 2005; Kellerer-Pirklbauer, 2008), and bedrock (Shakesby et al., 2006; Matthews et al., 2024; Santos-González et al., 2024).

The Schmidt hammer records an r-value (Tomkins et al., 2016) which is proportional to the compressive strength of the rock surface (Rode and Kellerer-Pirklbauer, 2011). This r-value is calculated by the distance the spring-loaded bolt travels after being rebounded off the surface (Goudie 2006; Tomkins et al., 2016), therefore, the r-values taken from rock surfaces can be used to determine weathering rates such as Matthews et al. (2024) or to apply Schmidt hammer exposure dating (SHED) to rock surfaces (Tomkins et al., 2016). The principle of the Schmidt hammer is that higher r-values indicate higher rock hardness (Aydin and Basu, 2005), and therefore less weathering and a younger rock surface (Tomkins et al., 2016). While older, more weathered surfaces record lower r-values (Tomkins et al., 2016).

There is a gap in the literature regarding the application of the Schmidt hammer to more recently deglaciated landscapes, especially gneissic landscapes, that can be dated using aerial imagery. Most of the studies focus on surfaces dating to the LIA (Matthews and Shakesby, 1984) or Holocene (Shakesby et al., 2006), and even to the Late Pleistocene as shown by Kłapyta (2013). At the Schlatenkees, orthophotos have been taken of the site every decade since 1953 (Tyrolean State Government - Geoinformation

Department, 2025). There are historical photos from the 1920s and 30s of the glacier (Österreichische Nationalbibliothek, 2025) and also a painting from the LIA (Figure 1.4).

The Schmidt hammer has been successfully paired with other dating methods to gather a more accurate understanding of surface dates. Winkler (2009) first attempted to use terrestrial cosmogenic nuclide dating (absolute dating) and the Schmidt hammer together (relative age dating). This study concluded that using the two methods was successful with the Schmidt hammer showing that it was valuable in cross checking boulders that were absolutely dated in the glacier foreland. Lichenometry has also been paired with the Schmidt hammer in Norway (Rune Aa and Sjøstad, 2000; Matthews and Shakesby, 1984) and Iceland (Evans et al., 1999). In Iceland, Evans et al., (1999) found a reasonable correlation between r-value and lichen size at two glacier forelands. Rune Aa and Sjøstad (2000) found that both the r-values and lichen sizes indicated that the outermost moraine at Bøyabreen dates to the Early Holocene. This supports the historical evidence that they were not from the LIA and were older.

The Schmidt hammer has a variety of factors which have been known to affect r-values and this is well documented in the literature. These are joints, cracks, sharp edges and lichen/moss (Winkler, 2005; Shakesby et al., 2006; Matthews and Winkler, 2022; Matthews et al., 2024), irregular surface micro-topography and surface moisture (Rode and Kellerer-Pirklbauer, 2011; Matthews and Winkler, 2022). Internal rock moisture can also have an effect (Sumner and Nel, 2002); however, gneiss, the local lithology, has a low permeability (Duca et al., 2015; Liu et al., 2016). Another key factor to maintain Schmidt hammer accuracy when sampling is to keep the lithology homogenous across the sites and this is due to the significant differences in strength across varying lithologies

(Matthews et al., 2024). However, some lithologies such as gneiss can form with a variety of mineral compositions, leading to a variety of results across the same lithology (Tomkins et al., 2016).

Many studies have been undertaken on gneiss using the Schmidt hammer across the world. Pye et al. (1986) in Kenya recorded average *r*-values between 49.4-53.5, Brooks et al. (2004) in Northwest Scotland recorded a mean of 45.7 and Birdeau et al. (2004) recorded 24-42 in the Yukon, Canada, although only the study by Brooks et al. (2004) was conducted on a glaciated landscape. The suitability of gneiss for Schmidt hammer application was questioned by Tomkins et al. (2016) as they said that due to its coarse-grained texture (Fueten et al., 2003) and highly variable mineral content it can cause inaccurate *r*-values. Although, in Norway the Schmidt hammer has successful application to glacial gneissic landscapes, most notably Matthews et al. (2024) (bedrock) and Shakesby et al. (2006) (boulders and bedrock). Matthews et al. (2024) found that the Schmidt hammer was consistent in recording higher *r*-values in sites deglaciated for <300 years and lower values on sites deglaciated for ~10,000 years. The study by Shakesby et al. (2006) reported similar results as they found the Schmidt hammer was successful in differentiating surface ages (Figure 2.4).

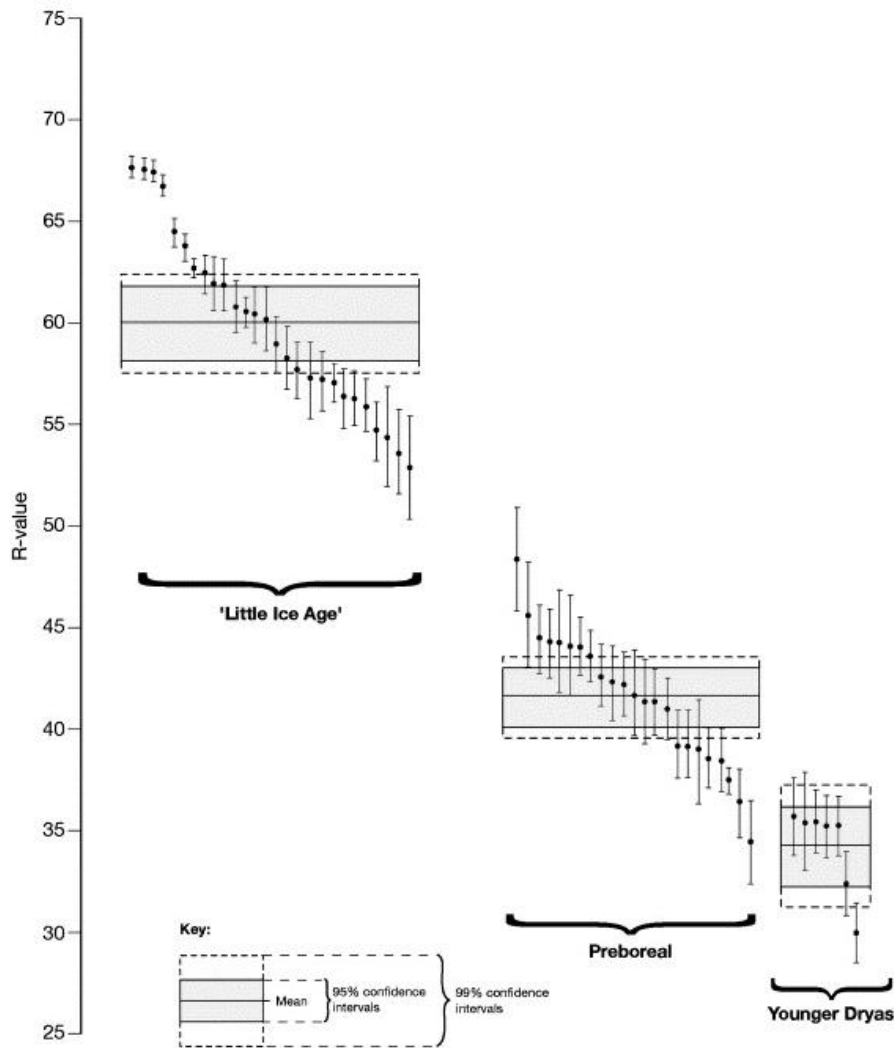


Figure 2. 4: Graph from Shakesby et al. (2006) showing the decrease in r-value from the LIA surfaces to the Younger Dryas surfaces.

A study by Matthews and Owen (2008), conducted on boulders and bedrock in a foreland in Norway focused on the effects of lichen biologically weathering surfaces leading to inaccurate r-values. This study highlighted a significant difference between lichen free surfaces and lichen colonised surfaces, showing that during the first 30-40 years of lichen colonisation, r-values on recently exposed bedrock (88 years), systemically declined from  $61 \pm 0.3$  to  $<40$ . They further discuss that the lichen affected surfaces have characteristics that would typically be seen on the lichen free surfaces after  $\sim 10,000$

years and that the intense biological weathering increased weathering rates on lichen affected surfaces by 200-300 times.

An important study by Niedzielski et al. (2009) aimed to find the minimum sample size required for Schmidt hammer measurements on 14 different lithologies, which was done across a total of 600 sites in Poland, and relevant to this study, they recommend 38 samples for gneiss when taking the mean of the r-values at a site. Niedzielski et al. (2009) also reported numerous sampling schemes for the Schmidt hammer from other studies. For example, Matthews et al. (1986) and Winkler (2005) applied one hit on 50 different boulders, Katz et al. (2000) used the average of the upper 50% out of the 32-40 impacts and Sumner and Nel (2002) took 15 readings at different points of the rock and removed the 5 worst outliers. They then obtained the mean form from the 10 remaining values.

There have been various studies which have applied the Schmidt hammer to glacial landscapes in Austria for dating glacial landforms (Rode et al., 2009), and on rock glaciers (Kellerer-Pirklbauer, 2008; Rode and Kellerer-Pirklbauer, 2011). A moderate correlation between the r-values increasing as the landforms decreased in age was observed by Czempiński and Dąbski (2017) on the foreland of the Kaunertaler Gletscher, in the Ötztal Alps. This shows that the Schmidt hammer has been used with some success on glacial forelands in Austria, although in the Venediger group or at the Schlatenkees specifically there has not been a documented application of the Schmidt hammer on glacial forelands.

## **Chapter 3.**

### **Methodology**

The first two sections of this chapter cover the methodology undertaken for the geomorphological map and Schmidt hammer data collection processes. The programmes/equipment used and the rationale behind the Schmidt hammer sampling are set out in these sections. The final section covers how the data analysis for the Schmidt hammer was completed such as the graphs were used and the statistical analysis conducted on the data.

#### **3.1 - Geomorphological Map**

The use of geomorphologic maps is becoming increasingly common to present the spread of various landforms within a specified area. They are key in communicating the history of the landscape to the reader (Gustavsson et al., 2006) which is becoming more important as receding glaciers are exposing landscapes that can help understand past glacier dynamics. In recent years with the rise of GIS applications and freely available satellite imagery, geomorphological mapping has seen a shift to these platforms (Chander et al., 2018). However, fieldwork remains integral to the foundation of geomorphological mapping (Gustavsson et al., 2006).

For this study geomorphological mapping of the site was undertaken using various forms of satellite imagery, including Orthophotos at a 20cm resolution (Tyrolean State Government - Geoinformation Department, 2025), and were available on ArcGIS Pro as

the basemap for the area so the mapping was carried out using them. Google, Bing and open street maps were also used to assist the mapping process and, in the field, ground truthing was applied to features identified on satellite imagery. The terrain basemap in ArcGIS Pro was used for checking moraines as it was a DEM which allowed moraines to be distinguished easier from the flat satellite imagery. Using a mix of various satellite imagery and field observations, the advantages of all methods could be used to create a more accurate map (Boston, 2012). Photos were taken of identified features, including GPS points which helped in verifying the location of features (Boston, 2012). For one moraine in particular, the length of the moraine was walked over two different days. GPS points were taken at curves of the moraine and a field sketch was made to understand its shape (Figure 3.1). This was later transferred to the GIS via a GPX file to help locate the feature for mapping.

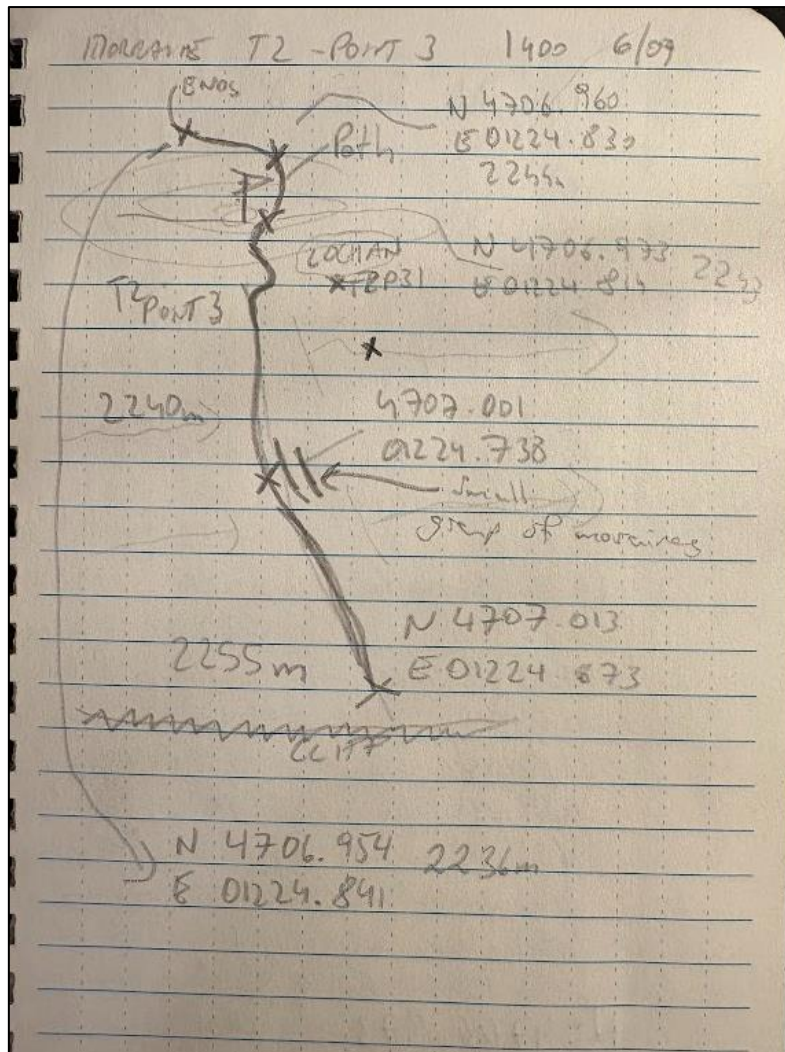


Figure 3. 1: Field sketch taken while walking a moraine in the site. Features such as where the path was and where a smaller group of moraines were noted down as well. Source: Author.

The mapping was all undertaken on ArcGIS Pro with separate shapefiles created for each feature using the 'Lambert Conformal Conic' coordinate system and the framework laid out by Chandler et al (2018) was followed. The scale used was 1:10,000 as it allowed for detail to be shown but also covered the whole valley to give further geographical context. Depending on the feature being mapped, a specific geometry for the shapefile was chosen, for example, mapping the ridges of moraines with lines or polygons for features which covered greater areas such as scree or the glacier (Table 3.1). Meltwater streams utilised both to aid in displaying the larger meltwater stream at the 1:10,000 scale used.

Using individual shapefiles for each feature enhanced the ability to calculate the size/length and quantity of each feature and this could aid in transferring the data to a larger dataset in the future (Chander et al., 2018). The feature types used in Table 3.1 were based off Lardeux et al., (2015) as they had similar features within their geomorphologic map.

*Table 3. 1: Table showing the features mapped within the foreland of the Schlatenkees along with its feature type classification and the geometry typed used to map the feature.*

<b>Feature Type</b>	<b>Feature</b>	<b>Shapefile geometry</b>
<i>Geomorphological</i>	Scoured bedrock	Polygon
<i>Geomorphological</i>	Moraine	Line
<i>Geomorphological</i>	Gully	Line
<i>Geomorphological</i>	Scree	Polygon
<i>Geomorphological</i>	Outwash plain	Polygon
<i>Geomorphological</i>	Braided river	Polygon
<i>Hydrological</i>	Meltwater stream	Line/Polygon
<i>Hydrological</i>	Meltwater pond	Polygon
<i>Hydrological</i>	Proglacial lake	Polygon
<i>Hydrological</i>	Seasonal snow-melt stream	Line
<i>Hydrological</i>	Stream	Line
<i>Hydrological</i>	Pond	Polygon
<i>Glaciological</i>	Glacier	Polygon
<i>Glaciological</i>	Debris covered glacier	Polygon
<i>Vegetation</i>	Trees	Polygon
<i>Vegetation</i>	Shrubs	Polygon

Careful consideration was put into the presentation of the map, as the presentation plays a key role in the communication of the features mapped and the ability to conduct analysis. The use of symbology and colours can help the readability of the map

(Gustavsson, et al., 2006) and help show the direction of ice advance/retreat (Clark et al., 2017). In this study the angle of the hatching for the scoured bedrock is used to indicate the general ice retreat direction, identified through analysis of old satellite imagery and striations in the field.

### 3.2- Schmidt Hammer

Various types of the Schmidt-hammer exist, but in this study an N-type Schmidt-hammer was used, specifically, the digital ‘Rockschmidt’, manufactured by ‘Proceq’ (Figure 3.2). The Schmidt hammer is seen as a non-destructive method (Matthews and Winkler, 2022) which meant access was granted to use it within the national park.



*Figure 3. 2: Image showing the digital N-type Schmidt hammer used in this study, specifically, the ‘Rockschmidt’ manufactured by Proceq in Switzerland. Source: Author.*

Most studies use it to apply relative dating to landforms, also known as, Schmidt-hammer Exposure Dating (SHED) (Winkler, 2005; Rode and Kellerer-Pirklbauer, 2011; Tomkins et al., 2016). However, in this study, it was possible to undertake absolute dating due to the available historical photos/aerial imagery. The historical imagery used was from the 1920-30s (Österreichische Nationalbibliothek, 2025), however some photos did not have dates, making it more challenging to date them accurately. Orthophotos and satellite imagery dating back to 1953 from the state of Tirol through their open access data portal (Tyrolean State Government - Geoinformation Department, 2025) were also used, providing detail with images every decade to identify the sites and their exposure dates.

Various factors had to be considered to obtain accurate r-values at each site. Sampling surfaces of the same lithology was important as varying lithologies can have significant effects on results (Shakesby et al., 2006; Rode and Kellerer-Pirklbauer, 2011) due to different weathering rates (Matthews and Winkler, 2022). Other important factors were, surface micro-topography (Goudie, 2006), lichen, joints, cracks, edges and surface moisture (Winkler, 2005; Rode and Kellerer-Pirklbauer, 2011). The angle at which the Schmidt-hammer is applied to the surface affects the readings (Aydin and Basu, 2005; Winkler, 2005), therefore it was hit at a perpendicular angle to the surface (Figure 3.3).



*Figure 3. 3: Image showing the author applying the Schmidt hammer to a section of bedrock at a perpendicular angle. Source: Author.*

The location of the transects were determined during a desktop study of the site by looking at old orthophotos and satellite images of the study area and identifying the direction of retreat of the Schlatenkees. Locations for the sites were placed along the transect, where it was thought the bedrock would be smooth and accessible. Some sites closer to the glacier were placed on known margins taken from the Austrian GI's (Fischer et al., 2015b; Buckel and Otto 2018) to allow for comparisons between sites on different glacier margins.

A handheld GPS system had the site coordinates loaded before visiting the area which was used to reach each site. Before sampling had taken place, notes were taken about the site's characteristics (Figure 3.4) and five of the smoothest sections of bedrock were

identified. Ten r-values were taken at each of the five bedrock sections. During sampling a field assistant wrote down each r-value in a notebook. The ability of the digital Schmidt hammer to instantly calculate the r-value (Figure 3.5) allowed anomalies between the sites to be identified within the field. The r-value was written down and photographed to provide multiple backups of the data. Photos of each section of sampled bedrock were taken along with any other site characteristics such as vegetation or striations.

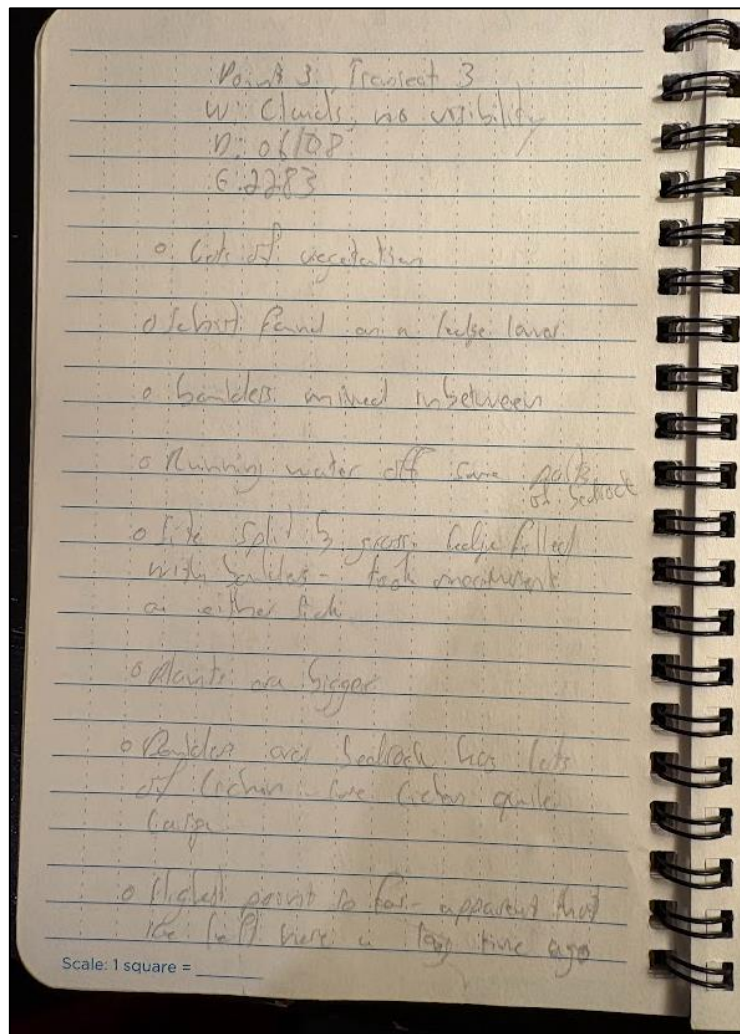


Figure 3. 4: Example of notes taken for site 3 on transect 3. Source: Author

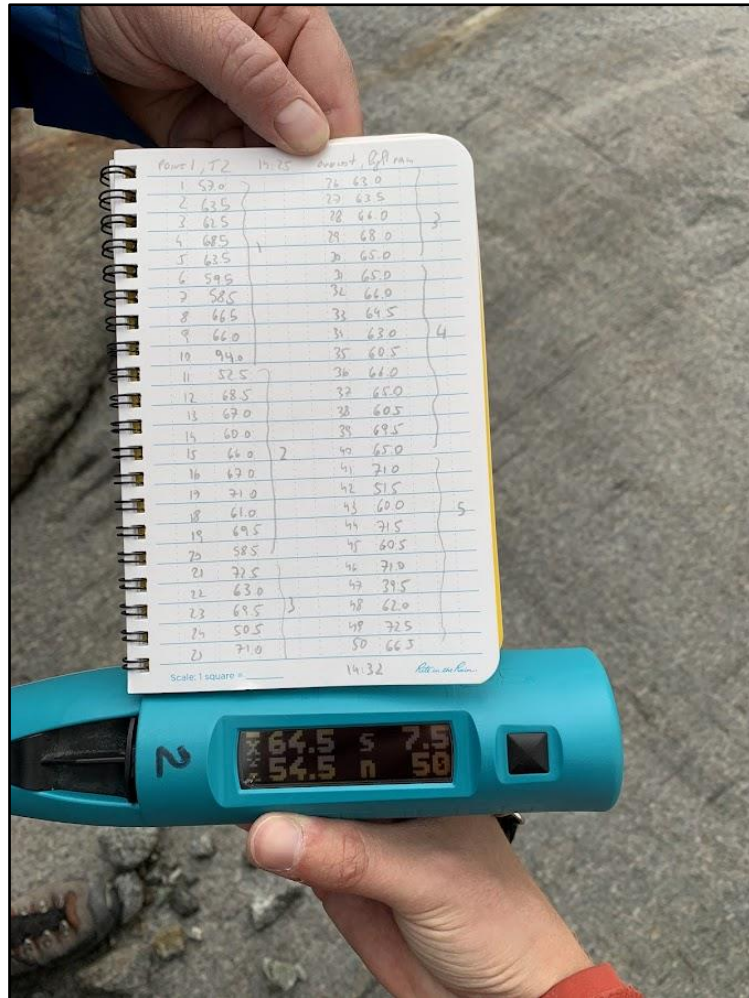


Figure 3. 5: Image showing the average r-value calculated in the field after data collection at the site was complete. Average r-value is displayed in the top left of the screen of the Schmidt hammer. Source: Author.

Three transects with 5 sites and one transect with 3 sites were sampled at the Schlattenkees, including eight additional sites (Figure 3.6) during the fieldtrip in September 2024. Transect 1 (with 3 sites) was added in the field along with numerous additional sites to fill in gaps where it was thought more data was needed. In total 22 out of the 26 sites consisted of bedrock, and the other four consisted of clasts. The minimum sample size for gneiss when taking the mean r-value at a site is 38 (Niedzielski et al., 2009), and with numerous studies using 50 R-values as their sample size (Winkler, 2005; Shakesby et al., 2006; Stahl et al., 2013), it was deemed sufficient to take 50 r-values at

each site. At the bedrock sites, Schmidt-hammer impacts were spread across the five selected bedrock surfaces to help avoid any factors which could have affected R-values, a technique used by Matthews and Owen, (2010) and Matthews et al. (2024). Sites where clasts were present saw 50 individual clasts impacted once, a method used on Holocene moraines by Winkler (2005). Clasts which had most of their surface covered were avoided to reduce inaccuracies caused by the soil dampening the impact of the Schmidt hammer on the surface (Stahl et al., 2013).

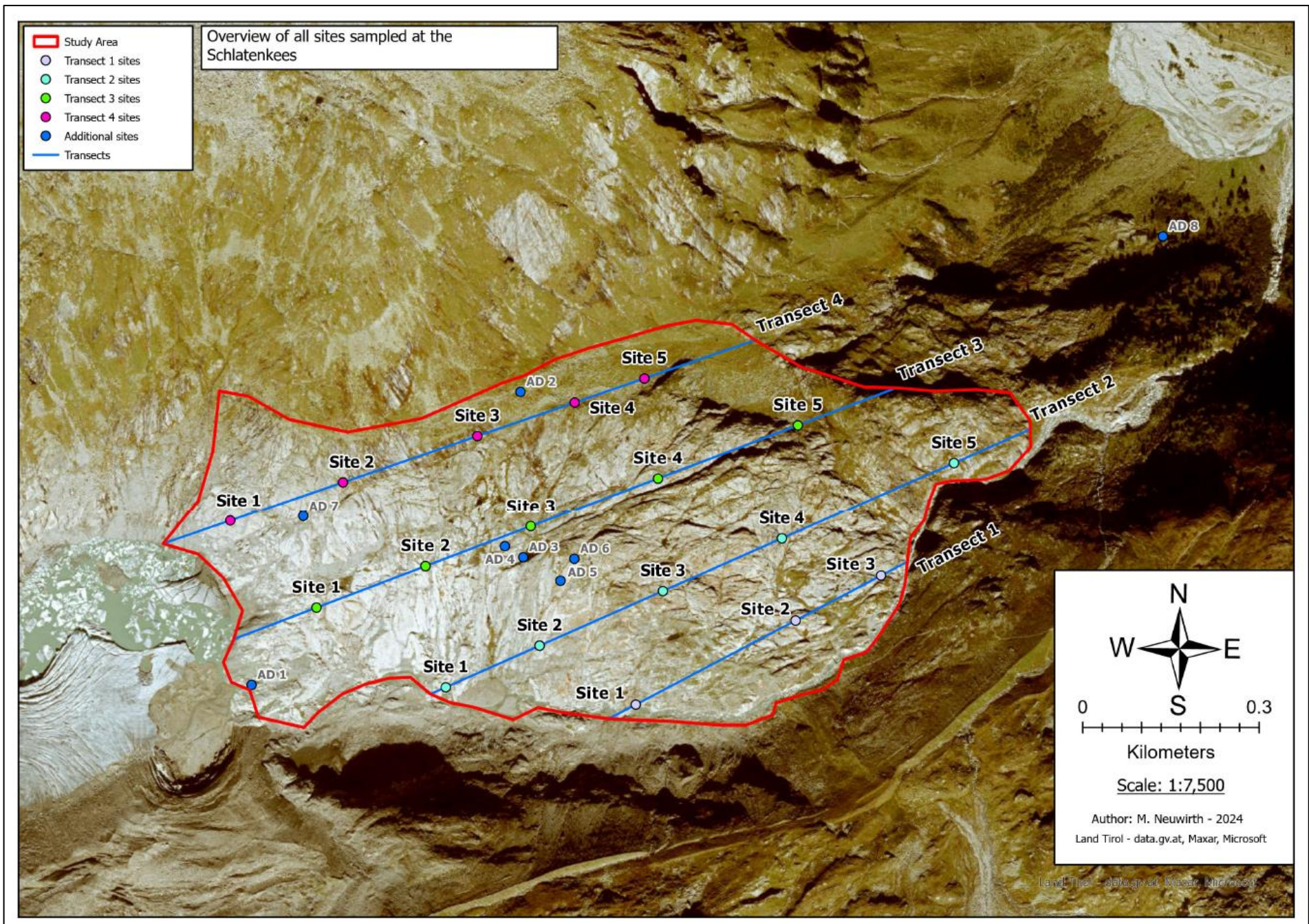


Figure 3. 6: Aerial image showing an overview of the sample sites on transects and the additional sites in the Schlattenkees foreland.

### 3.3- Data Analysis – Schmidt hammer

Data was transferred from the Schmidt hammer to the into the 'RockSchmidt' programme (Appendix A) and then exported as a text file into an Excel spread sheet, where the data was tidied up and the outliers were removed (Appendix B). These outliers were known to have been erroneous on behalf of the equipment operator, and far above or below the averages for the sites. The outliers on the boxplot diagrams are known to not be erroneous. The highest number of outliers removed from one site was 3, keeping within a 10% threshold, however, the removal of outliers did affect the r-value of some sites. The standard deviation (SD) for each site was also noted down as this was calculated by the Schmidt-hammer. Multiple CSV sheets were created to be imported into R-studio for further analysis.

Analysis in R-studio involved creating scatter graphs of each site and plotting the R-value against distance from the glacier and adding the SD to graphs as error bars (for code see Appendix C). For measuring the distance, all sites were measured to the same point of the proglacial lake on the GIS. A graph showing all four transects together was also created to help in comparing the transects between one another. Boxplot diagrams were created to analyse the spread of r-values for each site. Additionally, the average r-value on each transect was calculated and plotted against the average elevation of each transect. Correlation tests between the r-value and the distance from the ice were undertaken for each transect (for code see Appendix C), as well as a correlation test for the average transect r-value against the average transect elevation. A p-value threshold of  $<0.05$  was used to determine the significance of the correlation. Along with the graphs, the average r-values were added as labels to each site on the GIS and then the Austrian

GI's were overlaid to help analyse the difference between r-values on different glacial margins from the past.

## **Chapter 4.**

### **Results**

In this chapter, section 4.1 covers results from the geomorphological map (Figure 4.1) and section 4.2 presents the Schmidt hammers results. The geomorphological features are in separate sub-sections and the rest of the features are under their own subsections based on feature type. The individual transects for the Schmidt hammer are presented together, with other sections covering the additional sites and the average transect r-value against the average transect elevation.

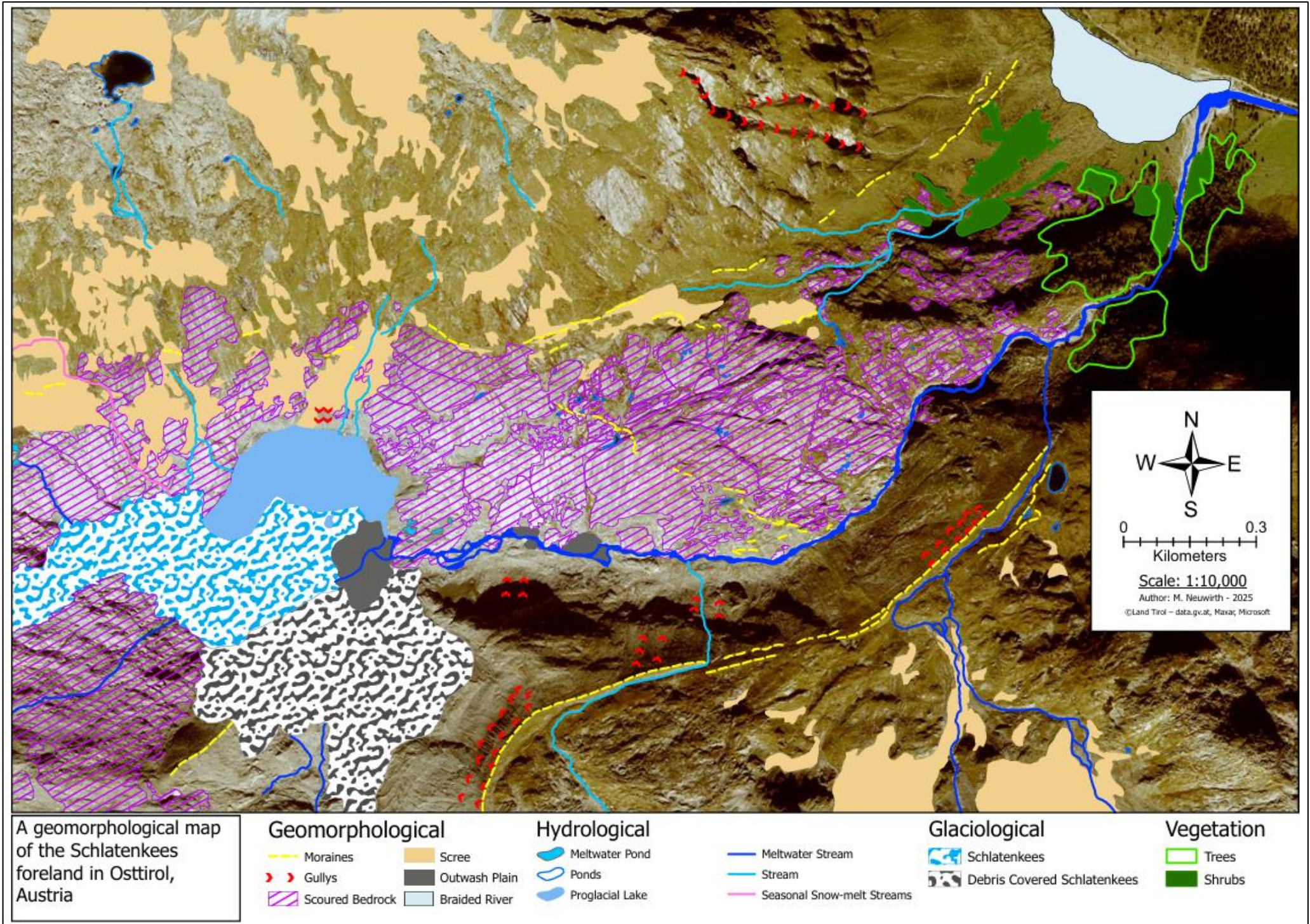


Figure 4. 1: Geomorphological map of the Schlatenkees foreland.

#### 4.1 - Geomorphological Map

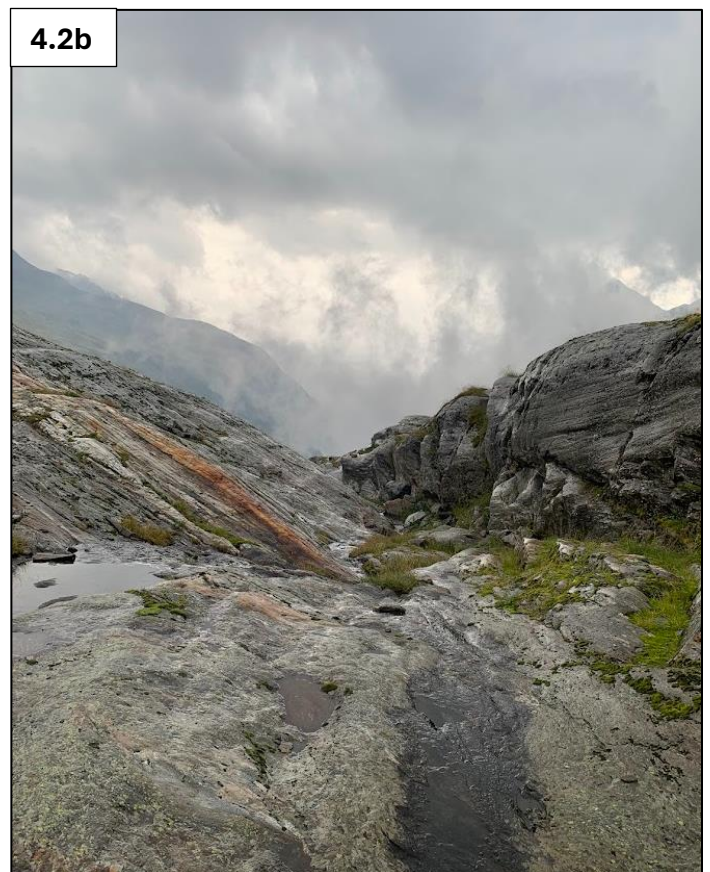
In total 16 features were mapped across and surrounding the foreland of the Schlatenkees (Figure 4.1; Table 4.1). Particular attention was given to the geomorphological features, especially the bedrock and the moraines as they can help indicate past extents of the ice and the direction of retreat (Roman, 2019).

*Table 4. 1: Table showing the total area (or highest length of a linear feature) of the mapped features across the Schlatenkees foreland. The feature type on the map and the occurrence of each feature is also acknowledged. Table based off (Kjær et al., 2008). <sup>1</sup>Gullies drawn only signify that gullies are present on that section of hillside. Does not signify quantity of gullies*

<b>Mapped feature</b>	<b>Total area (km<sup>2</sup>)</b>	<b>Greatest length (m)</b>	<b>Occurrence</b>
<i>Scoured Bedrock</i>	0.85 km <sup>2</sup>	-	205
<i>Scree</i>	0.61km <sup>2</sup>	-	76
<i>Moraines</i>	-	986m	58
<i>Gullies<sup>1</sup></i>	-	461m	29
<i>Braided River</i>	0.06km <sup>2</sup>	-	1
<i>Ponds</i>	0.01km <sup>2</sup>	-	40
<i>Fluvial Outwash Plain</i>	>0.01km <sup>2</sup>	-	5
<i>Seasonal Snowmelt Stream</i>	-	753m	1
<i>Streams</i>	-	896m	16
<i>Meltwater Streams</i>	-	2850m	9
<i>Meltwater Pond</i>	>0.01km <sup>2</sup>	-	6
<i>Proglacial Lake</i>	0.07km <sup>2</sup>	-	1
<i>Schlatenkees</i>	0.26km <sup>2</sup>	-	1
<i>Debris Covered Schlatenkees</i>	0.26km <sup>2</sup>	-	1
<i>Trees</i>	0.09km <sup>2</sup>	-	3
<i>Shrubs</i>	0.04km <sup>2</sup>	-	8

#### 4.1.1 - Geomorphological Features – Scoured Bedrock

Scoured bedrock covered the highest area at 0.85km<sup>2</sup> (Table 4.1) with most of the valley floor up to 1250m away from the glacier being scoured bedrock with only a few sections higher up on the northern slopes. Scree covered vast areas of the upper northern slopes above the bedrock. Through observations made in ground truthing, striations were identified on the bedrock surface (Figure 4.2a) in some areas. Channels incised into the bedrock (Figure 4.2b) and streamlined bedrock features, such as Roche moutonnées (Figure 4.2c) were also identified. Large areas of exposed bedrock can be seen either side of the narrowing tongue of the glacier (Figure 4.3).



4.2c



*Figure 4. 2a: Photo of striations in the bedrock at additional site 3; Figure 4. 2b: Channel incised into the bedrock below site 4 on transect 3; Figure 4. 2c: Streamlined features at additional site three. The feature under the furthest right red arrow is a small roche moutonnée. Red arrows indicate streamline features, green arrows show ice flow direction. Source: All photos – Author.*

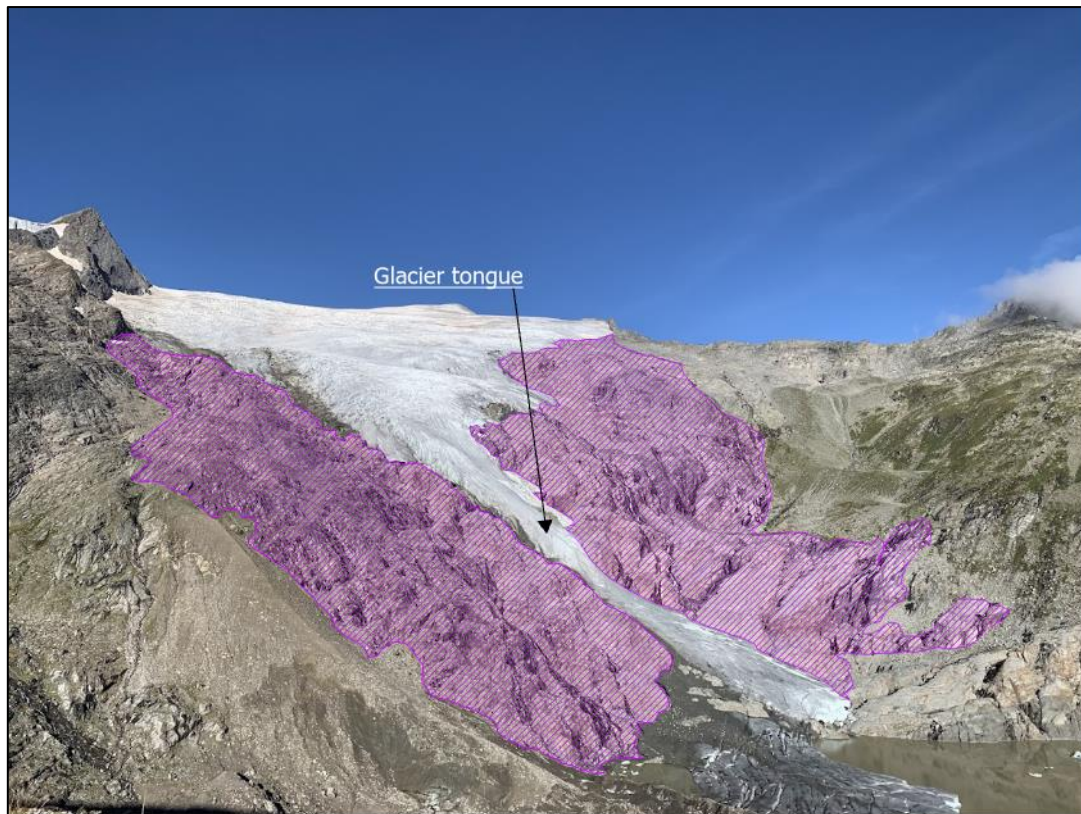


*Figure 4. 3: Image showing large sections of exposed bedrock either side of the narrow tongue of the Schlatenkees. Purple hatchings highlight bedrock either side of the tongue. Source: Author*

#### 4.1.2 - Geomorphological Features – Moraines

The moraines show a clear indication of the full glacier extent during the LIA (Fischer et al., 2015a) (Figure 4.4) with moraine ridges being observed on the valley floor in the north of the site. In total 58 moraines were identified, making it the 3<sup>rd</sup> most identified feature within the GIS database (Table 4.1). The two longest moraines are on the southern side (Figure 4.5a) of the site and sit approximately 100m above the scoured bedrock and have numerous gullies. The moraines to the north (Figure 4.5b) mostly consisted of larger boulders (observed during ground truthing), and the high and very distinct moraines in the south, consisted of smaller sediments. Within the study site, a set of moraines were identified that cut across the site from northwest to southeast (Figure 4.6a, 4.6b, 4.6c),

with the length of this moraine being walked during ground truthing as it follows the past glacier margins from GI's 1 and 2 (Figure 4.4) (Fischer et al., 2015b). Two more small groups of moraines can be observed on the northwestern edge of the bedrock.

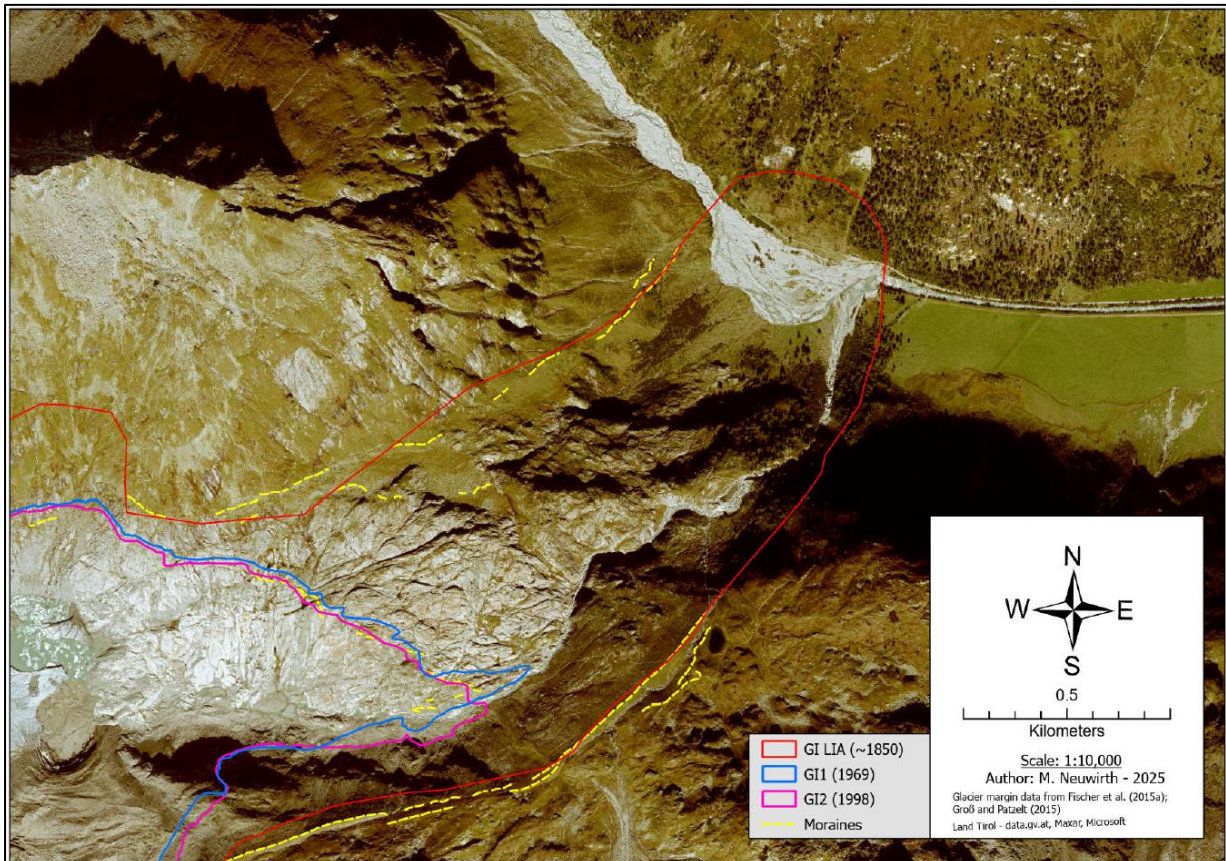


*Figure 4. 4: Map showing the LIA, 1969 and 1998 glacier margins for the Schlattenkees in comparison to the moraines. The LIA margin follows the lateral moraines whilst the 1969 and 1998 margins follow the moraine cutting across the site from north-west to south-east.*

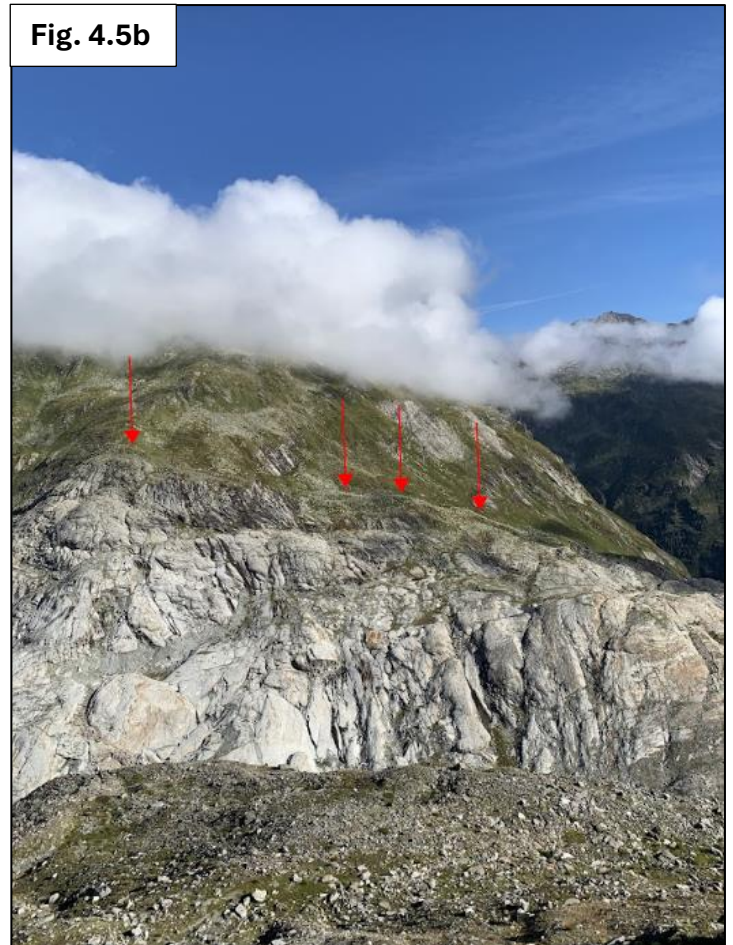


*Figure 4. 5a: Image showing the southern moraine which sits above the foreland of the Schlatenkees. Red lines highlight the ridges of the moraines; Figure 4. 5b: Image showing the moraines on the northern slope above the foreland of the Schlatenkees. Highlighted with red arrows. Source: Author.*

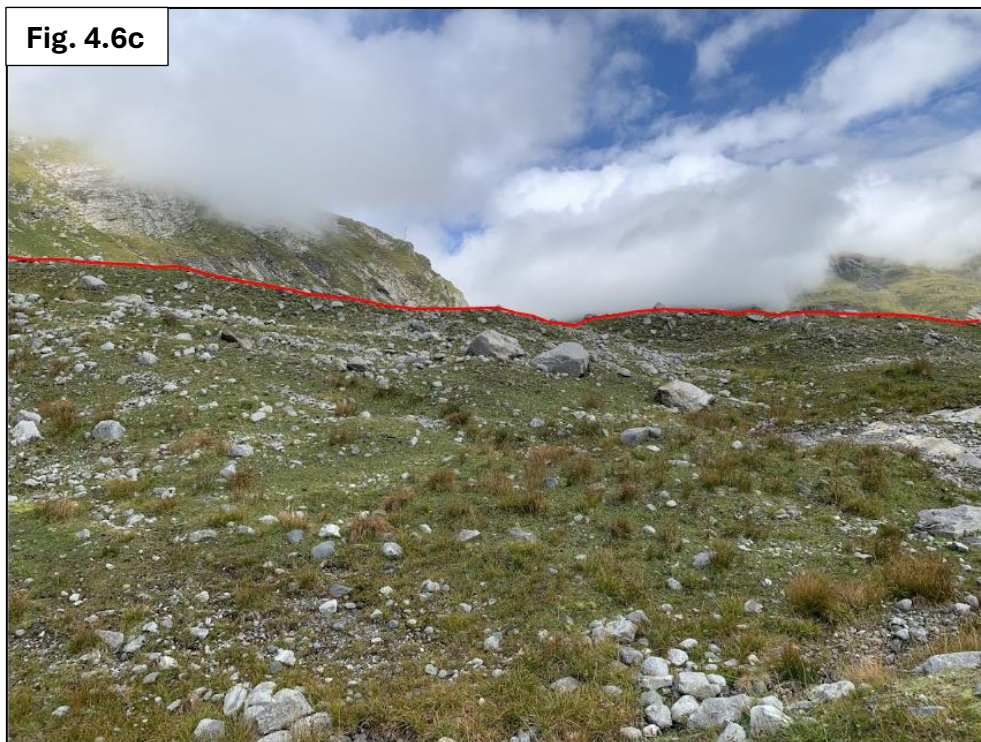


*Figure 4. 6 a: 3 Image looking downhill as the moraine cuts across the landscape; 4. 6b: Image showing the moraine where it was deposited on a section of bedrock at site 3, transect; 4. 6c: Side view of a section of the moraine further down from figures 4. 6a and 4. 6b. The red line shows the ridge of the moraines. Source: Author.*

### 4.1.3 - Geomorphological Features – Gullies

Gullies were predominantly found along the southern slope above the foreland. Extensive gullying can be observed in the finer sediments within the large moraine above the southern side of the site (Figure 4.7). There is continued gullying further east along the southern moraine. The longest gully was situated in the northwest and measured 461m (Table 4.1).



*Figure 4. 7: Photo showing gullying on the large moraine on the south side of the site. Source: Author.*

### 4.1.4 - Hydrological Features

There were 6 hydrological features identified within the mapping area, with the ponds being the most identified at 40, although they covered an area of <math><0.01\text{km}^2</math> (Table 4.1). The largest meltwater stream was 2850m in length (Table 4.1), which discharges water from the proglacial lake (Figure 4.8). In the southwest of the site the smaller meltwater streams are from the Karlskees (Figure 1.3). The meltwater streams from the

Schlatenkees and the Karleskees merge and flow further downstream to join the braided river. The largest body of water in the site was the pro-glacial lake at 0.07km<sup>2</sup> (Figure 4.9; Table 4.1), fed by both sections of the Schlatenkees and had various icebergs floating within it.



*Figure 4. 8: Image showing the meltwater stream which drains the proglacial lake at the Schlatenkees. Source: Author.*



*Figure 4. 9: Image showing the proglacial lake where the Schlatenkees terminates as seen from site 1 on transect 4. Various icebergs which have calved from the snout can be seen floating in the lake. Source: Author.*

#### 4.1.5 - Glaciological Features

The two glaciological features that were identified were the Schlatenkees and the debris covered section from the south (Figure 4.10a, 10b) which cover a combined area of 0.52km<sup>2</sup> (Table 4.1) and terminate in the proglacial lake. The Schlatenkees had a very narrow tongue, which was only 115m wide when measured on satellite imagery.



*Figure 4. 10 a: The Schlatenkees as seen from the proglacial lake where it terminates; Figure 4. 10b: The terminus of the debris covered section of the Schlatenkees. Source: Both photos - Author*

#### 4.1.6 – Vegetation

Only the larger types of vegetation were mapped, these being shrubs and trees. These were contained to lower elevations in the north/north-east of the site where the foreland drops down into the valley below (Figure 4.11), with the trees covering the most area at 0.09km<sup>2</sup> (Table 4.1).

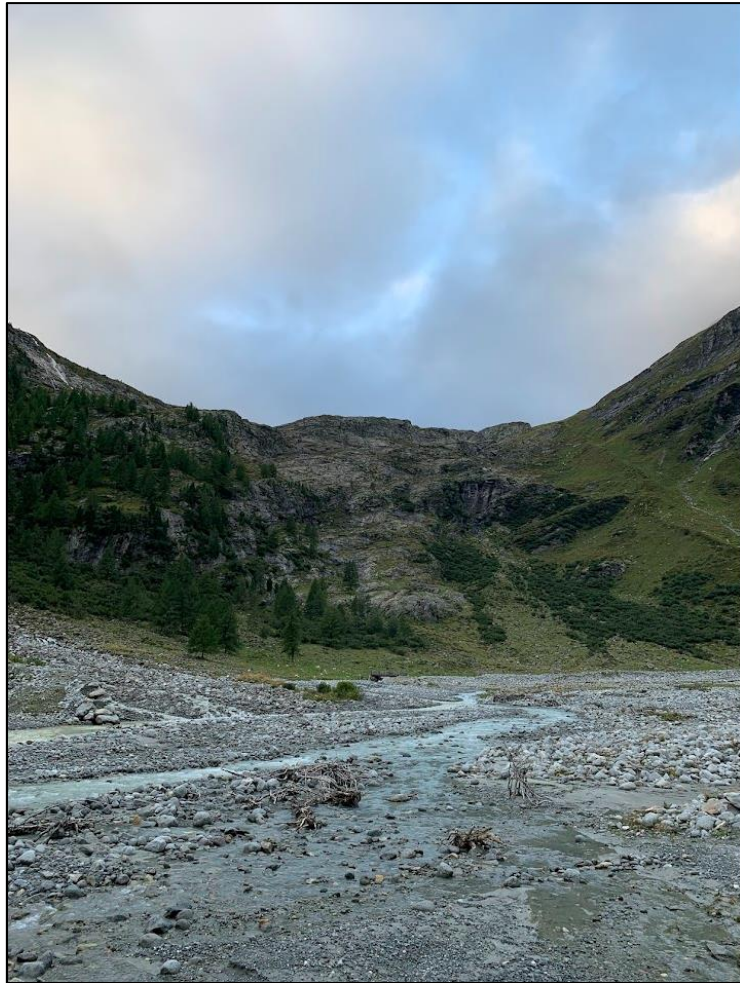


*Figure 4. 11: Photo from valley bottom showing trees and shrubs on the lower part of the Schlattenkees foreland which drops down into the valley floor. Source: Author.*

## 4.2 – Schmidt Hammer

Overall, including additional sites, there were 26 sites sampled at the Schlatenkees, with 18 on transects (Figure 4.12). A statistically significant relationship was found between the average transect r-value and the average transect elevation. There was a trend observed between all transects as the site closest to the glacier was higher than the site furthest away (Figure 4.12). A high SD was identified across the study area amongst the sites along the transects with an average SD of 9.1. The average mean r-value for all sites along the 4 different transects was 61. A range of 20 was identified between the highest and lowest recorded sites.

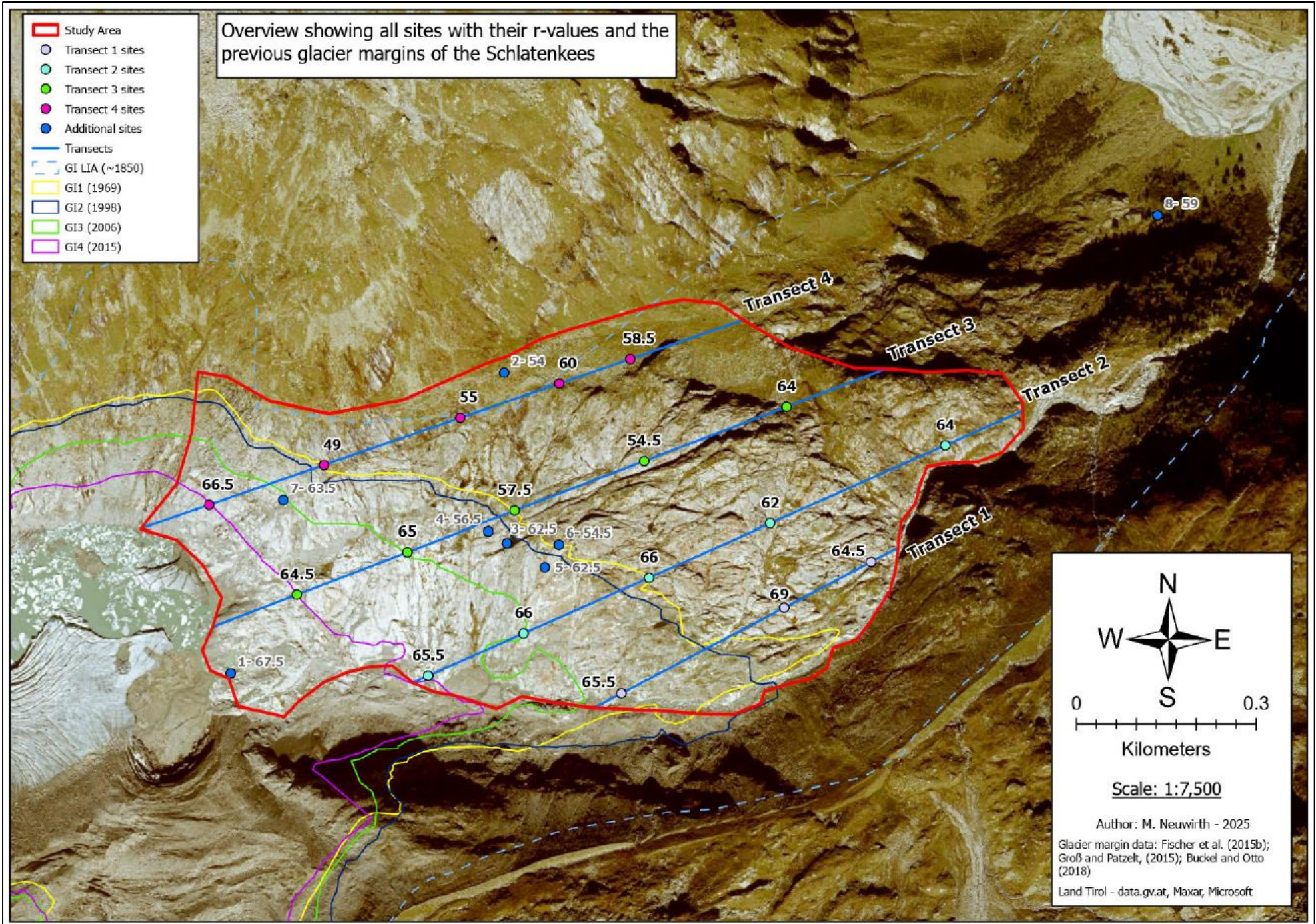


Figure 4. 12: Overview showing all sites with their r-values and the glacial margins from the glacial inventories.

### 4.2.1 – Transects

Transect 1 had the least number of sites at 3 (all bedrock) due to it being the shortest at 573m (Figure 4.12) This transect was at the lowest elevation with an average elevation of 2121m and very smooth bedrock (Figure 4.13). Transect 1 boasted the site with the highest overall r-value with site 2 recording an r-value out of 69 with a standard deviation (SD) of 5.7 (Figure 4.14). This transect recorded a p-value of 0.96 ( $>0.05$ ), showing a statistically insignificant relationship between r-value and distance from the glacier, whilst having site one higher than site five. The error bars showed a considerable variance within all three sites as they all had SDs above 5.7 (Figure 4.13) and the boxplot diagrams help highlight the variance in sites 1 and 3 (Figure 4.15).



*Figure 4. 13: A very smooth area of bedrock at site 2 on transect 1. Source: Author*

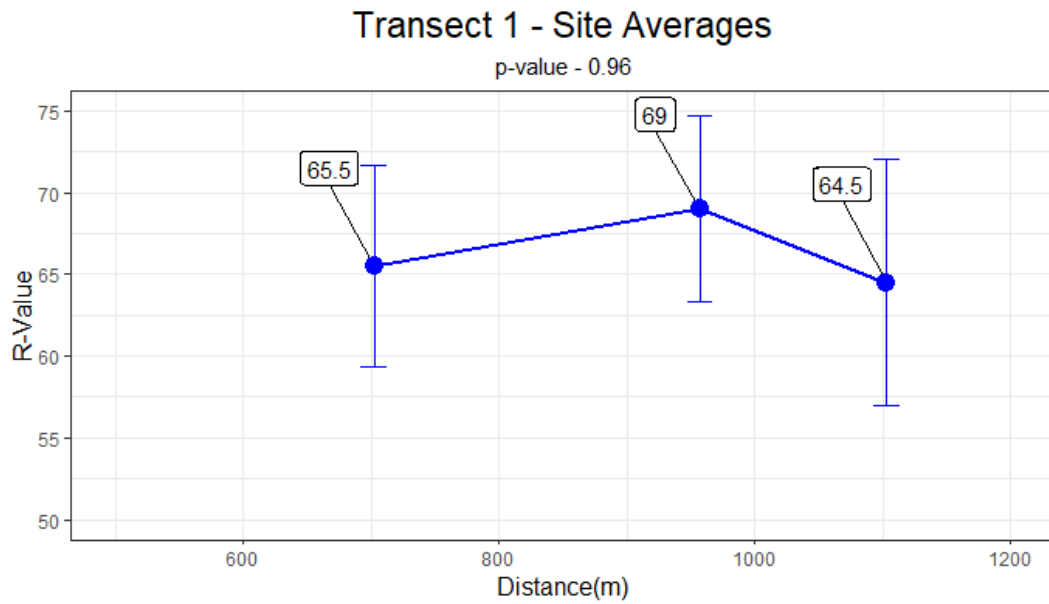


Figure 4. 14: Graph showing the average site r-value against the distance from the glacier for transect 1. With the standard deviations shown in the error bars. Source: Author.

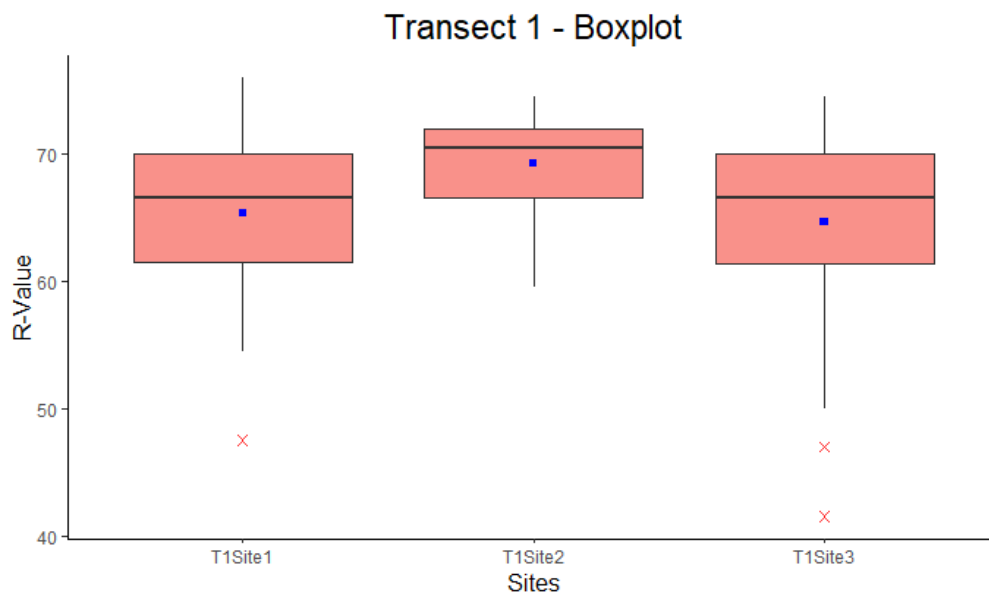


Figure 4. 15: Boxplot showing the differences between the sites on transect 1. Blue square represents the mean and red crosses represent outliers. Source: Author.

Transect 2 measured 1115m in length and included five sites, all of which were bedrock (Figure 4.12) and had an average elevation of 2143m. The statistically insignificant p-value of 0.26 ( $>0.05$ ) it is the lowest out of all transects, however, site 1 was still higher

than site 5. Sites 2 and 3 had the same average R-value of 66, the highest for this transect (Figure 4.16). There was little variation in values across the transect, with a range of 4 (Figure 4.16). The lowest SD was from site 2 at 4.3, which was the lowest overall. Both sites 3 and 4 had two outliers, while sites 3 and 5 have the highest interquartile range (Figure 4.17).

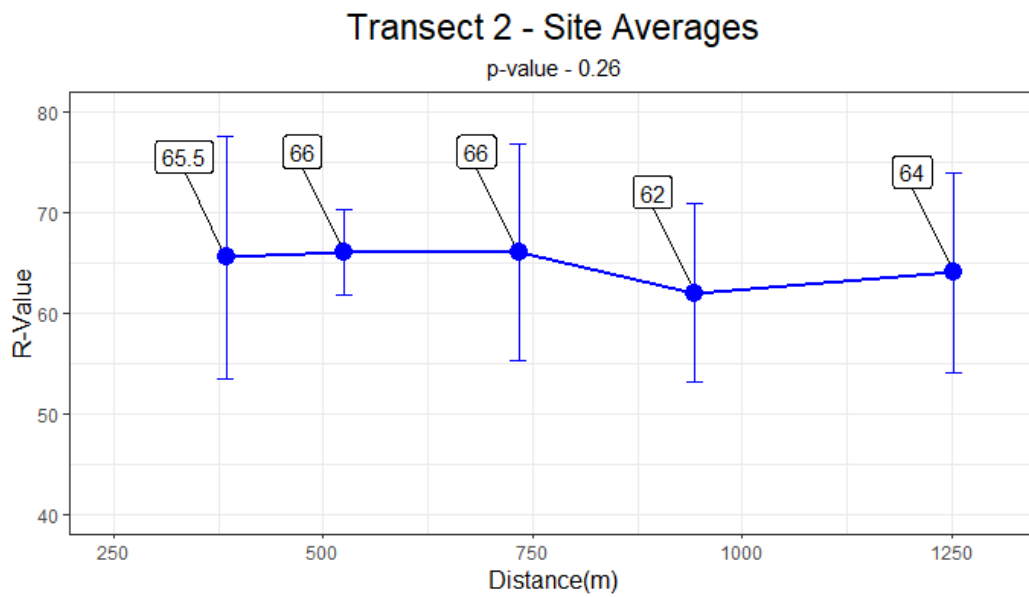


Figure 4. 16: Graph showing the average site r-value against the distance from the glacier for transect 2. With the standard deviations shown in the error bars. Source: Author.

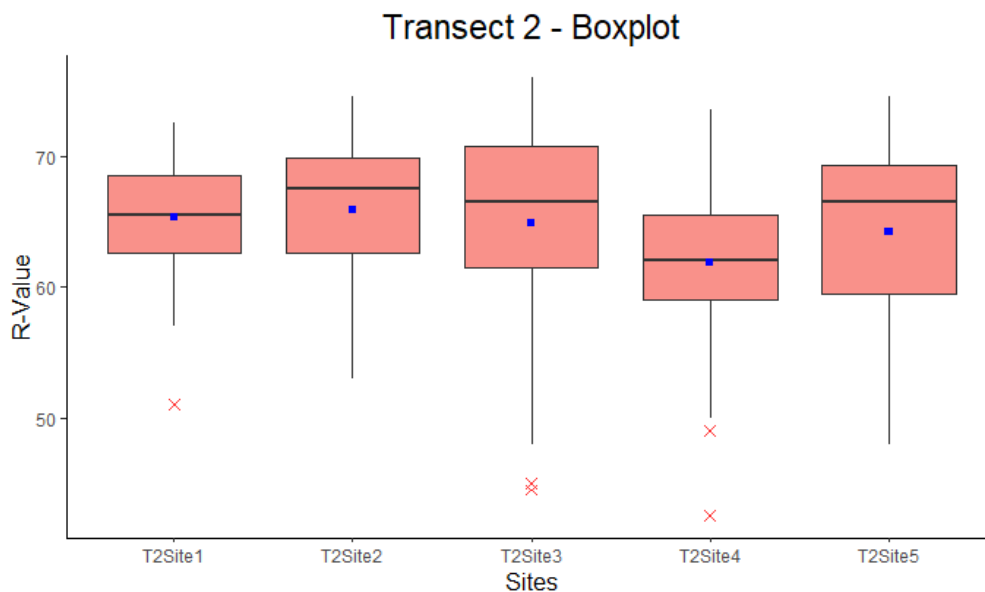


Figure 4. 17: Boxplot showing the differences between the sites on transect 2. Blue square represents the mean and red crosses represent outliers. Source: Author.

Transect 3 was the longest at 1205m (Figure 4.12). It had 5 sites, four of which were bedrock and one of which was clasts and was the second highest with an average elevation of 2201m. The p-value of 0.59 ( $>0.05$ ) made it the second lowest out the 4 transects. Site 2 had the highest R-value at 65 with an SD of 7.1, the lowest overall along the transect (Figure 4.18). A clear downward trend in average R-values is observed from sites 2 to 4. However, a sharp increase is observed at site 5 which had the highest value out of the 3 clast sites. The boxplot diagram (Figure 4.19) highlights a significant variance in site 4, which also had the highest SD of 12.1.

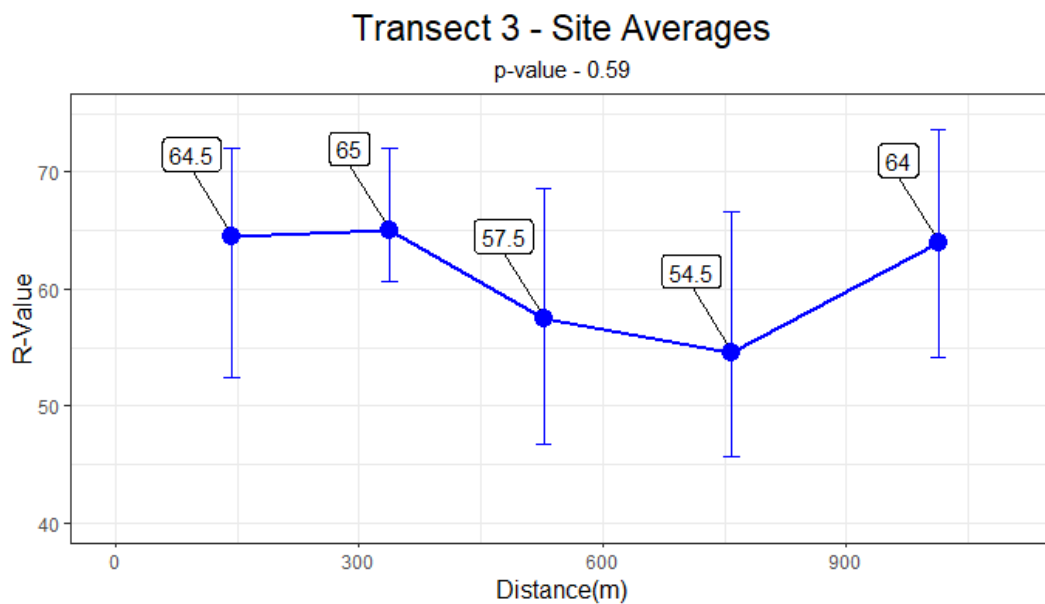


Figure 4. 18: Graph showing the average site r-value against the distance from the glacier for transect 3. With the standard deviations shown in the error bars. Source: Author.

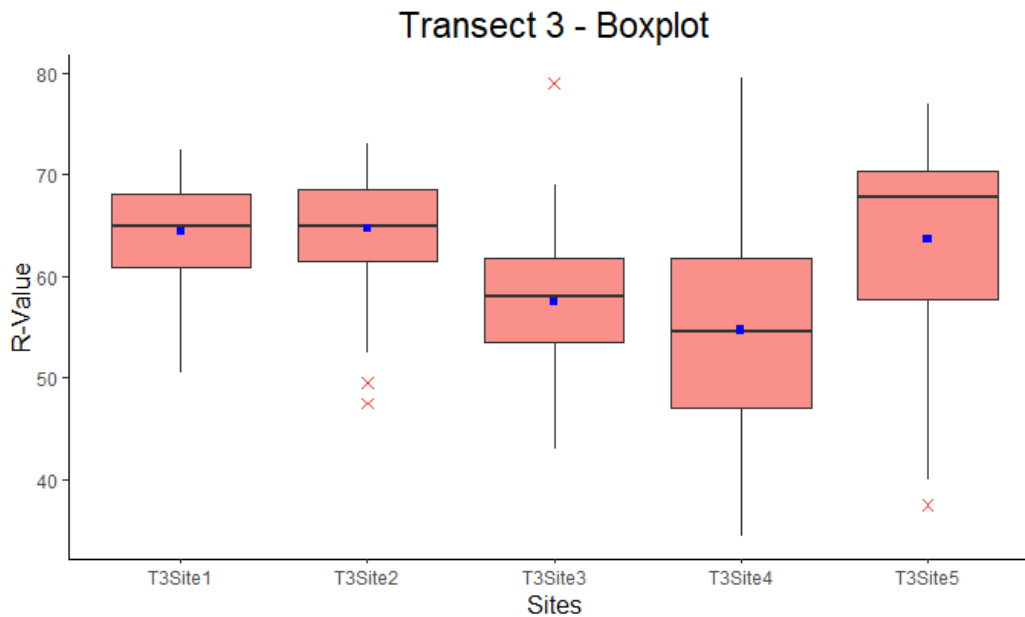


Figure 4. 19: Boxplot showing the differences between the sites on transect 3. Blue square represents the mean and red crosses represent outliers. Source: Author.

Transect 4 measured at 1065m (Figure 4.12) and had the highest average elevation out of all four transects at 2267 meters. It had 5 sites, 3 being bedrock and 2 being clasts. Although being statistically insignificant with a p-value of 0.89 ( $>0.05$ ), it recorded the highest difference between site 1 and 5, at eight, following the trend observed along the other transects (Figure 4.20). A sharp decline from site 1 to site 2 highlighted site 2 as a significant outlier with it having the lowest overall r-value at 49 and SD at 13.6 (Figure 4.20). It also had the greatest interquartile range overall as observed in Figure 4.21 and was the highest site overall at 2309 meters. This site had lots of vegetation present, with weathered bedrock surfaces across the site (Figure 4.22).

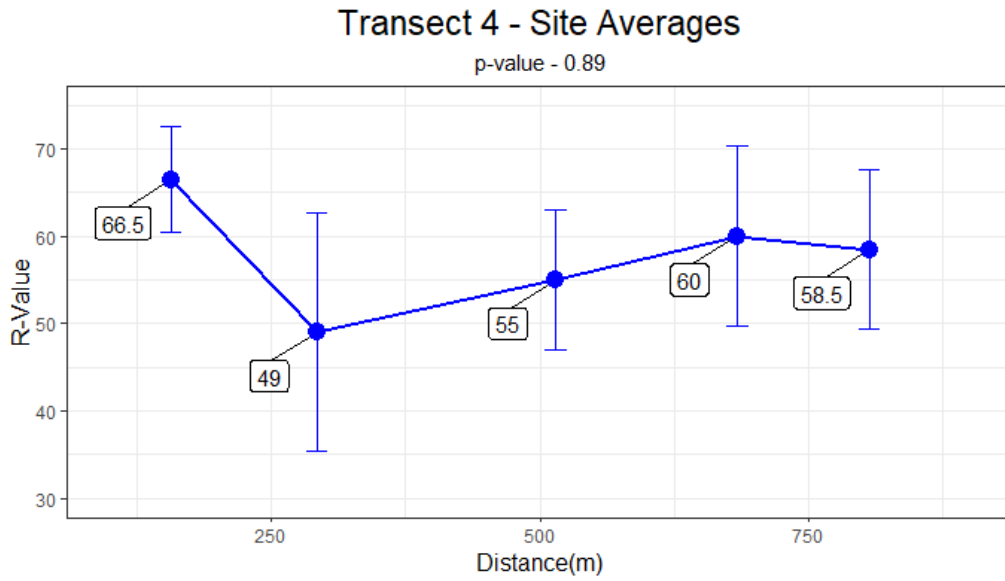


Figure 4. 20: Graph showing the average site r-value against the distance from the glacier for transect 4. With the standard deviations shown in the error bars. Source: Author.

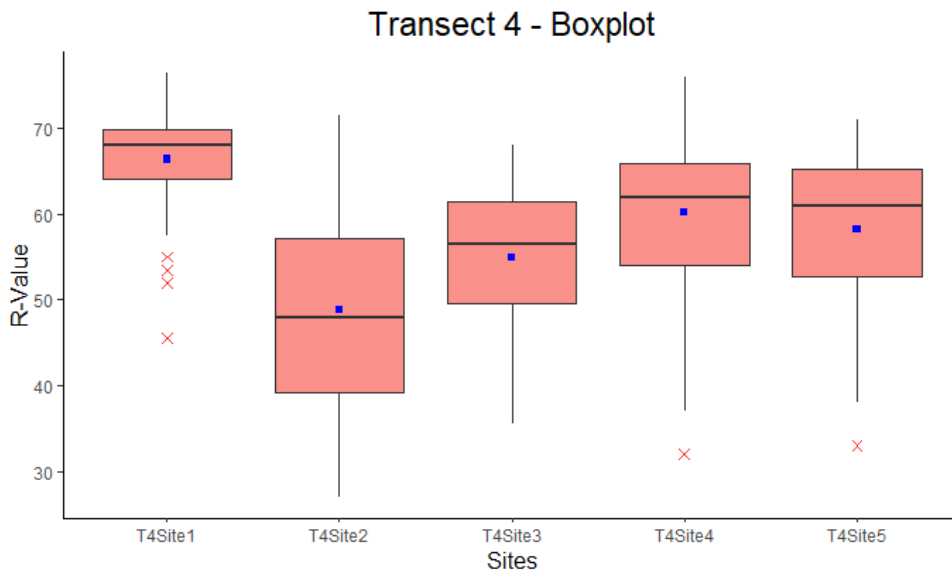


Figure 4. 21: Boxplot showing the differences between the sites on transect 4. Blue square represents the mean and red crosses represent outliers. Source: Author.



*Figure 4. 22: An area of bedrock sampled at site 2 on transect four. Vegetation and a rougher rock surface can be observed. Source: Author.*

#### 4.2.2 - Individual Transects Compared

The common theme across all transects is that sites closest to the glaciers were higher than the sites furthest away from the glacier. The outliers identified on the individual graphs were furthermore highlighted (Figure 4.23). Site 2 on transect 4 stuck out as the lowest value overall and the stark difference of 20 between the lowest and highest  $r$ -values was highlighted (Figure 4.23). Although transect 2 site 5 was the furthest away from the glacier, it was higher still than 39% of sites which are closer to the glacier. In total, eight sample points were on known glacial margins from the glacial inventories (Figure 4.12) and along G11 there was a range of 17 between all values.

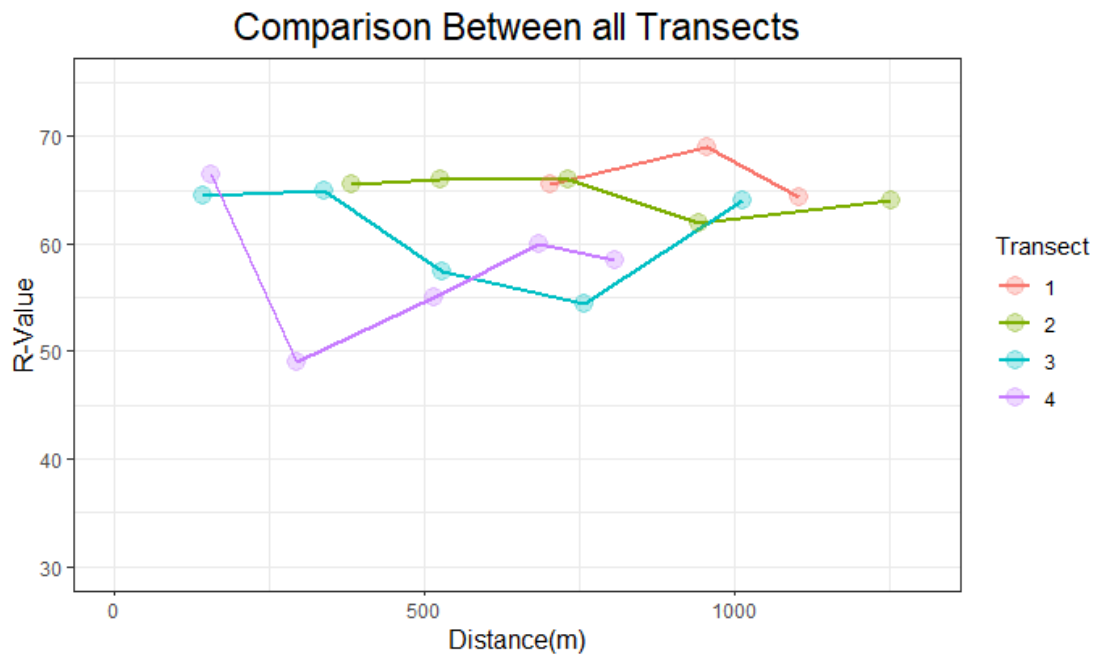


Figure 4. 23: Graph showing a comparison between all 4 transects plotted against the distance from the glacier. Source: Author.

#### 4.2.3 - Additional sites

The additional sites sampled at the Schlatenkees were chosen to be in specific locations that were thought to be important when determining the reliability of the Schmidt hammer; such as additional sites 5 and 6 being inside and outside a moraine or additional site 7 being located between sites 1 and 2 on transect 4 where there was a significant difference in r-values observed.

Additional site 1 (closest to the ice) (Figure 4.24) recorded an r-value of 67.5 which was higher than additional site 8 (furthest from the ice) at 59 (Table 4.2). For additional sites 5 and 6 which were either side of a moraine they recorded r-values which would be expected as site 6 recorded a lower value (Figure 4.24; Table 4.2). The site with the highest SD was additional site 2 at 11.0, however this was the only clast site, all other seven were

on bedrock. Additional site 7 recorded an r-value of 63.5 (SD. 6.9) and further highlighted the significance of site 2 transect 4 as an outlier.

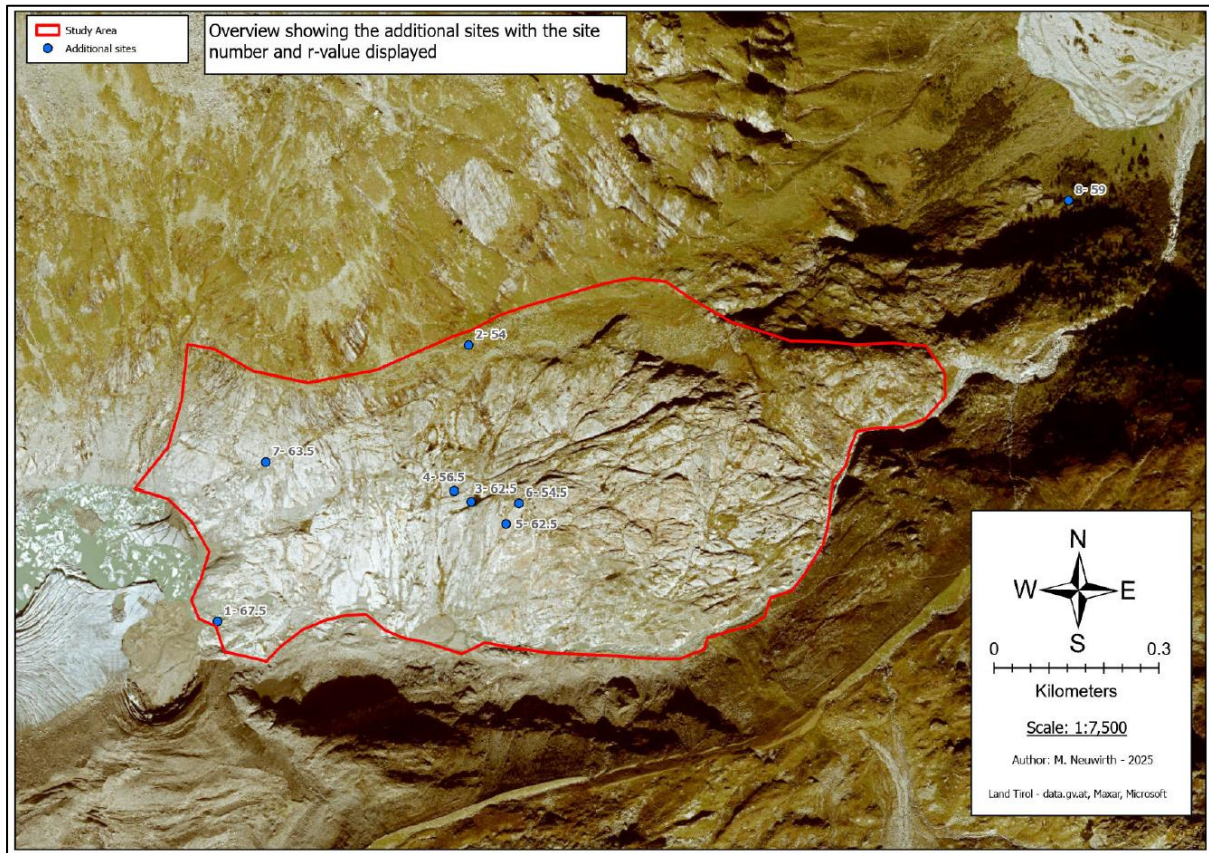


Figure 4. 24: Overview of the eight additional sites sampled at the Schlattenkees. See Table 4.2 for the distance from the ice and SD.

Table 4. 2: Table showing the data for the additional sites sampled at the Schlattenkees.

<b>Site</b>	<b>No. of Rebounds</b>	<b>Distance from Ice (m)</b>	<b>Standard Deviation</b>	<b>R-value</b>
<i>Additional site 1</i>	50	20 meters	4.6	67.5
<i>Additional site 2</i>	48	620 meters	11.0	54
<i>Additional site 3</i>	50	520 meters	4.7	62.5
<i>Additional site 4</i>	48	470 meters	5.5	56
<i>Additional site 5</i>	50	568 meters	6.6	62.5
<i>Additional site 6</i>	47	600 meters	9.6	56
<i>Additional site 7</i>	50	215 meters	6.9	63.5
<i>Additional site 8</i>	48	1728 meters	7.7	59

#### 4.2.4 – Transect Average Vs. Elevation

When comparing the average r-value of each transect (the average of all sites on a transect) against the average elevation of all sites on the transect, a linear relationship between the two variables was observed (Figure 4.25). The r-value decreased as the elevation increased showing a statically significant relationship with a p-value of 0.005 (<0.05).

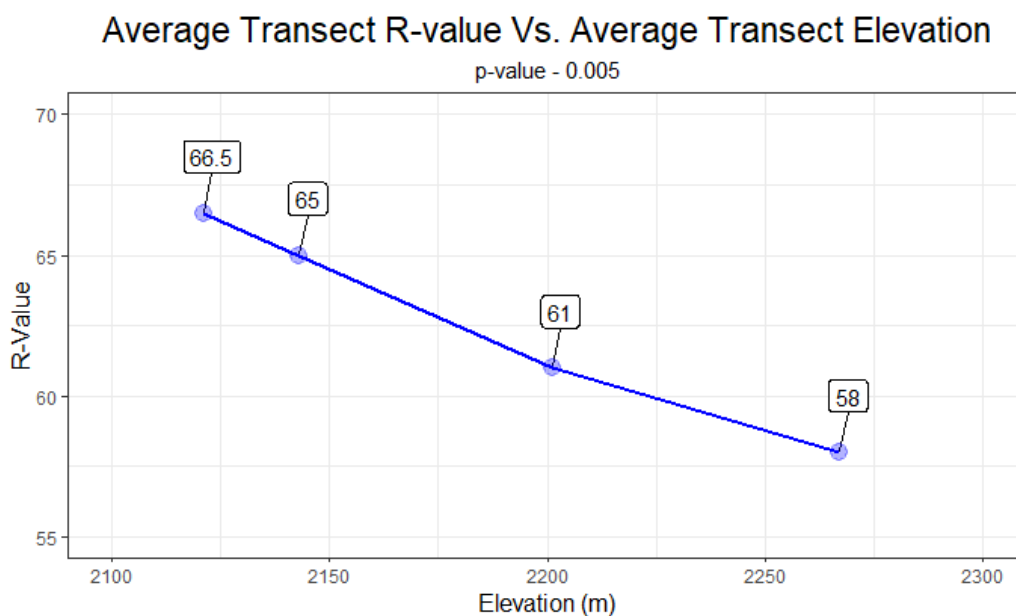


Figure 4. 25: Graph showing the average r-value of each transect plotted against the average elevation of each transect. Source: Author.

#### 4.2.5 – Exposure Dates of the Sites

Using historical photos which date to the 1920/30s from the Österreichische Nationalbibliothek, (2025) and aerial imagery going back to 1953 it was possible to get exposure dates for all sites (Table 4.3). The year exposed is the year it can be seen on satellite imagery; therefore, some sites may have been exposed before the next available aerial image.

Table 4. 3: Table showing the exposure date of the sites along the transects and for the additional sites.

<b>Transect</b>	<b>Site</b>	<b>Last Known Year Under Ice</b>	<b>Year exposed</b>	<b>Elevation (m)</b>	<b>R- value</b>
<b>1</b>	1	2004	2006	2131	65.5
<b>1</b>	2	1953	1969	2127	69
<b>1</b>	3	1928	1953	2106	64.5
<b>2</b>	1	2009	2015	2166	65.6
<b>2</b>	2	2004	2006	2181	66
<b>2</b>	3	1953	1969	2186	66
<b>2</b>	4	1928	1953	2136	62
<b>2</b>	5	1928	1953	2048	63
<b>3</b>	1	2009	2015	2219	64.5
<b>3</b>	2	2006	2009	2230	65
<b>3</b>	3	1953	1969	2233	57.5
<b>3</b>	4	1928	1953	2210	54.5
<b>3</b>	5	1928	1953	2113	64
<b>4</b>	1	2004	2006	2296	66.5
<b>4</b>	2	LIA	1928	2309	49
<b>4</b>	3	LIA	1953	2283	55
<b>4</b>	4	LIA	1928	2243	60
<b>4</b>	5	LIA	1928	2213	58.5
<b>Additional Sites</b>	<b>Site</b>	<b>Last Known Year Under Ice</b>	<b>Year exposed</b>	<b>Elevation (m)</b>	<b>R- value</b>
<b>1</b>	1	2015	2022		67.5
<b>2</b>	2	LIA	LIA		54
<b>3</b>	3	1953	1969		62.5
<b>4</b>	4	1953	1969		56.5
<b>5</b>	5	1953	1969		62.5
<b>6</b>	6	1928	1953		54.5
<b>7</b>	7	1997	2004		63.5
<b>8</b>	8	LIA	LIA		59

## **Chapter 5.**

### **Discussion**

This section aims to interpret some of the results and discuss them in a wider context. Features identified on the geomorphological map (Section 5.1) that are linked to glacial retreat are discussed to help achieve the first objective (see section 1.2). Section 5.2 focuses on the second and third objective (section 1.2) which cover the Schmidt hammer. In this section the variety in the Schmidt hammer results are discussed, along the possibilities for this variety and the final sub-section discusses the limitations of the Schmidt hammer.

#### **5.1 - Geomorphological Map**

During the site visit in September 2024 a multitude of features relating to glacial retreat were identified through the combination of analysis of satellite imagery and ground truthing. The ability to ground truth in this study was highly important as it allowed the opportunity to identify features in the bedrock, walk the length of moraines and identify the sediments that make up the two lateral moraines above the study area.

### 5.1.1 – Scoured Bedrock

The scoured bedrock dominates the study area from west to east with large sections north and south of the narrow tongue and smaller sections within more vegetated areas (Figure 4.1). The study area itself was also predominantly bedrock. It is possible that there is more scoured bedrock further down the valley, however, the vegetation cover is too substantial to confirm. This widespread glacial erosion can be referred to as ‘areal scouring’ and is widely observed in regions such as the north-west of Scotland (Rea and Evans, 1996) and are characterized by streamlined features and over-deepened rock basins (Benn and Evans, 2010).

Streamlined features such as Roche moutonnées were identified within the study area (Figure 4.1c), with some having striations, giving an indication of ice flow (Rea and Evans, 1996; Ray et al., 2021). This kind of landscape allows for many ponds to form between the high and low points and at the Schlatenkees twenty-eight ponds were observed within the bedrock. These features are formed during the advance of the ice and are only revealed after the retreat of the ice; however, they are important in understanding local glacier dynamics, including ice flow direction, plucking, abrasion and quarrying.

### 5.1.2 – Moraines

Moraines are an indication of past glacier extent in a region and are formed by deposition of sediment in various forms (Benn and Evans, 2010). The two types of moraines identified in the Schlatenkees foreland were lateral and recessional and these are discussed in the following two sections. No terminal moraines were identified at the bottom of the valley. Evidence from old photos and the GI LIA (Groß and Patzelt, 2015),

indicates that it may have been located where the braided river is in the present day and likely eroded and washed downstream through fluvial processes.

#### 5.1.2.1 – Lateral Moraines

Lateral moraines primarily consist of supraglacial debris, typically from rockfall on the slopes above the glacier (Small, 1983; Benn and Evans, 2010). There is a profound difference in the sediment size between the northern and southern moraines. The northern moraines are comprised of large clasts (Figure 5.1a) which may be due to the large coverage of scree slopes above the northern side of the site consisting of larger material. The southern moraine consists of finer and more angular sediment (Figure 5.1b) which is causing numerous gullies to appear on the slopes of the moraine. This may be a consequence of the high concentration of rock fall from the north face of the Kristallwand and the scree slopes above the debris covered section of the Schlatenkees (Figure 5.2). Historical imagery helps to show the difference in debris cover on the northern and southern margins of the glacier and why the sediment characteristics are vastly different between the moraines (Figure 5.3). The lateral moraines align closely with the GI LIA (Groß and Patzelt, 2015), particularly the along the southern moraines (Figure 4.3) strongly suggesting that these are from the Schlatenkees' LIA maximum.



*Figure 5. 1 a: Photograph showing a section of the moraine on the northern side of the site comprised of larger clasts surrounded by vegetation; Figure 5. 1b: Photograph looking down the southern moraine above the debris covered tributary of the Schlattenkees which shows some clasts mixed in with finer sediments. Both photos sourced from Author.*

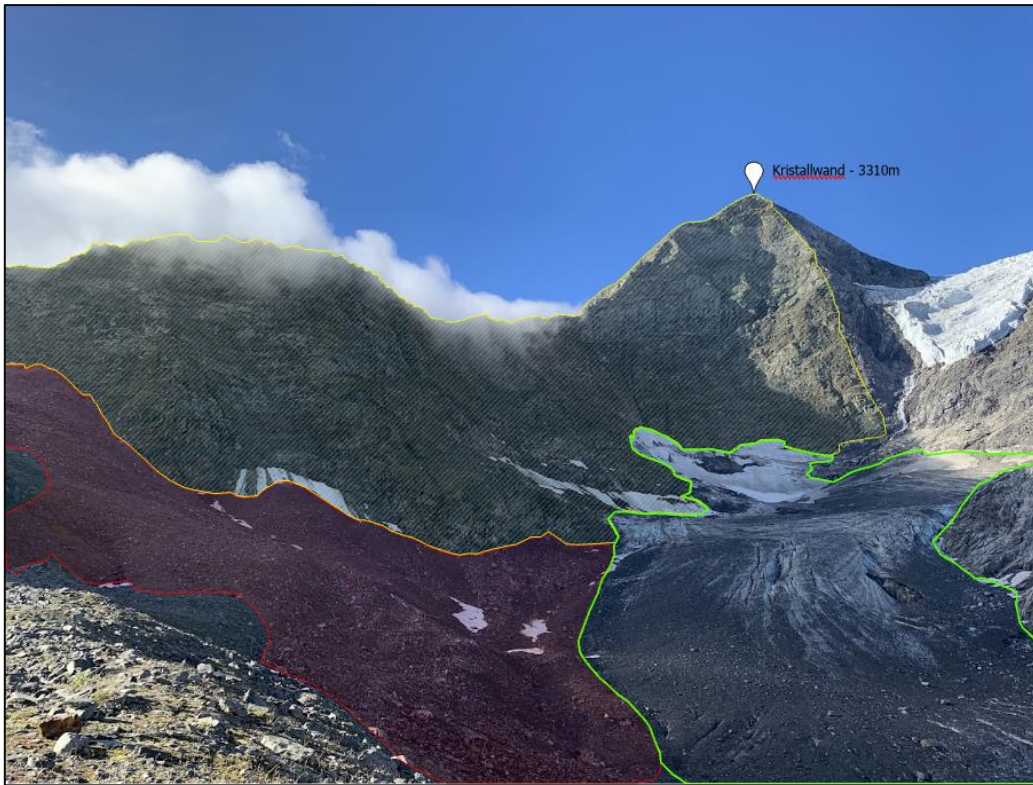


*Figure 5. 2: Annotated photo showing the possible sources for the abundance of debris covering the debris covered tributary of the Schlattenkees which had formed the southern lateral moraine. The area shaded in red is a scree slope, the north face of the Kristallwand is shaded in a yellow hatching and the glacier is outlined in green. Source: Author.*

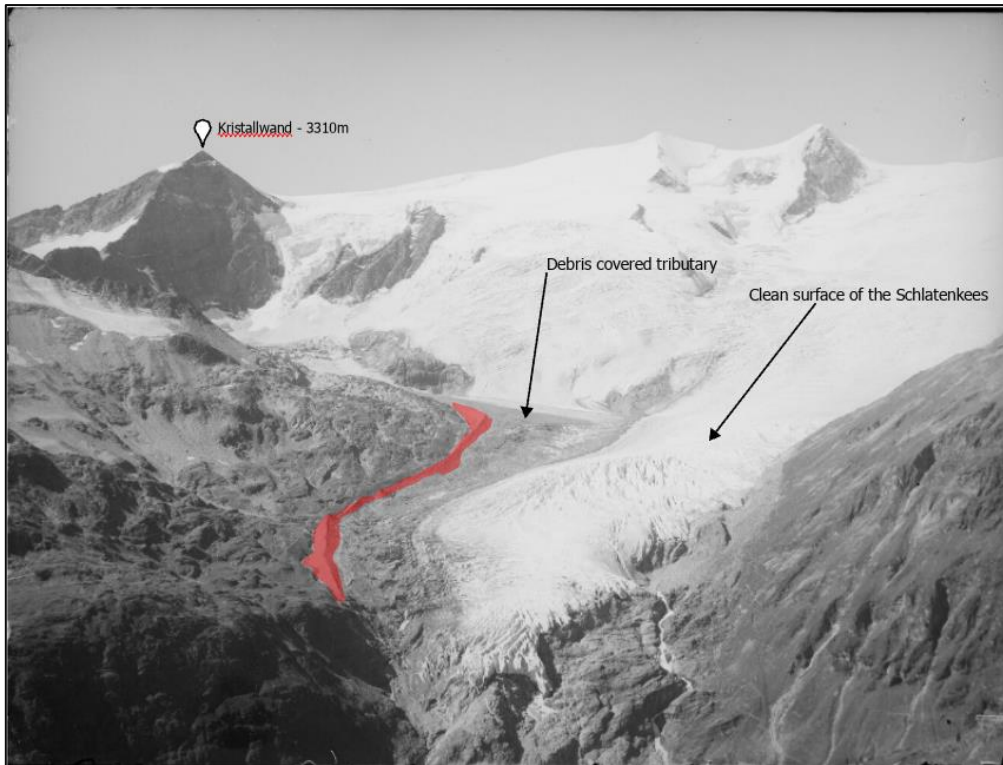


*Figure 5. 3: Annotated photo of the Schlatenkees from between 1920-1940, showing the difference between the clean surface of the Schlatenkees on the right compared to the debris covered tributary on the left. The southern moraine is highlighted in red. Source: Austrian National Library – Photo L 51918-B POR MAG ([https://data.onb.ac.at/rep/BAG\\_18956337](https://data.onb.ac.at/rep/BAG_18956337)).*

### 5.1.2.2 – Recessional Moraines

The second type of moraine identified were recessional moraines. These are moraines which are within the limits of the outermost moraines and are formed during recession of a glacier (Benn and Evans, 2010). The most prominent recessional moraine went from northwest to southeast and was split into different segments (Figure 4.1). Using the Austrian GI's, it revealed that GI1 and GI2 (Patzelt, 1980; Lambrecht and Kuhn, 2007) closely aligned with this moraine. The margin of GI2 follows the shape of the moraine closer compared to GI1, although they both do intersect the moraine at points (Figure 4.4).

When analysing Orthophotos of the Schlatenkees from the 1970/80s, a slight glacier advance was observed between 1974 and 1982. This is consistent with other observations made in the alps during the 1970/80s (Schöner et al., 2000; Lambrecht and Kuhn, 2007; Fischer et al., 2015a). This moraine was likely formed during this advancing period and with the feature being no younger than 51 years old, it shows the change in terminus positions in the last half century at the Schlatenkees. However, there was an error observed with the margin from GI2 on the GIS, as seen in Figure 5.4 the glacier terminus had receded away from the moraine by some distance by 1997 compared to what is shown by GI2 on the GIS (Figure 4.4).

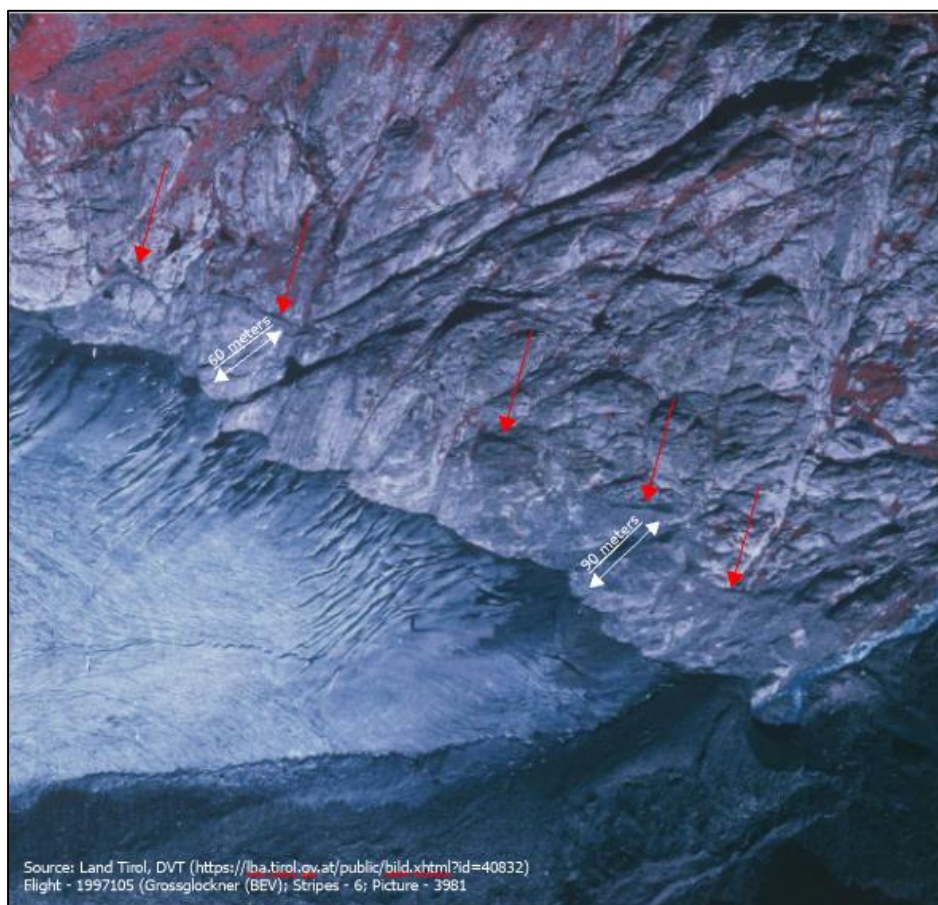


*Figure 5. 4: Satellite imagery from 1997 showing the actual distance the glacier had receded from the recessional moraine. Red arrows show sections of the moraine and white arrows show the rough distance between the moraine and terminus. Source: See bottom left of figure.*

Older recessional moraines were identified in the northeast of the study area, with historical imagery from the 1920s-30s (Figure 5.5, 5.6) indicating they were formed during this period. Site 4 on transect 4 was located directly west of the most westerly moraine in group one (as labelled on Figure 5.6) and recorded an r-value of 60. These moraines are below the northern slope and are comprised of the same type of clasts seen in the northern lateral moraines.

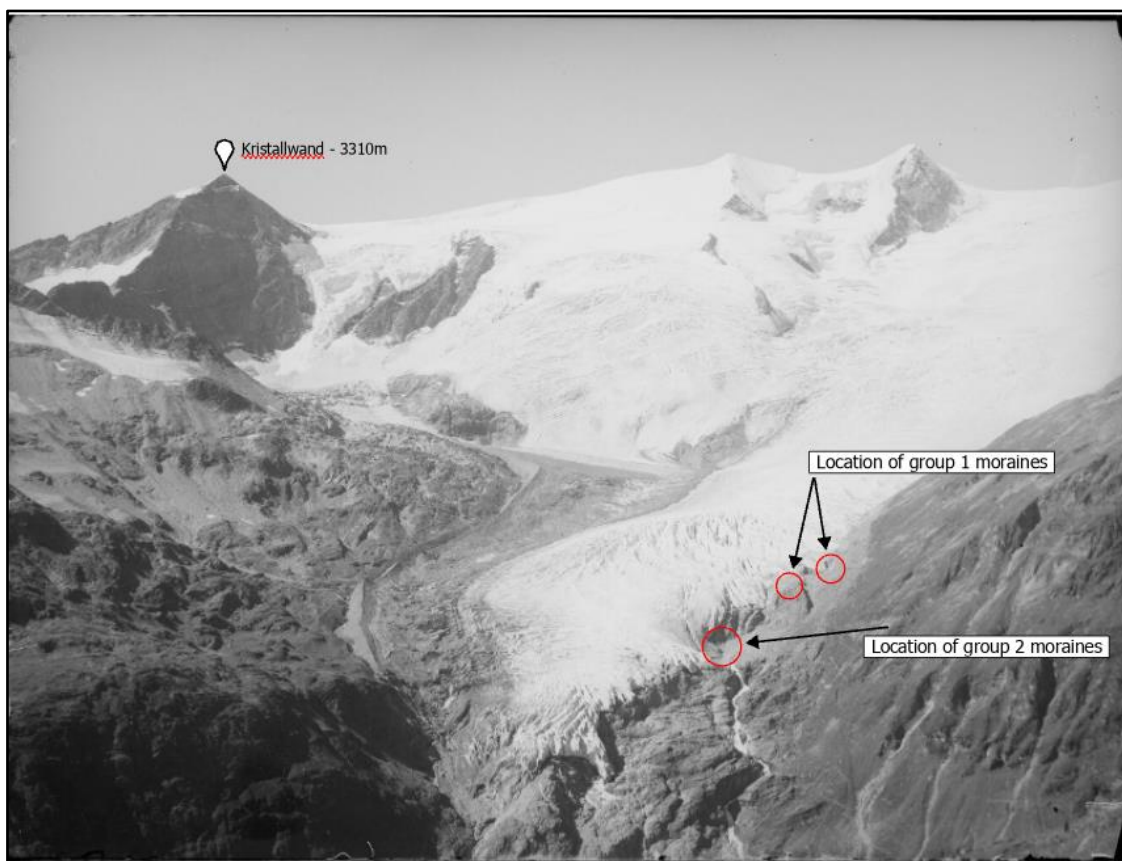


*Figure 5. 5: Annotated historical Image between the 1920s-1930s showing the glacial margin at points where recessional moraines were identified on the geomorphological map. Source: Austrian National Library – Photo L 51918-B POR MAG ([https://data.onb.ac.at/rep/BAG\\_18956337](https://data.onb.ac.at/rep/BAG_18956337))*

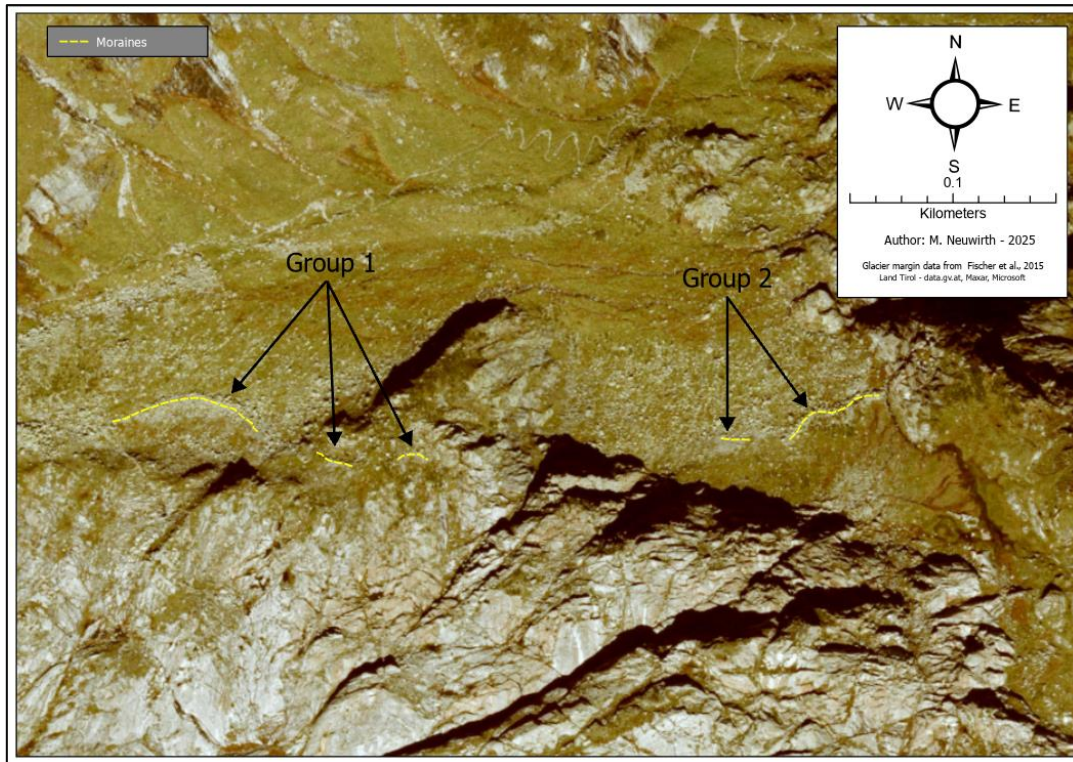


*Figure 5. 6: Aerial imagery showing the location of the recessional moraines which were left behind by the glacier as it retreated from the location seen in Figure 5.5.*

### 5.1.3 – Hydrological Features

Due to the current state of glaciers in the alps, ice-contact proglacial lakes, such as observed at the Schlatenkees (Figure 4.1, 4.9) are becoming more common. Various icebergs were observed in the proglacial lake at the Schlatenkees showing the retreat and disintegration of the snout at the lake (Figure 4.9). These lakes have also been identified at the Miage Glacier in Italy (Diolaiuti et al., 2006) and the Pazterze Glacier in Austria (Kellerer-Pirklbauer et al., 2021).

Throughout the world, proglacial lakes are becoming an increasing indicator of glacier retreat (Otto, 2019) such as in the New Zealand Alps (Tweed and Carrivick, 2015). In Austria, the Venediger group has one of the highest densities of proglacial lakes in, as highlighted in an inventory compiled by Buckel et al. (2018) (Figure 5.7). Although, there

was no lake at the Schlatenkees at the time of the study by Buckel et al. (2018), it highlights a trend of increasing temperatures and decreasing glacier area in Austria, which is accelerating the formation of these proglacial lakes. A few interesting observations were identified within this inventory by Buckel et al. (2018) such as an increase of 264 new lakes between the LIA and 2015 with bedrock dammed lakes being the predominant type observed. The study also linked the formation of these lakes to changing climatic conditions and glacier retreat.

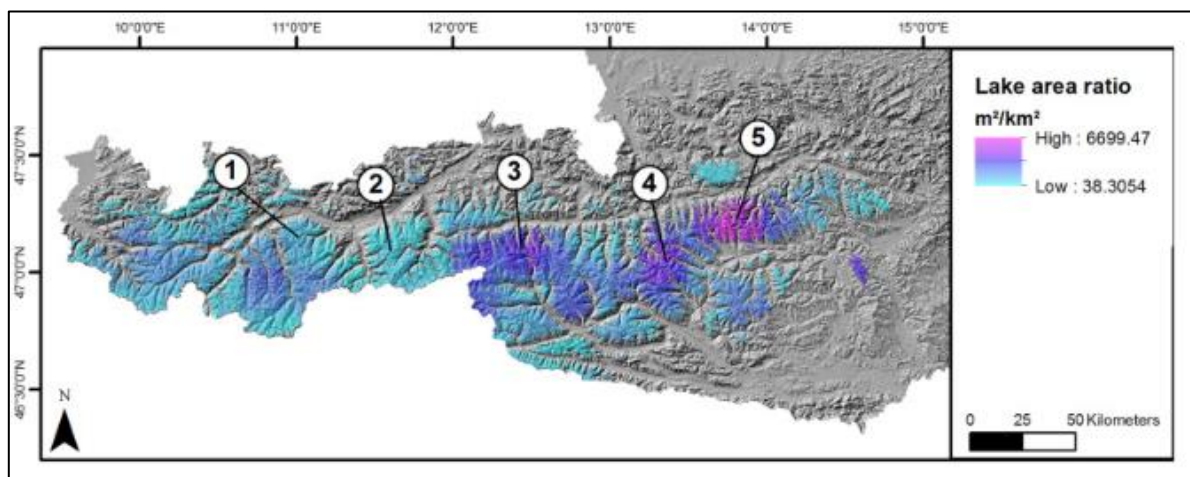


*Figure 5. 7: Map of glacial lakes in Austria, showing the Venediger group (labelled as group '3') with the 3<sup>rd</sup> highest lake density in the Austrian Alps. Source: Buckel et al. (2018).*

The proglacial lake at the Schlatenkees has been a recent development in the foreland. Satellite imagery from 2015 shows little evidence of proglacial lake formation, however imagery from 2019 shows clear indication of snout disintegration and a lake forming beneath the ice. In 2022, the proglacial lake is a prominent feature in the landscape (Figure 5.8a 5.8b, 5.8c).

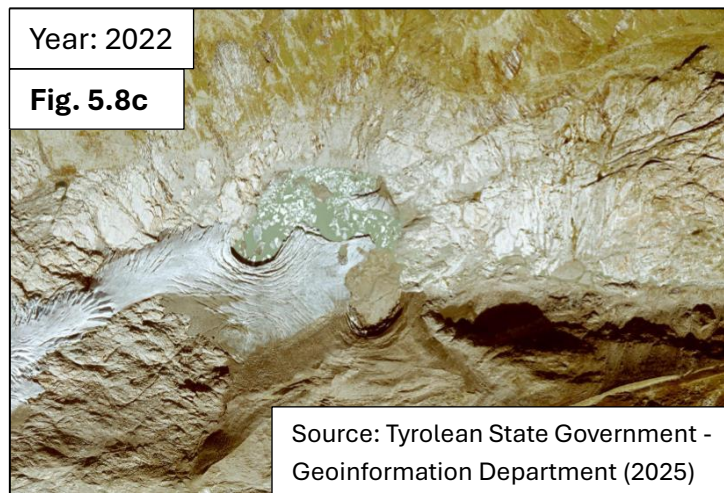
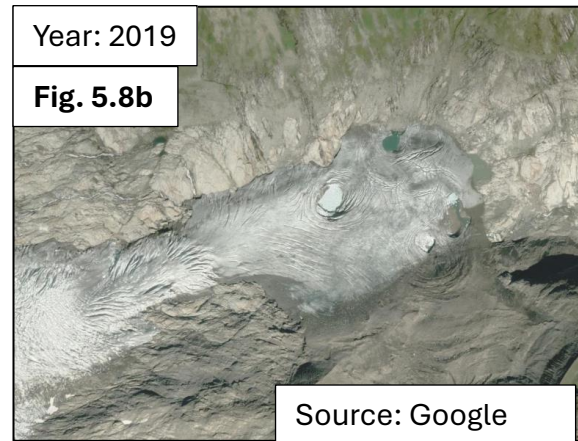
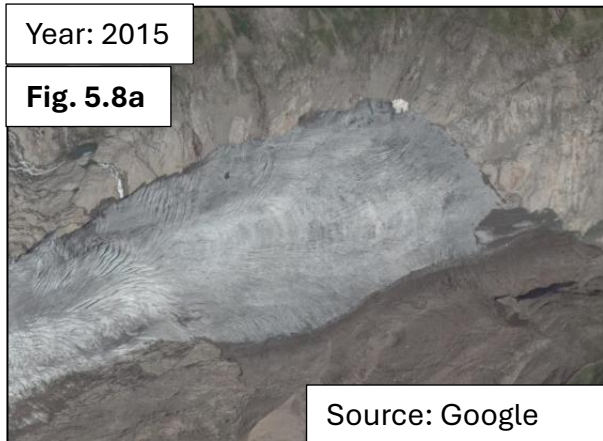


*Figure 5. 8 a: Satellite imagery of the Schlatenkees in 2015 showing little indication of proglacial lake development; Figure 5.8b; Satellite imagery of the Schlatenkees from 2019 showing circular crevasses and disintegration of the snout with the proglacial lake in development; Figure 5.8c: Satellite imagery of the Schlatenkees from 2022 showing the proglacial lake which has become a prominent feature in the landscape.*

## 5.2 - Schmidt Hammer

Twenty-six sites were sampled across the Schlatenkees foreland using the Schmidt hammer with the aim of testing its reliability. A relationship was identified between the r-value and the distance from the glacier, with site one on each transect recording a higher value than site five, indicating that the sites further away have been exposed longer. At two additional sites either side of a moraine, the site inside the moraine recorded a higher r-value, which is consistent with findings by Matthews et al. (2024) in Norway.

### 5.2.1 – R-values across the Schlatenkees Foreland

Shakesby et al. (2006) demonstrated a statistically significant relationship on different surface types in southern Norway (Figure 2.4), on a similar lithology to the Schlatenkees. This showed that Schmidt hammer r-values could be used to clearly distinguish surfaces of different ages. The Schmidt hammer's ability to quantify glacial recession accurately at the Schlatenkees was more subtle, with none of the transects being statistically significant. However, the transects showed a trend of the furthest away site recording a lower r-value (Figure 4.12), and additionally a difference of 8.5 was recorded between the two additional sites furthest away from each other (Table 4.2). Indicating, that the Schmidt hammer did show some reliability, although it was not as effective as demonstrated by, Shakesby et al. (2006) in Norway.

Although a multitude of studies have applied the Schmidt hammer to gneiss, (See Table in Goudie, 2006), there is a gap in the literature regarding its application and reliability to recently deglaciated gneiss. Matthews and Owen (2008) suggest a preliminary dating

curve for surfaces exposed <50 years by retreating glaciers in Norway, suggesting a mean r-value of ~61.0 for unweathered and freshly deglaciated rock surfaces. At the Schlatenkees, eight sites were deglaciated <50 years ago (Table 4.3), with a mean r-value of 65.5, 4.5 lower Matthews and Owens' (2008) dating curve. This does indicate some minor inaccuracies with the Schmidt hammer, however, the mean r-value of sites deglaciated >50 years ago was 59.0. This does show the general reliability of the Schmidt hammer to distinguish younger and newer surfaces.

### 5.2.2 – Retreat Pattern of Schlatenkees Affecting R-Values

There was no statistically significant relationship identified between r-value and distance from the glacier. However, the trend of site five on each transect being higher than site one indicates a moderate correlation.

Understanding the retreat pattern of the Schlatenkees is important. The site slopes downwards from north to south, with the low point being where the present-day meltwater stream is located. From analysing historical photos and satellite imagery, the glacier retreats into this low point, with it being the point of the glacier that extends furthest downslope. As it is known that the glacier retreated from a higher elevation to a lower one, it helps demonstrate the statistically significant relationship (p-value- 0.005) between the transect elevation and r-value. This further supports the Schmidt hammer as a reliable piece of equipment in measuring the glacial recession at this site. The use of historical photos and orthophotos/satellite imagery helped to provide further insight into the relationship observed.

### 5.2.3 – Assessing the Outlier of Site 2 on Transect 4

The Schmidt hammer values collected across the Schlatenkees foreland had considerable variability with an average SD across all sites of 8.4, with a range from 4.3 (Figure 4.16) to 13.6 (Figure 4.20), highlighting concerns about its reliability. A possibility for this variance may be the local lithology, gneiss, which can feature a coarse grain on the surface (Fueten et al., 2003). The heterogeneity between the rock surfaces between and within transects was clear, quartz veins, oxidization and varying mineral compositions were all identified (Figure 5.9a, 5.9b). These likely did contribute to inaccuracies in the r-values at the Schlatenkees, a point also identified by Tomkins et al. (2016) on features linked to recession of the British Ice Sheet. There was also a difference of 4.5 in r-values observed by Shakesby et al. (2006) on two different compositions of gneiss. Both Tomkins et al. (2016) and Czempiński and Dąbski (2017) suggested that based on their results, gneiss may not be suitable for Schmidt hammer application due to its coarse surface grain and varying mineral composition.

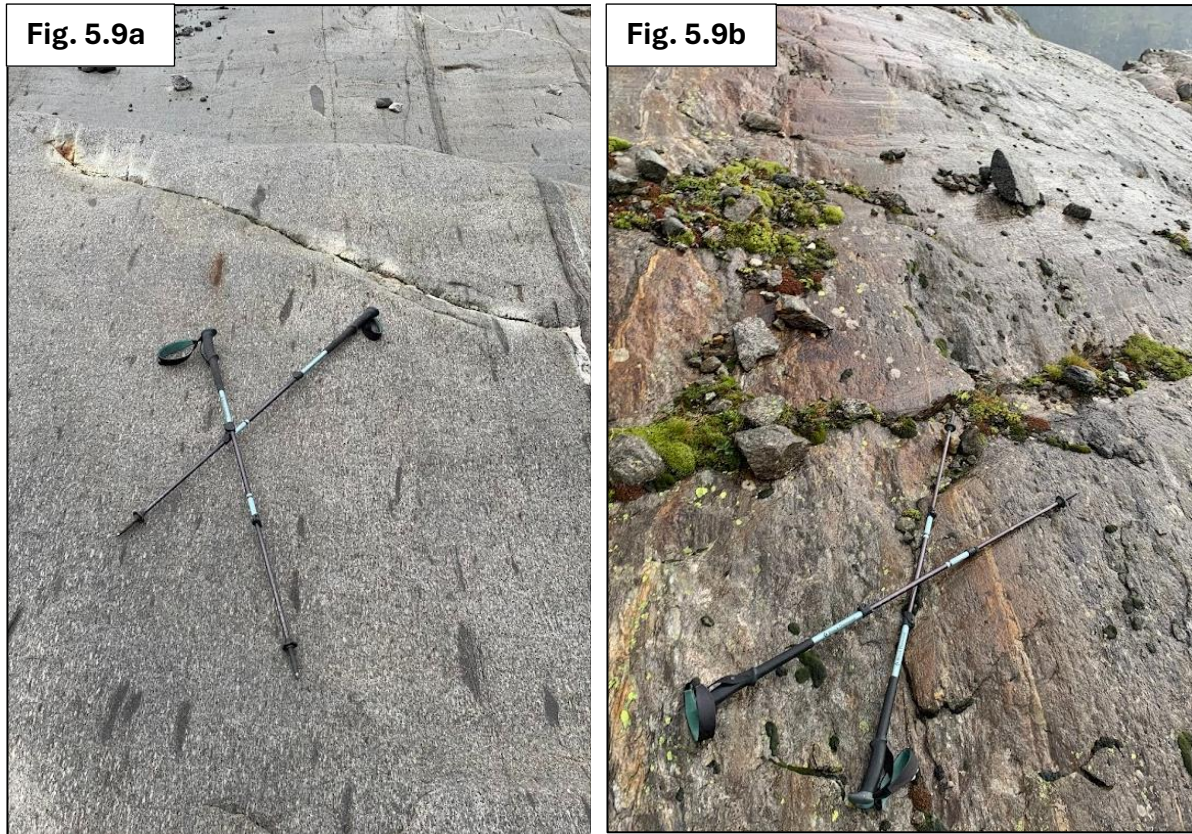


*Figure 5. 9a: Smooth bedrock surface at site 1 on transect 3. Figure 5.9b: Rougher and lichen covered section of bedrock at site 4, transect 3 with moss, lichen and oxidisation, highlighting the difference between two sites on the same surface.  
Source: Both photos – Author.*

The largest difference between two sites on one transect is site 1 (66.5) and 2 (49) on transect 4 (Figure 4.20); a difference of 17.5. These two sites are approximately 200 meters apart, with site 2 being further away from the glacier and 13m higher and the sites were deglaciated at least 78 years apart (Table 4.3). To help investigate large difference between these two sites, additional site seven was placed in between the two sites, recording an r-value of 63.5 (Table 4.2). There was a clear difference in surfaces at site 1 and 2, with site one being smooth and lichen free, whilst site two exhibited a coarser texture and significant lichen cover (Figure 5.10a, 10b). The presence of lichen on the rock surface at site two may have influenced the r-value, a point also made by Matthews and

Owen, (2008), who found a 28-point r-value reduction between lichen covered surfaces and lichen free surfaces on bedrock exposed in 1951. They further discuss that the lichen was enhancing weathering rates on rock surfaces 200-300 times greater than the normal weathering rate in that region (Matthews and Owen, 2008).

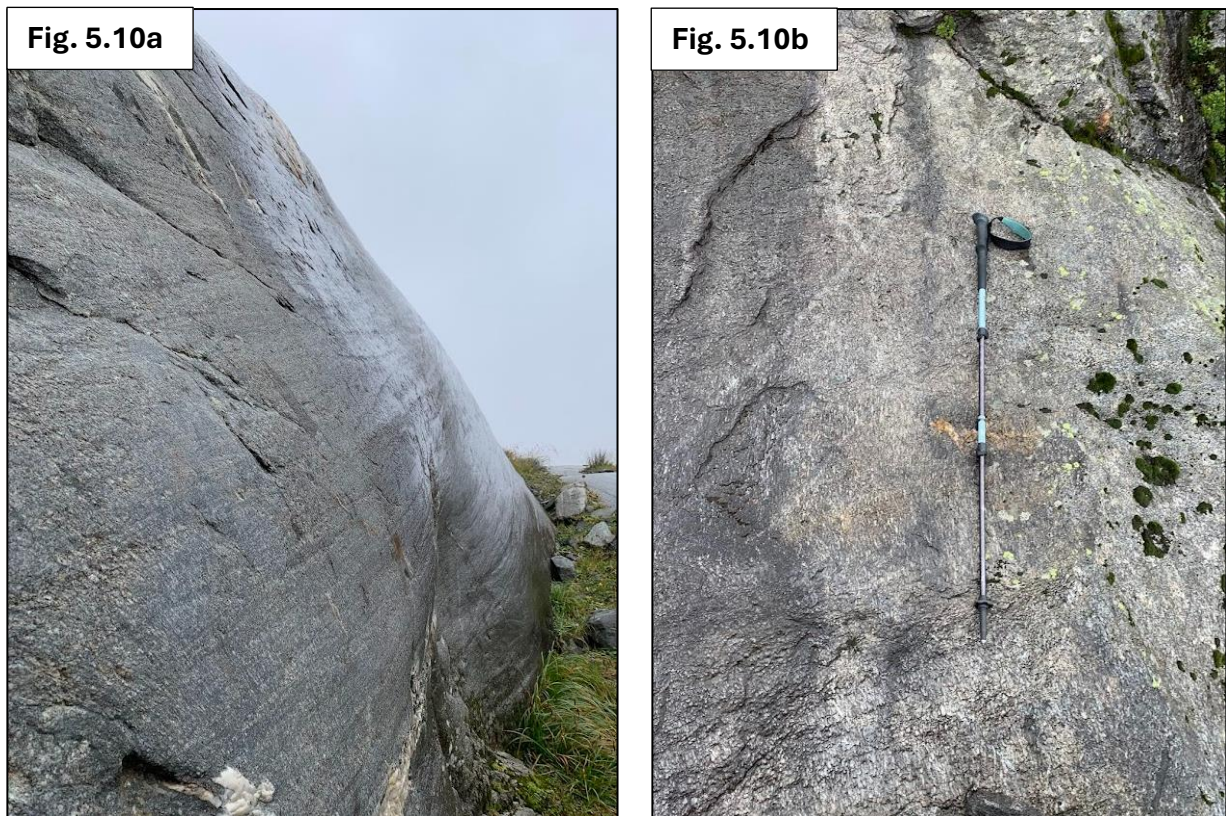


*Figure 5. 10a: Bedrock sampled from site 1 on transect 4 (r-value 66.5), showing a smooth profile with no lichen present. Figure 5. 10b: Bedrock sampled at site 2 on transect 4 (r-value 49) showing the presence of lichen and a rougher profile.*

*Source: Both photos – Author.*

The observed outlier of site 2 on transect 4 (Figure 4.20) does raise some questions around the reliability of the Schmidt hammer on gneiss and lichen covered surfaces. Further analysis on the weathering rates and mineral composition may help suggest the observed difference in r-value and analysis of the lichen at the site would aid in getting a better understanding of the difference in r-values. Using the Schmidt hammer in conjunction with lichenometry for example (Matthews and Shakesby, 1984; Rune Aa and

Sjåstad, 2000) may help to provide a more robust value at sites where the Schmidt hammer is limited.

#### 5.2.4 – Limitations of the Schmidt Hammer

Throughout this study various limitations were identified with the Schmidt hammer, which may have influenced the recorded r-values at certain sites. The difference in surface texture and the presence of lichen on the rock surfaces may have impacted the r-values. These findings raise questions surrounding gneiss and if it is a suitable lithology for Schmidt hammer application due to it not being homogenous in structure. This leads to there being scope for future studies to explore the application of the Schmidt hammer to more homogenous lithologies such as sandstone. The effects of the lichen and variability in gneiss was mentioned in the previous section and has also been documented in previous studies (Matthews and Owen, 2008; Tomkins et al., 2016). Future work on the effects of lichen and mineral variability on r-values would help gather a more robust understanding on the Schmidt hammer's reliability on recently deglaciated gneissic glacial landscapes which can be dated through historical/aerial imagery.

Local glacier mechanics can influence the surface of the bedrock and thus the Schmidt hammer results. Differences in basal sliding speed affecting abrasion rates, ice thickness (Hallet, 1981) and concentration of basal debris (Ugelvig and Egholm, 2018) affect the subglacial erosion of a glacier, and consequently the rock surface characteristics. For example, a difference in local glacier dynamics could explain the difference of 14 in r-value between site 2 transect 1 and site 3 transect 4. At site 2 transect 1 there may have

been a higher basal debris concentration due to its location debris covered section, leading to the smoother bedrock observed.

## **Chapter 6.**

### **Conclusion**

The aim of this study was to test the reliability of the Schmidt hammer to measure glacial recession in the Austrian Alps and this was done by sampling twenty-six different sites across the foreland of the Schlatenkees. Overall, the Schmidt hammer proved moderately reliable as a cheap, lightweight piece of equipment, with each transect having a higher r-value at site 1 opposed to site 5. The two furthest additional sites further away from each other also saw a reduction in r-value as distance increased. The Schmidt hammer was tested either side of a moraine and the results tied in with expectations that the r-value was higher inside the moraine closer to the glacier. The sites where the rock surface was smooth, such as transect 1 site 2 (Figure 4.13), produced higher r-values and on more weathered and rougher rock, such as transect 4 sites 2 (Figure 4.22) or 3, lower r-value were produced, staying consistent with expectations. These results have helped broaden the literature on the reliability of the Schmidt hammer on recently deglaciated surfaces.

However, inaccuracies in r-value between smooth and weathered bedrock with lichen present on the surface do question its reliability on some surface types and it was evident that the latter surface type did affect r-values. Although, the variety in gneiss must not be overlooked and that between sites, even on the same transect, the mineral composition differed. This furthers the point made by Tomkins et al. (2016), suggesting that gneiss may not be suitable for Schmidt hammer application and can cause inaccurate results, leading to a less reliable data.

## 6.1 – Addressing the Objectives

The first objective was to identify any features relating to glacial retreat or former glacial terminus positions and this was achieved with lateral and recessional moraines showing clear former terminus positions which lined up with the various GI's. The proglacial lake at the Schlatenkees highlighted glacier in more recent times and follows a trend of proglacial development in the Austrian Alps since the LIA (Buckel et al., 2018).

The second objective involved collecting Schmidt hammer r-values across the Schlatenkees foreland to identify old glacier positions. Using various historical photos, orthophotos and satellite imagery it was possible to apply absolute dating to these sites to know when they were exposed. These dates can be paired with r-values (Table 4.3) to aid in identifying these former positions.

Finally, the third objective was to identify a relationship between the r-values and the distance from the glacier and this was achieved to a moderate extent. There was a relationship identified between sites one and five on each transect and some additional sites, however, these were not statistically significant as there was a mix of r-values between the two furthest away sites. Although there was a statistically relationship between the average transect r-value and elevation, showing that the Schmidt hammer proved reliable in measuring the recession of the Schlatenkees as it retreated from a higher elevation.

## **7 – Reference List**

Alpenverein (2016). *Alpenverein präsentiert Gletscherbericht*. [online] Alpenverein.at.

Available at:

[https://www.alpenverein.at/portal/news/aktuelle\\_news/2016/2016\\_04\\_08\\_gletscherbericht.php](https://www.alpenverein.at/portal/news/aktuelle_news/2016/2016_04_08_gletscherbericht.php) [Accessed 14 Mar. 2025].

Alpenverein (2018). *Aktueller Gletscherbericht*. [online] Alpenverein.at. Available at:

[https://www.alpenverein.at/portal/news/aktuelle\\_news/2018/2018\\_04\\_06\\_gletscherbericht.php](https://www.alpenverein.at/portal/news/aktuelle_news/2018/2018_04_06_gletscherbericht.php) [Accessed 14 Mar. 2025].

Alpenverein (2020). *Gletscherbericht 2018/19: Das ewige Eis schmilzt*. [online]

Alpenverein.at. Available at:

[https://www.alpenverein.at/portal/news/aktuelle\\_news/2020/2020\\_04\\_01\\_gletscherbericht-2019.php](https://www.alpenverein.at/portal/news/aktuelle_news/2020/2020_04_01_gletscherbericht-2019.php) [Accessed 14 Mar. 2025].

Alpenverein (2021). *09.04.2021 - Gletscherbericht 2019/20*. [online] Alpenverein.at.

Available at:

[https://www.alpenverein.at/portal/service/presse/2021/2021\\_04\\_09\\_gletscherbericht-2020.php](https://www.alpenverein.at/portal/service/presse/2021/2021_04_09_gletscherbericht-2020.php) [Accessed 14 Mar. 2025].

Alpenverein (2022). *01.04.2022 - Gletscherbericht 2020/21*. [online] Alpenverein.at.

Available at:

[https://www.alpenverein.at/portal/service/presse/2022/2022\\_04\\_01\\_gletscherbericht-2020-21.php](https://www.alpenverein.at/portal/service/presse/2022/2022_04_01_gletscherbericht-2020-21.php) [Accessed 25 Feb. 2025].

Alpenverein (2023a). *Alpenverein Gletschermonitor*. [online] Alpenverein.at. Available

at: <https://www.alpenverein.at/gletschermonitor/> [Accessed 15 Mar. 2025].

Alpenverein (2023b). *31.03.2023 - Gletscherbericht 2021/22*. [online] Alpenverein.at.

Available at:

[https://www.alpenverein.at/portal/service/presse/2023/2023\\_03\\_31\\_gletscherbericht-2021-22.php](https://www.alpenverein.at/portal/service/presse/2023/2023_03_31_gletscherbericht-2021-22.php) [Accessed 25 Feb. 2025].

Alpenverein (2024). *05.04.2024 - Gletscherbericht 2022/23*. [online] Alpenverein.at.

Available at:

[https://www.alpenverein.at/portal/service/presse/2024/2024\\_04\\_05\\_gletscherbericht-2022-23.php](https://www.alpenverein.at/portal/service/presse/2024/2024_04_05_gletscherbericht-2022-23.php) [Accessed 12 Mar. 2025].

Alpenverein (2025). 07.03.2025 - Gletscherbericht 2023/24. [online] Alpenverein.at.

Available at:

[https://www.alpenverein.at/portal/service/presse/2025/2025\\_03\\_07\\_Gletscherbericht.php](https://www.alpenverein.at/portal/service/presse/2025/2025_03_07_Gletscherbericht.php) [Accessed 12 Mar. 2025].

Alps, A., Abermann, J., Lambrecht, A., Fischer, A. and Kuhn, M. (2009). The Cryosphere Quantifying changes and trends in glacier area and volume in the). *The Cryosphere*, [online] 3, pp.205–215. Available at: <https://tc.copernicus.org/articles/3/205/2009/tc-3-205-2009.pdf>.

Aydin, A. and Basu, A. (2005). The Schmidt hammer in rock material characterization. *Engineering Geology*, 81(1), pp.1–14. doi:<https://doi.org/10.1016/j.enggeo.2005.06.006>.

Benn, D.I. and Evans, D.J.A. (2010). *Glaciers & glaciation*. London: Hodder Education.

Birdeau, M.-A., Stead, D., Huscroft, C. and Fecova, K. (2005). Quaternary, structural and engineering geology of the Aishihik River landslide, Cracker Creek area (NTS 115A/15), Yukon. *Yukon Exploration and Geology 2004, D.S. Emond, L.L. Lewis and G.D. Bradshaw (eds.)*, [online] pp.83–94. Available at:

<https://citeseerx.ist.psu.edu/document?repid=rep1&type=pdf&doi=c59474b935e5a8cefa8eeebf7b6e9a323b5d60e4> [Accessed 29 Jan. 2025].

Boston, C.M. (2012). A glacial geomorphological map of the Monadhliath Mountains, Central Scottish Highlands. *Journal of Maps*, 8(4), pp.437–444.

doi:<https://doi.org/10.1080/17445647.2012.743865>.

Brook, M.S., Kirkbride, M.P. and Brock, B. (2004). Rock strength and development of glacial valley morphology in the scottish highlands and northwest iceland. 86(3), pp.225–234. doi:<https://doi.org/10.1111/j.0435-3676.2004.00227.x>.

Buckel, J. and Otto, J.-C. (2018). The Austrian Glacier Inventory GI 4 (2015) in ArcGis (shapefile) format. doi:<https://doi.org/10.1594/pangaea.887415>.

- Buckel, J., Otto, J.C., Prasicek, G. and Keuschnig, M. (2018). Glacial lakes in Austria - Distribution and formation since the Little Ice Age. *Global and Planetary Change*, 164, pp.39–51. doi:<https://doi.org/10.1016/j.gloplacha.2018.03.003>.
- Chandler, B.M.P., Lovell, H., Boston, C.M., Lukas, S., Barr, I.D., Benediktsson, Í.Ö., Benn, D.I., Clark, C.D., Darvill, C.M., Evans, D.J.A., Ewertowski, M.W., Loibl, D., Margold, M., Otto, J.-C., Roberts, D.H., Stokes, C.R., Storrar, R.D. and Stroeven, A.P. (2018). Glacial geomorphological mapping: A review of approaches and frameworks for best practice. *Earth-Science Reviews*, [online] 185, pp.806–846. doi:<https://doi.org/10.1016/j.earscirev.2018.07.015>.
- Clark, C.D., Ely, J.C., Greenwood, S.L., Hughes, A.L.C., Meehan, R., Barr, I.D., Bateman, M.D., Bradwell, T., Doole, J., Evans, D.J.A., Jordan, C.J., Monteys, X., Pellicer, X.M. and Sheehy, M. (2017). BRITICE Glacial Map, version 2: a map and GIS database of glacial landforms of the last British-Irish Ice Sheet. *Boreas*, 47(1), pp.11-e8. doi:<https://doi.org/10.1111/bor.12273>.
- Diolaiuti, G., Citterio, M., Carnielli, T., D'Agata, C., Kirkbride, M. and Smiraglia, C. (2006). Rates, processes and morphology of freshwater calving at Miage Glacier (Italian Alps). *Hydrological Processes*, 20(10), pp.2233–2244. doi:<https://doi.org/10.1002/hyp.6198>.
- Czempiński, J. and Dąbski, M., 2017. Lichenometry and Schmidt hammer tests in the Kaunertal glacier foreland (Ötztal Alps) during the AMADEE-15 Mars Mission Simulation. *Miscellanea Geographica. Regional Studies on Development*, 21(4), pp.190-196.
- Duca, S., Alonso, E.E. and Scavia, C. (2015). A permafrost test on intact gneiss rock. *International Journal of Rock Mechanics and Mining Sciences*, 77, pp.142–151. doi:<https://doi.org/10.1016/j.ijrmms.2015.02.003>.
- Evans, D.J.A., Archer, S. and Wilson, D.J.H. (1999). A comparison of the lichenometric and Schmidt hammer dating techniques based on data from the proglacial areas of some Icelandic glaciers. *Quaternary Science Reviews*, 18(1), pp.13–41. doi:[https://doi.org/10.1016/s0277-3791\(98\)00098-5](https://doi.org/10.1016/s0277-3791(98)00098-5).

Fischer, A. and Kuhn, M. (2013). Ground-penetrating radar measurements of 64 Austrian glaciers between 1995 and 2010. *Annals of Glaciology*, 54(64), pp.179–188.  
doi:<https://doi.org/10.3189/2013aog64a108>.

Fischer, A., Seiser, B., Stocker Waldhuber, M., Mitterer, C. and Abermann, J. (2015a). Tracing glacier changes in Austria from the Little Ice Age to the present using a lidar-based high-resolution glacier inventory in Austria. *The Cryosphere*, 9(2), pp.753–766.  
doi:<https://doi.org/10.5194/tc-9-753-2015>.

Fischer, A., Seiser, B., Stocker-Waldhuber, M., Mitterer, C. and Abermann, J. (2015b). The Austrian Glacier Inventories GI 1 (1969), GI 2 (1998), GI 3 (2006), and GI LIA in ArcGIS (shapefile) format. doi:<https://doi.org/10.1594/pangaea.844988>.

Fricke, H.A., Galton-Fenzi, B.K., Walker, C.C., Freer, B.I.D., Padman, L. and DeConto, R. (2025). Antarctica in 2025: Drivers of deep uncertainty in projected ice loss. *Science*, 387(6734), pp.601–609. doi:<https://doi.org/10.1126/science.adt9619>.

Fueter, F., Robin, P.-Y.F. and Stephens, R. (2003). A model for the development of a domainal quartz c-axis fabric in a coarse-grained gneiss. *Journal of Structural Geology*, [online] 13(10), pp.1111–1124. doi:[https://doi.org/10.1016/0191-8141\(91\)90072-Q](https://doi.org/10.1016/0191-8141(91)90072-Q).

Geological Survey of Austria (1987). *152 Matri in Osttirol*. Available at:  
[https://opac.geologie.ac.at/wwwopacx/wwwopac.ashx?command=getcontent&server=images&value=GK0152\\_000\\_A.pdf](https://opac.geologie.ac.at/wwwopacx/wwwopac.ashx?command=getcontent&server=images&value=GK0152_000_A.pdf) [Accessed 6 Mar. 2025].

Geyman, E.C., J. J. van Pelt, W., Maloof, A.C., Aas, H.F. and Kohler, J. (2022). Historical glacier change on Svalbard predicts doubling of mass loss by 2100. *Nature*, 601(7893), pp.374–379. doi:<https://doi.org/10.1038/s41586-021-04314-4>.

Goudie, A.S. (2006). The Schmidt Hammer in geomorphological research. *Progress in Physical Geography: Earth and Environment*, 30(6), pp.703–718.  
doi:<https://doi.org/10.1177/0309133306071954>.

Groß, G., 1987. Der Flächenverlust der Gletscher in Österreich 1850-1920-1969 (GI 1), shapefile archive.

Groß, G. and Patzelt, G. (2015). The Austrian Glacier Inventory for the Little Ice Age Maximum (GI LIA) in ArcGIS (shapefile) format.  
doi:<https://doi.org/10.1594/pangaea.844987>.

Gustavsson, M., Kolstrup, E. and Seijmonsbergen, A.C. (2006). A new symbol-and-GIS based detailed geomorphological mapping system: Renewal of a scientific discipline for understanding landscape development. *Geomorphology*, 77(1-2), pp.90–111.  
doi:<https://doi.org/10.1016/j.geomorph.2006.01.026>.

Haines, D. (2017). *Rivers Divided*. *Oxford Scholarship Online*. Oxford University Press.  
doi:<https://doi.org/10.1093/acprof:oso/9780190648664.001.0001>.

Hallet, B. (1981). Glacial Abrasion and Sliding: their Dependence on the Debris Concentration in Basal Ice. *Annals of Glaciology*, 2, pp.23–28.  
doi:<https://doi.org/10.3189/172756481794352487>.

Han, P., Long, D., Zhao, F. and Slater, L.J. (2023). Response of Two Glaciers in Different Climate Settings of the Tibetan Plateau to Climate Change Through Year 2100 Using a Hybrid Modeling Approach. *Water Resources Research*, 59(4).  
doi:<https://doi.org/10.1029/2022wr033618>.

Hugonnet, R., McNabb, R., Berthier, E., Menounos, B., Nuth, C., Girod, L., Farinotti, D., Huss, M., Dussailant, I., Brun, F. and Käab, A. (2021). Accelerated global glacier mass loss in the early twenty-first century. *Nature*, [online] 592(7856), pp.726–731.  
doi:<https://doi.org/10.1038/s41586-021-03436-z>.

Katz, O., Reches, Z. and Roegiers, J.-C. . (2000). Evaluation of mechanical rock properties using a Schmidt Hammer. *International Journal of Rock Mechanics and Mining Sciences*, 37(4), pp.723–728. doi:[https://doi.org/10.1016/s1365-1609\(00\)00004-6](https://doi.org/10.1016/s1365-1609(00)00004-6).

Kehrwald, N.M., Thompson, L.G., Tandong, Y., Mosley-Thompson, E., Schotterer, U., Alfimov, V., Beer, J., Eikenberg, J. and Davis, M.E. (2008). Mass loss on Himalayan glacier endangers water resources. *Geophysical Research Letters*, 35(22).  
doi:<https://doi.org/10.1029/2008gl035556>.

Kellerer-Pirklbauer, A. (2008). The Schmidt-Hammer as a Relative Age Dating Tool for Rock Glacier Surfaces. *Quaternary International*, 279-280, p.239.

doi:<https://doi.org/10.1016/j.quaint.2012.08.546>.

Kellerer-Pirklbauer, A., Avian, M., Benn, D.I., Bernsteiner, F., Krisch, P. and Ziesler, C. (2021). Buoyant calving and ice-contact lake evolution at Pasterze Glacier (Austria) in the period 1998–2019. *The Cryosphere*, 15(3), pp.1237–1258.

doi:<https://doi.org/10.5194/tc-15-1237-2021>.

Kjær, K.H., Korsgaard, N.J. and Schomacker, A. (2008). Impact of multiple glacier surges—a geomorphological map from Brúarjökull, East Iceland. *Journal of Maps*, 4(1), pp.5–20. doi:<https://doi.org/10.4113/jom.2008.91>.

Kłapyta, P. (2013). Application of Schmidt hammer relative age dating to Late Pleistocene moraines and rock glaciers in the Western Tatra Mountains, Slovakia. *CATENA*, 111, pp.104–121. doi:<https://doi.org/10.1016/j.catena.2013.07.004>.

Koboltschnig, G.R. and Schöner, W. (2011). The relevance of glacier melt in the water cycle of the Alps: the example of Austria. *Hydrology and Earth System Sciences*, 15(6), pp.2039–2048. doi:<https://doi.org/10.5194/hess-15-2039-2011>.

Lambrecht, A. and Kuhn, M. (2007). Glacier changes in the Austrian Alps during the last three decades, derived from the new Austrian glacier inventory. *Annals of Glaciology*, (46), pp.177–184. doi:<https://doi.org/10.3189/172756407782871341>.

Lardeux, P., Glasser, N., Holt, T. and Hubbard, B. (2015). Glaciological and geomorphological map of Glacier Noir and Glacier Blanc, French Alps. *Journal of Maps*, 12(3), pp.582–596. doi:<https://doi.org/10.1080/17445647.2015.1054905>.

Liu, L., Xu, W.Y., Wang, H.L., Wang, W. and Wang, R.B. (2016). Permeability Evolution of Granite Gneiss During Triaxial Creep Tests. *Rock Mechanics and Rock Engineering*, 49(9), pp.3455–3462. doi:<https://doi.org/10.1007/s00603-016-0999-8>.

Luterbacher, J., Werner, J.P., Smerdon, J.E., Fernández-Donado, L., González-Rouco, F.J., Barriopedro, D., Ljungqvist, F.C., Büntgen, U., Zorita, E., Wagner, S., Esper, J., McCarroll, D., Toreti, A., Frank, D., Jungclauss, J.H., Barriendos, M., Bertolin, C., Bothe, O., Brázdil, R. and Camuffo, D. (2016). European summer temperatures since Roman

times. *Environmental Research Letters*, 11(2), p.024001.

doi:<https://doi.org/10.1088/1748-9326/11/2/024001>.

Matthews, J.A., Dawson, A.G. and Shakesby, R.A. (1986). Lake shoreline development, frost weathering and rock platform erosion in an alpine periglacial environment, Jotunheimen, southern Norway. *Boreas*, 15(1), pp.33–50.

doi:<https://doi.org/10.1111/j.1502-3885.1986.tb00741.x>.

Matthews, J.A., Mourne, R.W., Wilson, P., Hill, J.L., Robbins, C. and Winkler, S. (2024). Schmidt-hammer R-values from glacially-scoured bedrock surfaces across glacier-foreland boundaries: Insights into Holocene weathering rates with implications for exposure-age dating. *Geomorphology*, pp.109139–109139.

doi:<https://doi.org/10.1016/j.geomorph.2024.109139>.

Matthews, J.A. and Owen, G. (2010). Schmidt hammer exposure-age dating: developing linear age-calibration curves using Holocene bedrock surfaces from the Jotunheimen–Jostedalsglacier regions of southern Norway. *Boreas*, 39(1), pp.105–115.

doi:<https://doi.org/10.1111/j.1502-3885.2009.00107.x>.

Matthews, J.A. and Owen, G. (2008). Endolithic lichens, rapid biological weathering and schmidt hammer r-values on recently exposed rock surfaces: storbreen glacier foreland, jotunheimen, norway. *Geografiska Annaler: Series A, Physical Geography*, 90(4), pp.287–297. doi:<https://doi.org/10.1111/j.1468-0459.2008.00346.x>.

Matthews, J.A. and Shakesby, R.A. (1984). The status of the ‘Little Ice Age’ in southern Norway: relative-age dating of Neoglacial moraines with Schmidt hammer and lichenometry. *Boreas*, 13(3), pp.333–346. doi:<https://doi.org/10.1111/j.1502-3885.1984.tb01128.x>.

Matthews, J.A. and Winkler, S. (2022). Schmidt-hammer exposure-age dating: a review of principles and practice. *Earth-Science Reviews*, 230, p.104038.

doi:<https://doi.org/10.1016/j.earscirev.2022.104038>.

Niedzielski, T., MigońP. and Placek, A. (2009). A minimum sample size required from Schmidt hammer measurements. *Earth Surface Processes and Landforms*, 34(13), pp.1713–1725. doi:<https://doi.org/10.1002/esp.1851>.

Österreichische Nationalbibliothek (2025). [online] ÖNB Digital. Available at: <https://onb.digital/search/1136962> [Accessed 6 Mar. 2025].

Otto, J.-C. (2019). Proglacial Lakes in High Mountain Environments. In: T. Heckmann and D. Morche, eds., *Geomorphology of Proglacial Systems*. [online] Springer Cham. Available at: [https://doi.org/10.1007/978-3-319-94184-4\\_14](https://doi.org/10.1007/978-3-319-94184-4_14) [Accessed 28 Feb. 2025].

Palacios, D., Hughes, P.D., Jomelli, V. and Tanarro, L.M. (2024). Chapter 30 - Recent evolution and perspectives of European glacial landscapes. In: D. Palacios, P.D. Hughes, V. Jomelli and L.M. Tanarro, eds., *European Glacial Landscapes*. [online] Elsevier, p.Pages 587-599. Available at: <https://doi.org/10.1016/B978-0-323-99712-6.00031-3> [Accessed 22 Mar. 2025].

Patzelt, G., 1980. The Austrian glacier inventory: status and first results.

Patzelt, G. (2019). *Gletscher: Klimazeugen von der Eiszeit bis zur Gegenwart*. 1st ed. Hatje Cantz Verlag.

Pye, K., Goudie, A.S. and Watson, A. (1986). Petrological influence on differential weathering and inselberg development in the Kora area of central Kenya. *Earth Surface Processes and Landforms*, 11(1), pp.41–52.  
doi:<https://doi.org/10.1002/esp.3290110106>.

Ray, Y., Sen, S., Sen, K. and Beg, M.J. (2021). Quantifying the past glacial movements in Schirmacher Oasis, East Antarctica. *Polar Science*, 30, p.100733.  
doi:<https://doi.org/10.1016/j.polar.2021.100733>.

Rea, B.R. and Evans, D.J.A. (1996). Landscapes of areal scouring in N.W. Scotland. *Scottish Geographical Magazine*, 112(1), pp.47–50.  
doi:<https://doi.org/10.1080/00369229618736977>.

Reinthal, J. and Paul, F. (2024). Reconstructed glacier area and volume changes in the European Alps since the Little Ice Age. [online] doi:<https://doi.org/10.5194/egusphere-2024-989>.

Rode, M. and Kellerer-Pirklbauer, A. (2011). Schmidt-hammer exposure-age dating (SHD) of rock glaciers in the Schöderkogel-Eisenhut area, Schladminger Tauern Range,

Austria. *The Holocene*, 22(7), pp.761–771.

doi:<https://doi.org/10.1177/0959683611430410>.

Rode, M., Kranabeter, R. and Kellerer-Pirklbauer, A. (2009). The use of the Schmidt-hammer for dating paraglacial and glacial landforms in central Austria. *EGU General Assembly Conference Abstracts*, [online] p.8043. Available at:

<https://ui.adsabs.harvard.edu/abs/2009EGUGA..11.8043R/abstract> [Accessed 25 Feb. 2025].

Roman, M. (2019). Ice-flow directions of the last Scandinavian Ice Sheet in central Poland. *Quaternary International*, 501, pp.4–20.

doi:<https://doi.org/10.1016/j.quaint.2017.11.035>.

Rounce, D.R., Hock, R., Maussion, F., Hugonnet, R., Kochtitzky, W., Huss, M., Berthier, E., Brinkerhoff, D., Compagno, L., Copland, L., Farinotti, D., Menounos, B. and McNabb, R.W. (2023). Global glacier change in the 21st century: Every increase in temperature matters. *Science*, [online] 379(6627), pp.78–83.

doi:<https://doi.org/10.1126/science.abo1324>.

Rune Aa, A. and Sjøstad, J.A. (2000). Schmidt hammer age evaluation of the moraine sequence in front of Bøyabreen, western Norway. *Norsk Geologisk Tidsskrift*, 80(1), pp.27–32. doi:<https://doi.org/10.1080/002919600750042654>.

Santos-González, J., R.B. González-Gutiérrez, A. Gómez-Villar, S.A. Peña-Pérez, A. Melón-Nava, A. Pisabarro and J.M. Redondo-Vega (2024). Application of the Schmidt-hammer for relative-age dating of glacial and periglacial landforms in the Cantabrian Mountains (NW Spain). *Geomorphology*, pp.109210–109210.

doi:<https://doi.org/10.1016/j.geomorph.2024.109210>.

Schöner, W., Auer, I. and Böhm, R. (2000). Climate variability and glacier reaction in the Austrian eastern Alps. *Annals of Glaciology*, 31, pp.31–38.

doi:<https://doi.org/10.3189/172756400781819806>.

Shakesby, R.A., Matthews, J.A. and Owen, G. (2006). The Schmidt hammer as a relative-age dating tool and its potential for calibrated-age dating in Holocene glaciated

environments. *Quaternary Science Reviews*, 25(21-22), pp.2846–2867.

doi:<https://doi.org/10.1016/j.quascirev.2006.07.011>.

Small, R.J. (1983). Lateral Moraines of Glacier De Tsidjiore Nouve: Form, Development, and Implications. *Journal of Glaciology*, 29(102), pp.250–259.

doi:<https://doi.org/10.3189/s0022143000008303>.

Sommer, C., Malz, P., Seehaus, T.C., Lippl, S., Zemp, M. and Braun, M.H. (2020). Rapid glacier retreat and downwasting throughout the European Alps in the early 21st century. *Nature Communications*, [online] 11(1). doi:<https://doi.org/10.1038/s41467-020-16818-0>.

Stahl, T., Winkler, S., Quigley, M., Bebbington, M., Duffy, B. and Duke, D. (2013). Schmidt hammer exposure-age dating (SHD) of late Quaternary fluvial terraces in New Zealand. *Earth Surface Processes and Landforms*, 38(15), pp.1838–1850.

doi:<https://doi.org/10.1002/esp.3427>.

Stocker-Waldhuber, M., Fischer, A., Keller, L., Morche, D. and Kuhn, M. (2017). Funnel-shaped surface depressions — Indicator or accelerant of rapid glacier disintegration? A case study in the Tyrolean Alps. *Geomorphology*, 287, pp.58–72.

doi:<https://doi.org/10.1016/j.geomorph.2016.11.006>.

Sumner, P. and Nel, W. (2002). The effect of rock moisture on Schmidt hammer rebound: tests on rock samples from Marion Island and South Africa. *Earth Surface Processes and Landforms*, 27(10), pp.1137–1142. doi:<https://doi.org/10.1002/esp.402>.

Tomkins, M.D., Dortch, J.M. and Hughes, P.D. (2016). Schmidt Hammer exposure dating (SHED): Establishment and implications for the retreat of the last British Ice Sheet. *Quaternary Geochronology*, 33, pp.46–60.

doi:<https://doi.org/10.1016/j.quageo.2016.02.002>.

Tweed, F.S. and Carrivick, J.L. (2015). Deglaciation and proglacial lakes. *Geology Today*, 31(3), pp.96–102. doi:<https://doi.org/10.1111/gto.12094>.

Tyrolean State Government - Geoinformation Department (2025). [1] LBA. [online] Laser & Aerial Atlas of Tyrol. Available at: <https://lba.tirol.gv.at/public/karte.xhtml> [Accessed 6 Mar. 2025].

Ugelvig, S.V. and Egholm, D.L. (2018). The influence of basal-ice debris on patterns and rates of glacial erosion. *Earth and planetary science letters*, 490, pp.110–121. doi:<https://doi.org/10.1016/j.epsl.2018.03.022>.

Wahr, J., Burgess, E. and Swenson, S. (2016). Using GRACE and climate model simulations to predict mass loss of Alaskan glaciers through 2100. *Journal of Glaciology*, [online] 62(234), pp.623–639. doi:<https://doi.org/10.1017/jog.2016.49>.

Winkler, S. (2005). The Schmidt hammer as a relative-age dating technique: Potential and limitations of its application on Holocene moraines in Mt Cook National Park, Southern Alps, New Zealand. *New Zealand Journal of Geology and Geophysics*, 48(1), pp.105–116. doi:<https://doi.org/10.1080/00288306.2005.9515102>.

Winkler, S. (2009). First attempt to combine terrestrial cosmogenic nuclide ( $^{10}\text{Be}$ ) and Schmidt hammer relative-age dating: Strauchon Glacier, Southern Alps, New Zealand. *Open Geosciences*, 1(3). doi:<https://doi.org/10.2478/v10085-009-0026-3>.

Wytiachlowsky, H., Busfield, M.E., Hepburn, A.J. and Lukas, S. (2024). Deglaciation patterns in the Upper Zemmgrund, Austria: An exploration of clean-ice disintegration scenarios. *Geomorphology*, pp.109113–109113. doi:<https://doi.org/10.1016/j.geomorph.2024.109113>.

Zekollari, H., Huss, M. and Farinotti, D. (2019). Modelling the future evolution of glaciers in the European Alps under the EURO-CORDEX RCM ensemble. *The Cryosphere*, 13(4), pp.1125–1146. doi:<https://doi.org/10.5194/tc-13-1125-2019>.

Zemp, M. (2006). *Glaciers and climate change: spatio-temporal analysis of glacier fluctuations in the European Alps after 1850*.

Zemp, M., Frey, H., Gärtner-Roer, I., Nussbaumer, S.U., Hoelzle, M., Paul, F., Haeberli, W., Denzinger, F., Ahlstrøm, A.P., Anderson, B., Bajracharya, S., Baroni, C., Braun, L.N., Cáceres, B.E., Casassa, G., Cobos, G., Dávila, L.R., Delgado Granados, H., Demuth, M.N. and Espizua, L. (2015). Historically unprecedented global glacier decline in the early 21st century. *Journal of Glaciology*, [online] 61(228), pp.745–762. doi:<https://doi.org/10.3189/2015jog15j017>.

Zemp, M., Huss, M., Thibert, E., Eckert, N., McNabb, R., Huber, J., Barandun, M., Machguth, H., Nussbaumer, S.U., Gärtner-Roer, I., Thomson, L., Paul, F., Maussion, F., Kutuzov, S. and Cogley, J.G. (2019). Global glacier mass changes and their contributions to sea-level rise from 1961 to 2016. *Nature*, 568(7752), pp.382–386.

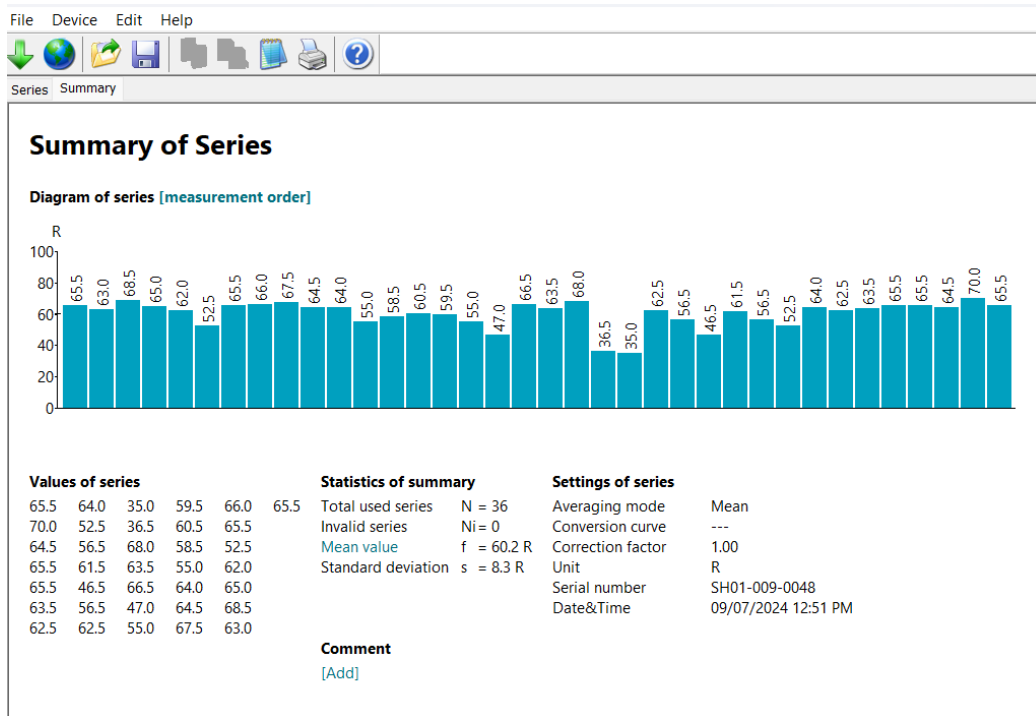
doi:<https://doi.org/10.1038/s41586-019-1071-0>.

Zemp, M., Jakob, L., Dussaillant, I., Nussbaumer, S.U., Gourmelen, N., Dubber, S., A, G., Abdullahi, S., Andreassen, L.M., Berthier, E., Bhattacharya, A., Blazquez, A., Boehm Vock, L.F., Bolch, T., Box, J., Braun, M.H., Brun, F., Cicero, E., Colgan, W. and Eckert, N. (2025). Community estimate of global glacier mass changes from 2000 to 2023. *Nature*. [online] doi:<https://doi.org/10.1038/s41586-024-08545-z>.

Zemp, M., Paul, F., Hoelzle, M. and Haeberli, W. (2008). Glacier Fluctuations in the European Alps, 185-2000. In: B. Orlove, E. Wiegandt and B.H. Luckman, eds., *Darkening Peaks: Glacier Retreat, Science, and Society*. University of California Press.

# 8 – Appendices

## Appendix A – ‘RockSchmidt’ programme



Summary page of all the series' taken with the Schmidt hammer. B – Page showing all off the series' taken

## Appendix B – Excel spreadsheet with outliers removed

Transect 2					Furthest from ice	Closest to ice	Transect 3					Furthest from ice	Closest to ice	Transect 4					Furthest from ice
Site 1	Site 2	Site 3	Site 4	Site 5			Site 1	Site 2	Site 3	Site 4	Site 5			Site 1	Site 2	Site 3	Site 4	Site 5	
65.5	66	66	62	64	<Average>		64.5	65	57.5	54.5	64	<Average>		66.5	49	55	60	58.5	
68	67.5	75.5	64				57	71	63	54.5	63			68.5	54	61.5	66	59.5	
64	70	66	62	56			63.5	60		68	69.5			68	48	65	68.5	62	
67.5	74.5	53.5	56.5	50.5			62	68	63	43	59			53.5	56.5	61	51.5	61.5	
71	74	74	73	74.5			68.5	72.5	62.5	43.5	40.5			68.5	41	59.5	60	58	
64	53	69		66.5			63.5	70	59.5	57	68.5			67.5	53	55	52.5	38	
68	63	69	61.5	66.5			59.5	71.5	59	62.5	71.5			67.5	60.5	61.5	54	62	
57	59.5	70.5	53.5	48			58.5	59	59	52.5	54			72.5	64.5	61.5	66	71	
67.5	71.5	72	58	61			66.5	62.5	63	42	69.5			66.5	68	62.5	51.5	55.5	
68.5	73	69.5	59	68.5			66	61.5	64.5	40.5	64			68	59	59.5	60.5	33	
69	68.5	63		62.5				71.5	59.5	44	71			75	56.5	58	55	65.5	
65	72	64	42.5	73.5			52.5	67.5	66	58.5	52			68.5	40.5	44		67	
72	64	71	62	59.5			68.5	65	52	65	69			66.5	61.5	48.5	74	45	
67.5	67.5	66.5	63.5	62.5			67	63	58	52	69.5			57.5	48.5	35.5	76	63	
66.5	74	61	69	62			60	62		40.5	69.5			68.5	45	68	67	51.5	
51	72.5	66.5	65.5	61			66	69		39.5	68			71.5	67.5	59.5	60.5	41.5	
60.5	57.5	95	55.5	68			67	47.5	55	46	56			64	27	59	58	62	
66.5	68	99.5	61.5	52			71	65	57	56.5	57.5			52	51	50	51	66.5	
62.5	53.5	62	60	59			61	68.5	56	48.5	71			67.5		51.5	73.5	64.5	
57.5	66.5	72.5	56.5	65.5			69.5	57.5	50	73	52			69	46	47.5	67	52	
69.5	68	67	60.5	56.5			58.5	65.5	59.5	59	52.5			69	47	53.5	63	69	
68.5	67.5	60.5	72.5	69			72.5	61	53	76.5	37.5			45.5	59.5	46	58.5	60.5	
70.5	67.5	45	65.5	59.5			63	64	58.5	60	64.5			70	37	43.5	61	63.5	
65	62		63.5	71.5			69.5	60.5	44	60.5	63.5			60	29	51.5	37	61	
61.5	70.5	67.5	69.5	69			50.5	69.5	50	52	68.5			70.5	51.5	49.5	65	69.5	
63.5	68.5	71	67.5	69.5			71		58		70.5			73	35	45.5	40	67.5	
69.5	71	66	63.5	68			63	58.5	52	68	65			70	57.5	58	56	61	
65.5	72.5	69.5	65.5	71.5			63.5	65	79	65.5	72			71	56.5	56.5	70	66	
70	70	61	73.5	71.5			66	68.5	50.5		66.5			64.5	35.5	44	63	68	
63	69.5	58	60.5	73			68	64	47	47	40			60.5	66	44	49	59	
61	68.5	69	66.5	70.5			65	66	62	57.5	51.5			72	36	36.5	63.5	40.5	
70	61	64.5	65	68.5			65	49.5	48	79.5	77			64	38.5	61	32	43	
67	62.5	54.5	73.5	70			66	67	59.5	66	69			70	55	66.5	43.5	52.5	
68	67.5	48	63.5	68			64.5	69	65	45	72.5			66	71.5	61.5	65	57	
60	64.5	53.5	66	71.5			63	70	57.5	61.5	58.5			68	57	45.5	54	47.5	
69.5	53.5	53	50	67			60.5	68.5	55	51	74			65	33	63	67.5	67.5	
62.5	69	64.5	62	63.5			66	67	54	61	62			64	48	56	71.5	54.5	
68.5	66.5	73	62	72			65	72	69	59	73.5			73	43	64.5	66	69.5	
65	63	53.5	60.5	69			60.5	63.5	65		49.5			67.5	67.5	63	67.5	64.5	
68.5	65	44.5	53.5	65.5			69.5	67.5	50.5	50	72			60.5	67	43.5	65.5	68.5	
72.5	65.5	67.5	55	71			65	73	59.5	35	67.5			76.5		60.5	65	56	
65	62	65	59	58			71	68.5	61.5	62	76			69	43.5	63	70.5	66.5	
60.5	53	67.5	64	67			51.5	67.5	62	49.5	63.5			61.5	36	54	59.5	52.5	
67.5	60	65	64	60			60	59	58.5	48.5	71			69.5	52.5	53.5	66.5	63	
65.5	61	72.5	49	60			71.5	62.5	43	34.5	74			69	36	60	61.5	55.5	
64	70.5	71.5	59	53			60.5	60.5	56	63	50			68.5		52.5	59	60.5	
65	69	71	63				71	64.5	56.5	52.5	54			67.5	31.5	56.5	53.5	44.5	
62	66.5	63.5	66.5					65	60	55	66			64.5	40	64.5	69.5	48	
61.5	65	71.5	66.5	54.5			62	65.5	57.5	53.5	68.5			55	28	50	52.5	61.5	
63.5	67	76	62	53			72.5	61.5	45	47	70			61.5	44.5	51.5	62	53.5	
58	58.5	70.5	53	58.5			66.5	52.5	58	65	68.5			73	46	62	64	64.5	

Example of transects 2, 3, 4 in the excel spreadsheet with the outliers removed shown as a red cell.

## Appendix C – R-studio code

```
27 library(ggplot2)
28 library(ggrepel)
29 library(tidyverse)
30
31
32 head(TranUpdate)
33 head(Tnew)
34 View(Tnew)
35 theme_set(theme_bw())
36
37 #Transect 1
38 TranUpdateError%>%
39   ggplot(aes(x=Distance1, y=T1avg, label=T1avg)) +
40   geom_errorbar(aes(ymin=T1avg-sd1,ymax=T1avg+sd1),width=20, colour = "blue") +
41   geom_label_repel(nudge_x = -35,
42                   nudge_y = 6) +
43   geom_line(color="blue", size=1) +
44   geom_point(size = 4, colour = "blue",fill = "blue",shape = 21) +
45   xlim(500,1200) + ylim(50,75) +
46
47
48   xlab("Distance(m)") + ylab("R-Value") +
49   ggtitle("Transect 1 - Site Averages",
50           subtitle = "p-value = 0.96") +
51   theme_bw() +
52   theme(plot.title = element_text(hjust = 0.5, size = 17),
53         axis.title = element_text(size = 12),
54         plot.subtitle = element_text(hjust = 0.5)) +
55   labs(tag = "")
56
57 #Correlation - Transect 1
58
59 cor.test(TranUpdateError$Distance1,TranUpdateError$T1avg) #P,Value of 0.96 - i.e >0.05
60
```

Example of code for transect one to create the scatter graph and the correlation test applied to calculate the p-value